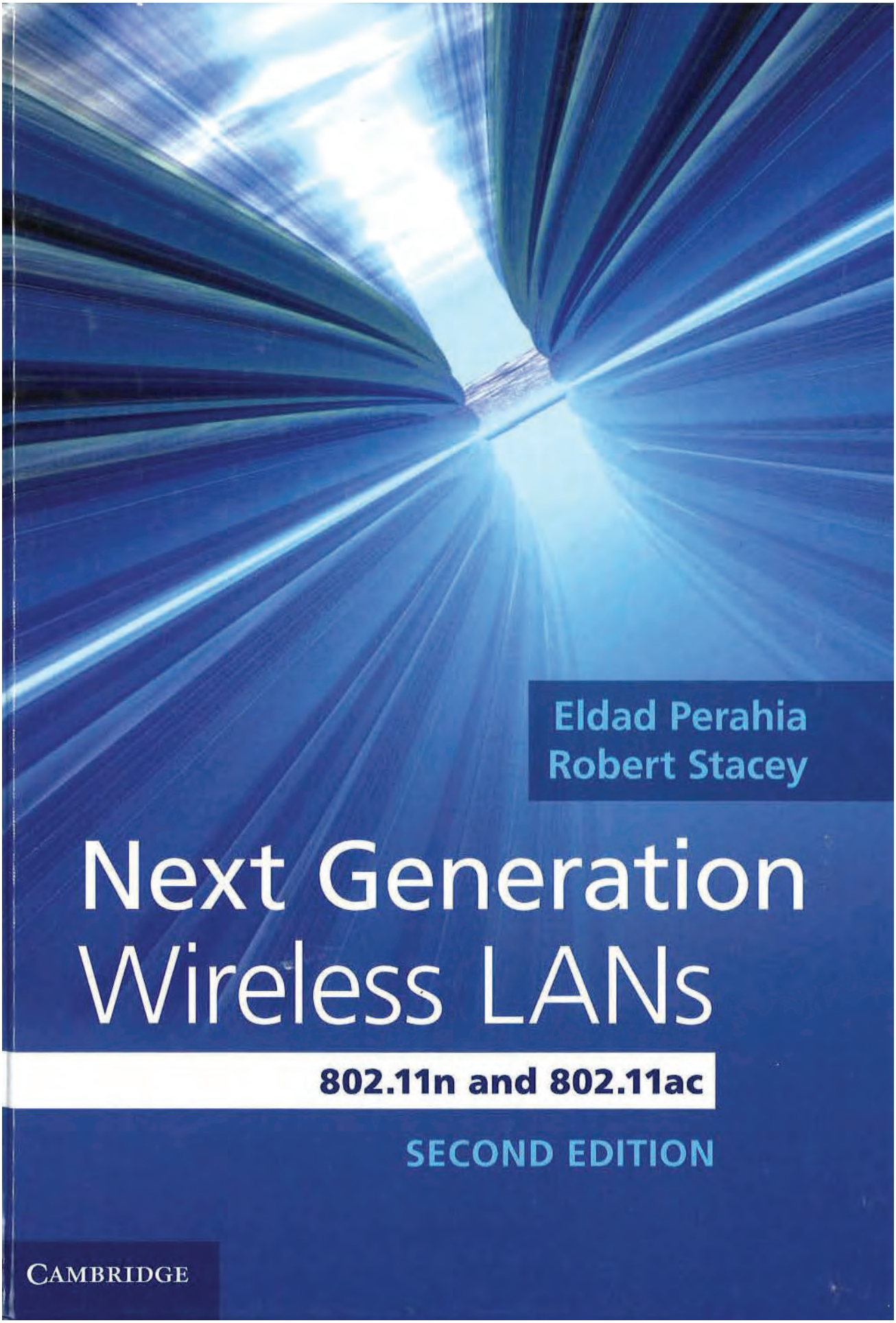
Eldad Perahia
Robert Stacey
Next Generation
Wireless LANs
802.11n and 802.11ac
SECOND EDITION
CAMBRIDGE

Next Generation Wireless LANs

If you've been searching for a way to get up to speed on IEEE 802.11n and 802.11ac WLAN standards without having to wade through the entire 802.11 specification, then look no further.

This comprehensive overview describes the underlying principles, implementation details, and key enhancing features of 802.11n and 802.11ac. For many of these features, the authors outline the motivation and history behind their adoption into the standard. A detailed discussion of the key throughput, robustness, and reliability enhancing features (such as MIMO, multi-user MIMO, 40\80\160 MHz channels, transmit beamforming, and packet aggregation) is given, in addition to clear summaries of the issues surrounding legacy interoperability and coexistence.

Now updated and significantly revised, this 2nd edition contains new material on 802.11ac throughout, including revised chapters on MAC and interoperability, as well as new chapters on 802.11ac PHY, and multi-user MIMO, making it an ideal reference for designers of WLAN equipment, network managers, and researchers in the field of wireless communication.

Eldad Perahia is a Principal Engineer in the Standards and Technology Group at Intel Corporation. He is Chair of the IEEE 802.11 Very High Throughput in 60 GHz Task Group (TGad), the IEEE 802.11 Very High Throughput in <6 GHz Task Group (TGac) Coexistence Ad Hoc Co-Chair, the IEEE 802.11 liaison from the IEEE 802.19 Wireless Coexistence Working Group, and the former Chair of the IEEE 802.11 Very High Throughout Study Group. He was awarded his Ph.D. in Electrical Engineering from the University of California, Los Angeles and holds 21 patents in various areas of wireless communications.

Robert Stacey is a Wireless Systems Architect at Apple, Inc. He is the IEEE 802.11 Very High Throughput in <6 GHz Task Group (TGac) Technical Editor and MU-MIMO Ad Hoc Co-Chair. He was a member of the IEEE 802.11 High Throughput Task Group (TGn) and a key contributor to the various proposals, culminating in the final joint proposal submission that became the basis for the 802.11n draft standard. He holds numerous patents in the field of wireless communications.

"The authors are renowned experts in the field. The book is a must read for engineers seeking knowledge of recent advances in WLAN technologies."

Dr Osama Aboul-Magd; IEEE 802.11ac Task Group Chair.

"First edition of the book "Next Generation Wireless LANs" by Eldad and Robert is excellent and very popular. The second edition adds newly developed IEEE 802.11ac standard with the same excellence in addressing technical features and easy to read writing style."

Vinko Erceg, Broadcom Corporation

"The 802.11 standard has been evolving for over 20 years and now contains nearly 3000 pages of information. The authors have had direct involvement in writing many of those pages. This book represents a significant accomplishment in conveying and explaining the engineering behind the features for two of the most important radio options provided by the standard. Radio engineers approaching the standard for the first time as well as those already engaged in product development will find this text remarkably rewarding."

Bruce Kraemer, Marvell Semiconductor and Chair, IEEE 802.11 Working Group

This endorsement solely represents the views of the person who is endorsing this book and does not necessarily represent a position of either the company, the IEEE or the IEEE Standards Association.

Next Generation Wireless LANs

802.11n and 802.11ac

ELDAD PERAHIA
Intel Corporation

ROBERT STACEY
Apple Inc.

CAMBRIDGE
UNIVERSITY PRESS

CAMBRIDGE
UNIVERSITY PRESS

University Printing House, Cambridge CB2 8BS, United Kingdom

Cambridge University Press is part of the University of Cambridge.

It furthers the University's mission by disseminating knowledge in the pursuit of education, learning and research at the highest international levels of excellence.

www.cambridge.org
Information on this title: www.cambridge.org/9781107016767

© Cambridge University Press 2008, 2013

This publication is in copyright. Subject to statutory exception and to the provisions of relevant collective licensing agreements, no reproduction of any part may take place without the written permission of Cambridge University Press.

First published 2008
Reprinted with corrections 2010
Second edition 2013
6th printing 2016

Printed in the United States of America by Sheridan Books, Inc.

A catalog record for this publication is available from the British Library

Library of Congress Cataloging-in-Publication Data
Perahia, Eldad, 1967 – author.
Next generation wireless LANs : 802.11n, 802.11ac, and Wi-Fi direct / Eldad Perahia, Intel Corporation, Robert Stacey, Apple Inc. – Second edition.
pages cm
ISBN 978-1-107-01676-7 (hardback)
1. Wireless LANs. I. Stacey, Robert, 1967 – author. II. Title.
TK5105.78.P47 2013
621.39′8–dc23

2012033809

ISBN 978-1-107-01676-7 Hardback

Cambridge University Press has no responsibility for the persistence or accuracy of URLs for external or third-party internet websites referred to in this publication, and does not guarantee that any content on such websites is, or will remain, accurate or appropriate.

To my wife Sarah and our son Nathan

— Eldad Perahia

To my wife Celia and son Zachary

— Robert Stacey

Contents

Foreword by Dr. Andrew Myles *page* xv
Preface to the first edition xix
Preface to the second edition xxi
List of abbreviations xxii

Chapter 1 Introduction 1

1.1 An overview of IEEE 802.11 3
1.1.1 The 802.11 MAC 3
1.1.2 The 802.11 PHYs 4
1.1.3 The 802.11 network architecture 6
1.1.4 Wi-Fi Direct 6
1.2 History of high throughput and 802.11n 7
1.2.1 The High Throughput Study Group 7
1.2.2 Formation of the High Throughput Task Group (TGn) 8
1.2.3 Call for proposals 10
1.2.4 Handheld devices 11
1.2.5 Merging of proposals 11
1.2.6 802.11n amendment drafts 11
1.3 Environments and applications for 802.11n 12
1.4 Major features of 802.11n 14
1.5 History of Very High Throughput and 802.11ac 17
1.6 Outline of chapters 20
References 22

Part I Physical layer 25

Chapter 2 Orthogonal frequency division multiplexing 27

2.1 Background 27
2.2 Comparison to single carrier modulation 29
References 31

Chapter 3 MIMO/SDM basics 32

3.1 SISO (802.11a/g) background 32
3.2 MIMO basics 32
3.3 SDM basics 34
3.4 MIMO environment 36
3.5 802.11n and 802.11ac propagation model 38
3.5.1 Impulse response 39
3.5.2 Antenna correlation 42
3.5.3 802.11n Doppler model 45
3.5.4 802.11ac Doppler model 46
3.5.5 Physical layer impairments 47
3.5.6 Path loss 50
3.6 Linear receiver design 51
3.7 Maximum likelihood estimation 54
References 56
Appendix 3.1 802.11n channel models 57

Chapter 4 PHY interoperability with 11a/g legacy OFDM devices 62

4.1 11a packet structure review 62
4.1.1 Short Training field 62
4.1.2 Long Training field 65
4.1.3 Signal field 68
4.1.4 Data field 69
4.1.5 Packet encoding process 70
4.1.6 Receive procedure 72
4.2 Mixed format high throughput packet structure 74
4.2.1 Non-HT portion of the MF preamble 75
4.2.2 HT portion of the MF preamble 81
4.2.3 Data field 88
4.2.4 HT MF receive procedure 96
References 102
Appendix 4.1 20 MHz basic MCS tables 103

Chapter 5 High throughput 105

5.1 40 MHz channel 105
5.1.1 40 MHz subcarrier design and spectral mask 106
5.1.2 40 MHz channel design 108
5.1.3 40 MHz mixed format preamble 108
5.1.4 40 MHz data encoding 113
5.1.5 MCS 32: high throughput duplicate format 116
5.1.6 20/40 MHz coexistence with legacy in the PHY 119
5.1.7 Performance improvement with 40 MHz 120

5.2 20 MHz enhancements: additional data subcarriers 121
5.3 MCS enhancements: spatial streams and code rate 122
5.4 Greenfield (GF) preamble 127
5.4.1 Format of the GF preamble 128
5.4.2 PHY efficiency 130
5.4.3 Issues with GF 130
5.4.4 Preamble auto-detection 134
5.5 Short guard interval 136
References 140
Appendix 5.1 Channel allocation 141
Appendix 5.2 40 MHz basic MCS tables 141
Appendix 5.3 Physical layer waveform parameters 146

Chapter 6 Robust performance 147

6.1 Receive diversity 147
6.1.1 Maximal ratio combining basics 148
6.1.2 MIMO performance improvement with receive diversity 149
6.1.3 Selection diversity 152
6.2 Spatial expansion 152
6.3 Space-time block coding 152
6.3.1 Alamouti scheme background 153
6.3.2 Additional STBC antenna configurations 156
6.3.3 STBC receiver and equalization 159
6.3.4 Transmission and packet encoding process with STBC 161
6.4 Low density parity check codes 164
6.4.1 LDPC encoding process 165
6.4.2 Effective code rate 175
6.4.3 LDPC coding gain 176
References 177
Appendix 6.1 Parity check matrices 177

Chapter 7 Very High Throughput PHY 182

7.1 Channelization 182
7.2 Single user (SU) VHT packet structure 184
7.3 VHT format preamble 185
7.3.1 Non-VHT portion of the VHT format preamble 185
7.3.2 VHT portion of the VHT format preamble 191
7.3.3 VHT data field 200
7.4 Modulation coding scheme 212
References 217

Part II Medium access control layer 219

Chapter 8 Medium access control 221

8.1 Protocol layering 222
8.2 Finding, joining, and leaving a BSS 223
8.2.1 Beacons 223
8.2.2 Scanning 224
8.2.3 Authentication 224
8.2.4 Association 225
8.2.5 Reassociation 226
8.2.6 Disassociation 226
8.2.7 802.1X Authentication 226
8.2.8 Key distribution 227
8.3 Distributed channel access 228
8.3.1 Basic channel access timing 229
8.4 Data/ACK frame exchange 231
8.4.1 Fragmentation 232
8.4.2 Duplicate detection 233
8.4.3 Data/ACK sequence overhead and fairness 234
8.5 Hidden node problem 234
8.5.1 Network allocation vector (NAV) 235
8.5.2 EIFS 236
8.6 Enhanced distributed channel access 236
8.6.1 Transmit opportunity 238
8.6.2 Channel access timing with EDCA 239
8.6.3 EDCA access parameters 239
8.6.4 EIFS revisited 240
8.6.5 Collision detect 240
8.6.6 QoS Data frame 241
8.7 Block acknowledgement 241
8.7.1 Block data frame exchange 243
8.8 Power management 243
8.8.1 AP TIM transmissions 244
8.8.2 PS mode operation 244
8.8.3 WNM-Sleep 246
8.8.4 SM power save 246
8.8.5 Operating Mode Notification 246
References 247

Chapter 9 MAC throughput enhancements 248

9.1 Reasons for change 248
9.1.1 Throughput without MAC changes 248

9.1.2 MAC throughput enhancements 250
9.1.3 Throughput with MAC efficiency enhancements 251
9.2 Aggregation 253
9.2.1 Aggregate MSDU (A-MSDU) 254
9.2.2 Aggregate MPDU (A-MPDU) 255
9.2.3 Aggregate PSDU (A-PSDU) 257
9.2.4 A-MPDU in VHT PPDUs 258
9.2.5 VHT single MPDU 259
9.3 Block acknowledgement 259
9.3.1 Immediate and delayed block ack 259
9.3.2 Block ack session initiation 260
9.3.3 Block ack session data transfer 261
9.3.4 Block ack session tear down 262
9.3.5 Normal ack policy in a non-aggregate 262
9.3.6 Reorder buffer operation 263
9.4 HT-immediate block ack 264
9.4.1 Normal Ack policy in an aggregate 264
9.4.2 Compressed block ack 265
9.4.3 Full state and partial state block ack 265
9.4.4 HT-immediate block ack TXOP sequences 269
9.5 HT-delayed block ack 269
9.5.1 HT-delayed block ack TXOP sequences 270
References 270

Chapter 10 Advanced channel access techniques 271

10.1 PCF 271
10.1.1 Establishing the CFP 271
10.1.2 NAV during the CFP 272
10.1.3 Data transfer during the CFP 272
10.1.4 PCF limitations 273
10.2 HCCA 274
10.2.1 Traffic streams 274
10.2.2 Controlled access phases 276
10.2.3 Polled TXOP 276
10.2.4 TXOP requests 277
10.2.5 Use of RTS/CTS 277
10.2.6 HCCA limitations 277
10.3 Reverse direction protocol 277
10.3.1 Reverse direction frame exchange 278
10.3.2 Reverse direction rules 279
10.3.3 Error recovery 279
10.4 PSMP 280
10.4.1 PSMP recovery 281

10.4.2 PSMP burst 281
10.4.3 Resource allocation 282
10.4.4 Block ack usage under PSMP 283
References 283

Chapter 11 Interoperability and coexistence 284

11.1 Station capabilities and operation 284
11.1.1 HT station PHY capabilities 285
11.1.2 VHT station PHY capabilities 285
11.1.3 HT station MAC capabilities 286
11.1.4 VHT station MAC capabilities 286
11.1.5 Advanced capabilities 286
11.2 BSS operation 287
11.2.1 Beacon transmission 288
11.2.2 20 MHz BSS operation 289
11.2.3 20/40 MHz HT BSS operation 289
11.2.4 VHT BSS operation 293
11.2.5 OBSS scanning requirements 294
11.2.6 Signaling 40 MHz intolerance 298
11.2.7 Channel management at the AP 299
11.2.8 Establishing a VHT BSS in the 5 GHz band 300
11.3 A summary of fields controlling 40 MHz operation 300
11.4 Channel access in wider channels 301
11.4.1 Overlapping BSSs 302
11.4.2 Wide channel access using RTS/CTS 303
11.4.3 TXOP rules for wide channel access 304
11.4.4 Clear channel assessment 304
11.4.5 NAV assertion in an HT and VHT BSS 306
11.5 Protection 306
11.5.1 Protection with 802.11b stations present 307
11.5.2 Protection with 802.11g or 802.11a stations present 307
11.5.3 Protection for OBSS legacy stations 308
11.5.4 RIFS burst protection 308
11.5.5 HT Greenfield format protection 309
11.5.6 RTS/CTS protection 309
11.5.7 CTS-to-Self protection 310
11.5.8 Protection using a non-HT, HT mixed, or VHT PPDU with non-HT response 311
11.5.9 Non-HT station deferral with HT mixed and VHT format PPDUs 311
11.5.10 L-SIG TXOP protection 312

11.6 Phased coexistence operation (PCO) 314
11.6.1 Basic operation 314
11.6.2 Minimizing real-time disruption 315
References 316

Chapter 12 MAC frame formats 317

12.1 General frame format 317
12.1.1 Frame Control field 317
12.1.2 Duration/ID field 321
12.1.3 Address fields 321
12.1.4 Sequence Control field 321
12.1.5 QoS Control field 322
12.1.6 HT Control field 324
12.1.7 Frame Body field 327
12.1.8 FCS field 327
12.2 Format of individual frame types 327
12.2.1 Control frames 327
12.2.2 Data frames 336
12.2.3 Management frames 337
12.3 Management frame fields 342
12.3.1 Fields that are not information elements 344
12.3.2 Information elements 344
References 361

Part III Transmit beamforming, multi-user MIMO, and fast link adaptation 363

Chapter 13 Transmit beamforming 365

13.1 Singular value decomposition 366
13.2 Transmit beamforming with SVD 369
13.3 Eigenvalue analysis 370
13.4 Unequal MCS 376
13.5 Receiver design 378
13.6 Channel sounding 379
13.7 Channel state information feedback 381
13.7.1 Implicit feedback 382
13.7.2 Explicit feedback 386
13.8 Improved performance with transmit beamforming 393
13.9 Degradations 399
13.10 MAC considerations 406
13.10.1 Sounding PPDUs 407
13.10.2 Implicit feedback beamforming 410
13.10.3 Explicit feedback beamforming 413

13.11 Comparison between implicit and explicit 416
13.12 Transmit beamforming in 802.11ac 417
13.12.1 VHT sounding protocol 418
References 419
Appendix 13.1 Unequal MCS for 802.11n 420
Unequal MCS for 20 MHz 420
Unequal MCS for 40 MHz 422

Chapter 14 Multi-user MIMO 424

14.1 MU-MIMO pre-coding 426
14.2 Receiver design 427
14.3 PHY considerations 428
14.3.1 VHT MU preamble 430
14.3.2 VHT MU data field 432
14.3.3 Compressed beamforming matrices 435
14.4 Group ID 435
14.4.1 Receive operation 435
14.4.2 Group ID management 435
14.5 MAC support for MU-MIMO 436
14.5.1 MU aggregation 436
14.5.2 MU acknowledgements 437
14.5.3 EDCA TXOPs for MU sequences 437
14.5.4 TXOP sharing 438
14.6 VHT sounding protocol for MU-MIMO 438
14.6.1 The basic sounding exchange 438
14.6.2 Support for fragmentation 439
References 439

Chapter 15 Fast link adaption 440

15.1 MCS feedback 441
15.2 MCS feedback mechanisms 442
15.3 MCS feedback using the HT variant HT Control field 442
15.4 MCS feedback using the VHT variant HT Control field 443

Index 445

1 Introduction

Wireless local area networking has experienced tremendous growth in the last ten years with the proliferation of IEEE 802.11 devices. Its beginnings date back to Hertz's discovery of radio waves in 1888, followed by Marconi's initial experimentation with transmission and reception of radio waves over long distances in 1894. In the following century, radio communication and radar proved to be invaluable to the military, which included the development of spread spectrum technology. The first packet-based wireless network, ALOHANET, was created by researchers at the University of Hawaii in 1971. Seven computers were deployed over four islands communicating with a central computer in a bi-directional star topology.

A milestone event for commercial wireless local area networks (WLANs) came about in 1985 when the United States Federal Communications Commission (FCC) allowed the use of the experimental industrial, scientific, and medical (ISM) radio bands for the commercial application of spread spectrum technology. Several generations of proprietary WLAN devices were developed to use these bands, including WaveLAN by Bell Labs. These initial systems were expensive and deployment was only feasible when running cable was difficult.

Advances in semiconductor technology and WLAN standardization with IEEE 802.11 led to a dramatic reduction in cost and the increased adoption of WLAN technology. With the increasing commercial interest, the Wi-Fi Alliance (WFA) was formed in 1999 to certify interoperability between IEEE 802.11 devices from different manufacturers through rigorous testing. Shipments of Wi-Fi certified integrated circuits exceeded a billion units per year in 2011 (ABIresearch, 2012) and are expected to exceed 2.5 billion units per year by 2016 (ABIresearch, 2012), as illustrated in Figure 1.1.

Such large and sustained growth is due to the benefits WLANs offer over wired networking. In existing homes or enterprises, deploying cables for network access may involve tearing up walls, floors, or ceilings, which is both inconvenient and costly. In contrast, providing wireless network connectivity in these environments is often as simple as installing a single wireless access point. Perhaps more importantly though, the proliferation of laptops and handheld devices has meant that people desire connectivity wherever they are located, not just where the network connection is located. Network connectivity in a conference room or while seated on the sofa in the living room are just two examples of the flexibility afforded by WLANs.

There has been a proliferation of small scale deployments providing Internet access in coffee shops, airports, hotels, etc., which have come to be known as hotspots. In recent

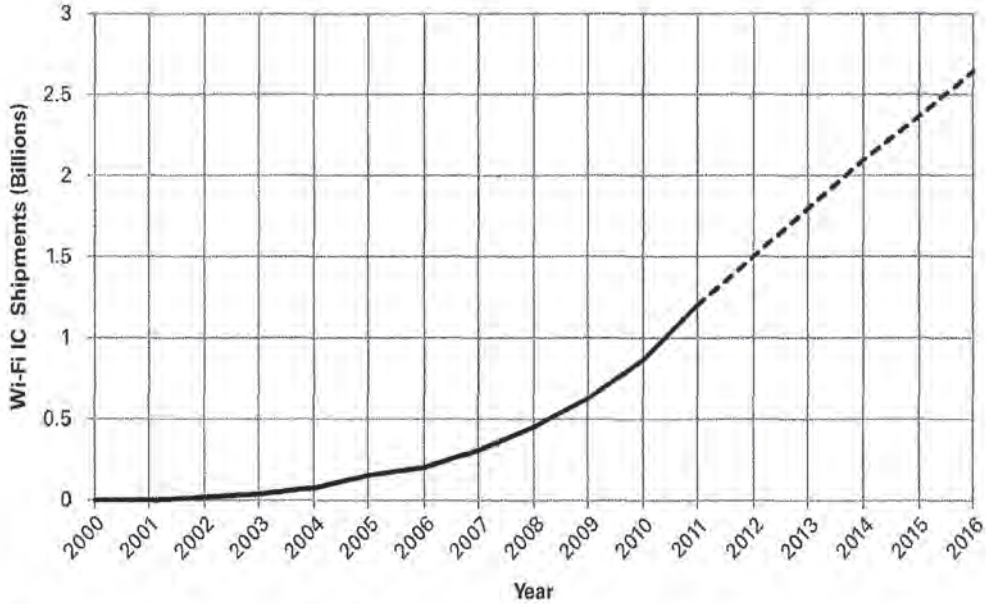

Figure 1.1 Wi-Fi IC shipments.Source: ABIresearch (2007, 2012).

years, carriers with heavily congested cellular networks are deploying hotspots to off-load traffic from their cellular networks. Additionally, when these networks are used in conjunction with virtual private network (VPN) technology, employees can securely access corporate networks from almost anywhere.

WLAN products and systems started with 802.11b, 802.11g, and 802.11a standard amendments, which provided throughput enhancements over the original 802.11 PHYs. Progress in WLAN technology continued with the development of 802.11n. Increased data rates were achieved with the multiple-input multiple-output (MIMO) concept, with its origins by Foschini (1996) at Bell Labs. In 2004, Atheros demonstrated that 40 MHz devices could be produced at almost the same cost as 20 MHz devices. During a similar time frame, the FCC and ETSI adopted new regulations in the 5 GHz band that added an additional 400 MHz of unlicensed spectrum for use by commercial WLANs.

These events paved the way for the broad acceptance of 40 MHz operating modes in 802.11n. When spectrum is free, increasing the channel bandwidth is the most cost effective way to increase the data rate.

Typically product development lags standardization efforts and products are released after the publication of the standard. An interesting event occurred in 2003 when Broadcom released a chipset based on a draft version of the 802.11g amendment, prior to final publication. This set a precedent for the flurry of "pre-n" products in 2005 and 2006, as industry players rushed to be first to market. Most of these products were either proprietary implementations of MIMO, or based on draft 1.0 of 802.11n, and thus unlikely to be compliant with the final standard.

Through early 2007, major improvements and clarifications were made to the 802.11n draft resulting in IEEE 802.11n draft 2.0. To continue the market momentum and forestall

interoperability issues, the IEEE took the unusual step of releasing 802.11n D2.0 to the public while work continued toward the final standard. This allowed the Wi-Fi Alliance (WFA) to begin interoperability testing and certification of devices based on a subset of the 802.11n D2.0 features in May 2007. Wi-Fi certified 802.11n D2.0 products provide consumers the assurance of interoperability between manufacturers that was not guaranteed by previous "pre-n" products. At the end of 2009, 802.11n was finally approved and the WFA updated the certification program to reflect support for the approved standard. Full interoperability was maintained between 802.11n D2.0 and the approved standard products. These were major steps in speeding up the standardization and certification process of new technology.

As this process was successful for the industry and beneficial for the consumers, 802.11ac will follow a similar path. It is expected that 802.11ac products based on an early draft will be certified and on the market in early 2013. Completion of the 802.11ac is expected by the end of 2013.[1] Certification based on the approved standard will take place in a similar time frame.

1.1 An overview of IEEE 802.11

The IEEE 802.11 standard defines multiple physical layers (PHYs) and a common medium access control (MAC) layer for wireless local area networking. As a member of the IEEE 802 family of local area networking (LAN) and metropolitan area networking (MAN) standards, 802.11 inherits the 802 reference model and 48-bit universal addressing scheme. The 802 reference model is based on the OSI reference model described in Table 1.1. In this model, the 802.11 MAC and 802.2 logical link control (LLC) sublayers form the data link layer and the 802.11 PHY the physical layer.

1.1.1 The 802.11 MAC

The initial version of the 802.11 standard was completed in 1997. Influenced by the huge market success of Ethernet (standardized as IEEE 802.3), the 802.11 MAC adopted the same simple distributed access protocol, carrier sense multiple access (CSMA). With CSMA, a station wishing to transmit first listens to the medium for a predetermined period. If the medium is sensed to be "idle" during this period then the station is permitted to transmit. If the medium is sensed to be "busy," the station has to defer its transmission. The original (shared medium) Ethernet used a variation called CSMA/CD or carrier sense multiple access with collision detection. After determining that the medium is "idle" and transmitting, the station is able to receive its own transmission and detect collisions. If a collision is detected, the two colliding stations backoff for a random period before transmitting again. The random backoff period reduces the probability of a second collision.

With wireless it is not possible to detect a collision with one's own transmission directly in this way: thus 802.11 uses a variation called CSMA/CA or carrier sense

[1] The reader is referred to http://grouper.ieee.org/groups/802/11/Reports/802.11_Timelines.htm for the latest update on the timeline of 802.11ac

Table 1.1 OSI reference model (adapted from ISO/IEC 7498-1, 1994)

OSI reference model layers	Description	Examples	Layer categories
Application	Interacts with the software applications that implement a communicating component	HTTP, FTP, SMTP	Application
Presentation	Establishes context between application-layer entities	MIME, TLS, SSL	
Session	Establishes, manages, and terminates communication sessions	Named pipe, NetBIOS	
Transport	Provides an end-to-end reliable data transfer service, including flow control, segmentation/desegmentation and error control	TCP, UDP	
Network	Provides the means for transferring variable length data sequences from a source device to a destination device. Maintains the quality of service requested by the transport layer	IP (IPv4, IPv6), ICMP, IPsec	
Data link	Provides the means for transferring data between devices	LLC 802.11 MAC	Data transport
Physical	Provides the electrical and physical specifications for devices	802.11 PHY	

multiple access with collision avoidance. With CSMA/CA, if the station detects that the medium is busy, it defers its transmission for a random period following the medium going "idle" again. This approach of always backing off for a random period following another station's transmission improves performance since the penalty for a collision is much higher on a wireless LAN than on a wired LAN. On a wired LAN collisions are detected electrically and thus almost immediately, while on wireless LAN collisions are inferred through the lack of an acknowledgement or other response from the remote station once the complete frame has been transmitted.

There is no doubt that the simplicity of this distributed access protocol, which enables consistent implementation across all nodes, significantly contributed to Ethernet's rapid adoption as the industry LAN standard. Likewise, the adoption by the industry of 802.11 as the wireless LAN standard is in no small part due to the simplicity of this access protocol, its similarity to Ethernet, and again the consistent implementation across all nodes that has allowed 802.11 to beat out the more complex, centrally coordinated access protocols of competing WLAN technologies such as HyperLAN.

1.1.2 The 802.11 PHYs

The original (1997) 802.11 standard included three PHYs: infrared (IR), 2.4 GHz frequency hopped spread spectrum (FHSS), and 2.4 GHz direct sequence spread

spectrum (DSSS). This was followed by two standard amendments in 1999: 802.11b built upon DSSS to increase the data rate in 2.4 GHz and 802.11a to create a new PHY in 5 GHz. 802.11b enhanced DSSS with complementary code keying (CCK), increasing the data rate to 11 Mbps. With higher data rates, IEEE 802.11b devices achieved significant market success, and markets for IR and FHSS PHYs did not materialize.

The development of 802.11a introduced orthogonal frequency division multiplexing (OFDM) to 802.11. Even though 802.11a introduced data rates of up to 54 Mbps, it is confined to the 5 GHz band and, as a result, adoption has been slow. New devices wishing to take advantage of the higher rates provided by 802.11a but retain backward compatibility with the huge installed base of 802.11b devices would need to implement two radios, one to operate using 802.11b in the 2.4 GHz band and one to operate using 802.11a in the 5 GHz band. Furthermore, international frequency regulations in the 2.4 GHz band uniformly allowed commercial use, whereas in 1999 and 2000 the non-military use of the 5 GHz band was limited to select channels in the United States.

In 2001, the FCC permitted the use of OFDM in the 2.4 GHz band. Subsequently, the 802.11 working group developed the 802.11g amendment, which incorporates the 802.11a OFDM PHY in the 2.4 GHz band, and adopted it as part of the standard in 2003. In addition, backward compatibility and interoperability is maintained between 802.11g and the older 802.11b devices. This allows for new 802.11g client cards to work in existing 802.11b hotspots, or older 802.11b embedded client devices to connect with a new 802.11g access point (AP). Because of this and new data rates of up to 54 Mbps, 802.11g experienced large market success. A summary of the high level features of each PHY is given in Table 1.2.

With the adoption of each new PHY, 802.11 has experienced a five-fold increase in data rate. This rate of increase continues with 802.11n with a data rate of 300 Mbps in 20 MHz and 600 Mbps in 40 MHz. Furthermore, in the 5 GHz band, 802.11ac provides a data rate of 1733 Mbps with 80 MHz and four spatial streams, and a maximum data rate of 6933 Mbps with 160 MHz and eight spatial streams. The exponential increase in data rate is illustrated in Figure 1.2.

Table 1.2 Overview of 802.11 PHYs

	802.11	802.11b	802.11a	802.11g	802.11n	802.11ac
PHY technology	DSSS	DSSS/ CCK	OFDM	OFDM DSSS/ CCK	SDM/OFDM	SDM/OFDM MU-MIMO
Data rates (Mbps)	1, 2	5.5, 11	6–54	1–54	6.5–600	6.5–6933.3
Frequency band (GHz)	2.4	2.4	5	2.4	2.4 and 5	5
Channel spacing (MHz)	25	25	20	25 MHz	20 and 40	20, 40, 80, and 160

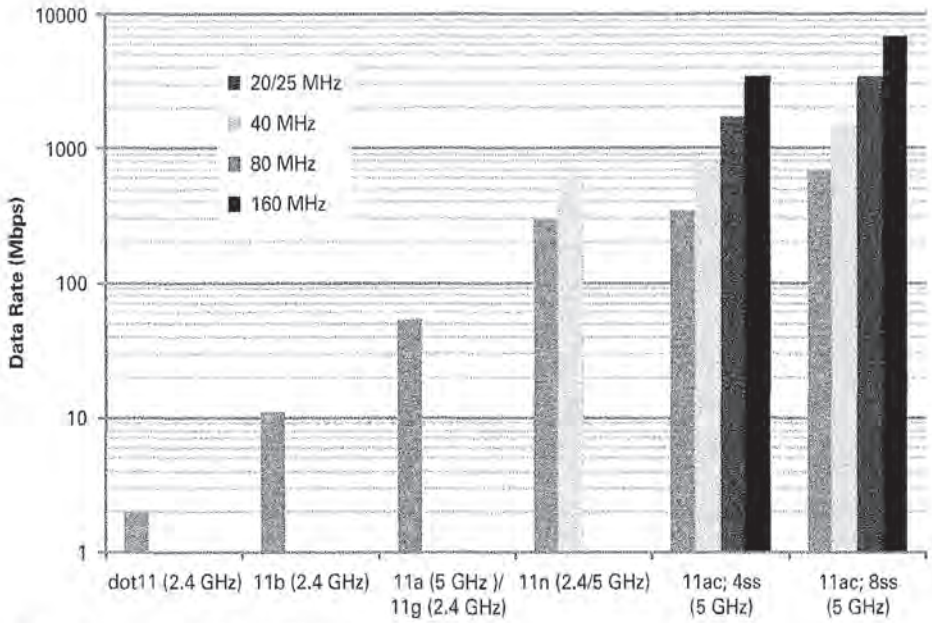

Figure 1.2 Increase in 802.11 PHY data rate.

1.1.3 The 802.11 network architecture

The basic service set (BSS) is the basic building block of an 802.11 LAN. Stations that remain within a certain coverage area and form some sort of association form a BSS. The most basic form of association is where stations communicate directly with one another in an ad-hoc network, referred to as an independent BSS or IBSS. This is illustrated as BSS 1 in Figure 1.3.

More typically, however, stations associate with a central station dedicated to managing the BSS and referred to as an access point (AP). A BSS built around an AP is called an infrastructure BSS and is illustrated by BSS 2 and BSS 3 in Figure 1.3. Infrastructure BSSs may be interconnected via their APs through a distribution system (DS).

The BSSs interconnected by a DS form an extended service set (ESS). A key concept of the ESS is that stations within the ESS can address each other directly at the MAC layer. The ESS, being an 802.11 concept, encompasses only the 802.11 devices and does not dictate the nature of the DS. In practice, however, the DS is typically an Ethernet (802.3) LAN and the AP functions as an Ethernet bridge. As such, stations in a BSS can also directly address stations on the LAN at the MAC layer.

1.1.4 Wi-Fi Direct

Recognizing the need for improved peer-to-peer operation, the Wi-Fi Alliance has developed a specification for direct communication between Wi-Fi devices without being associated with an infrastructure BSS. Such communication is possible using an

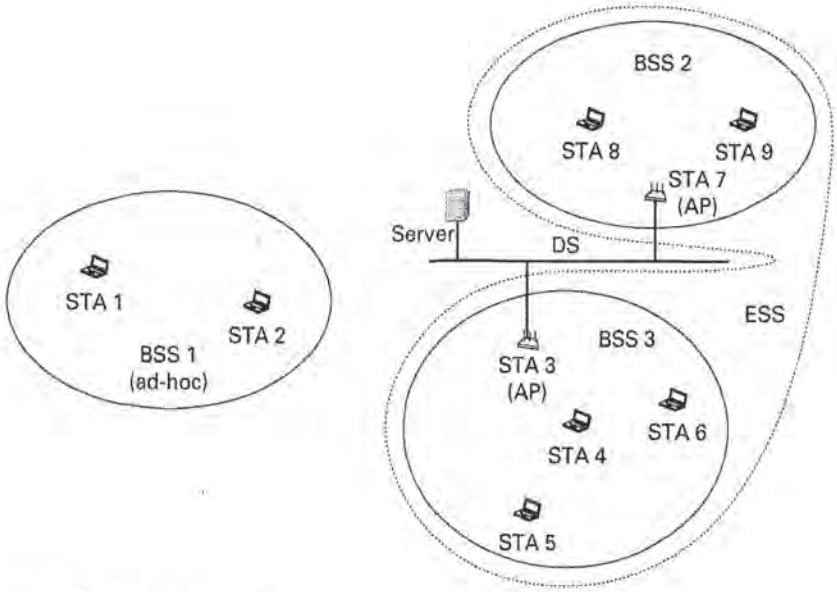

Figure 1.3 BSS, DS, and ESS concepts.

independent BSS, as defined in the 802.11 specification; however, it was preferable to create a mode of operation closer to that of the infrastructure BSS.

In a Wi-Fi Direct network, one device, called the group owner (GO), assumes a role similar to that of an AP while the other devices associate with that device as they would an AP. The Wi-Fi Direct network is thus similar to an infrastructure BSS except that (1) the GO does not provide access to a distribution system, and (2) like its peers, the GO could be a mobile, battery powered device, and thus also need to enter a low power sleep state when idle.

The Wi-Fi Direct standard builds on the 802.11 specification, specifying protocols by which devices can discover each other, how a device assumes the role of group owner and the protocol for absence from the session channel (for power management or to visit an infrastructure BSS channel).

1.2 History of high throughput and 802.11n

1.2.1 The High Throughput Study Group

Interest in a high data rate extension to 802.11a began with a presentation to the Wireless Next Generation Standing Committee (WNG SC) of IEEE 802.11 in January 2002. Market drivers were outlined, such as increasing data rates of wired Ethernet, more data rate intensive applications, non-standard 100+ Mbps products entering the market, and the need for higher capacity WLAN networks (Jones, 2002). The presentation mentioned techniques such as spatial multiplexing and doubling the bandwidth as potential approaches to study for increasing data rate.

After many additional presentations, the High Throughput Study Group (HTSG) was formed with its first meeting in September 2002. The primary objective of HTSG was to complete two documents necessary for the creation of the High Throughput Task Group (TGn). These are the project authorization request (PAR) form and five criteria form. The PAR defined the scope and purpose of the task group as follows:

The scope of this project is to define an amendment that shall define standardized modifications to both the 802.11 physical layers (PHY) and the 802.11 medium access control layer (MAC) so that modes of operation can be enabled that are capable of much higher throughputs, with a maximum throughput of at least 100 Mbps, as measured at the MAC data service access point (SAP). IEEE (2006)

By this statement, the standard amendment developed by TGn must contain modes of operation that are capable of achieving at least 100 Mbps *throughput*. Throughput is the measure of "useful" information delivered by the system and by using throughput as the metric, both MAC and PHY overhead must be considered. 802.11a/g systems typically achieve a maximum throughput of around 25 Mbps; thus this statement required at least a four-fold increase in throughput. Meeting this requirement would in essence mandate PHY data rates well in excess of 100 Mbps as well as significant enhancements to MAC efficiency.

Additional explanatory notes were included with the PAR outlining many evaluation metrics. These include throughput at the MAC SAP, range, aggregate network capacity, power consumption, spectral flexibility, cost complexity flexibility, backward compatibility, and coexistence (IEEE, 2006).

The five criteria form requires that the study group demonstrate the necessity of creating an amendment to the standard. The criteria include (1) broad market potential, (2) compatibility with existing IEEE 802.1 architecture, (3) distinct identity from other IEEE 802 standards, (4) technical feasibility, and (5) economic feasibility (Rosdahl, 2003). The goal is to create a standard amendment which results in marketable products, but that will also be differentiated from other potentially similar products.

In addition to completing the PAR and five criteria forms, HTSG also began development of new multipath fading MIMO channel models (Erceg *et al.*, 2004) and usage models (Stephens *et al.*, 2004). The channel models and usage models were used to create a common framework for simulations by different participants in the standard development process.

1.2.2 Formation of the High Throughput Task Group (TGn)

The PAR was accepted and approved by the 802 working group, creating Task Group n (TGn) with the first meeting of the task group held in September 2003. The standard amendment developed by the task group would be proposal driven, meaning that members of the task group would make partial or complete technical proposals, with the complete proposals proceeding through a down-selection process culminating in a single proposal upon which the standard amendment would be based. Partial proposals would be informative and could be incorporated in a complete proposal along the way. To

that end, the task group began development of the functional requirements (Stephens, 2005) and comparison criteria (Stephens, 2004) documents. These two documents would provide, respectively, the technical requirements complete proposals must meet and criteria by which complete proposals would be compared.

The task group began with nine functional requirements. One of the functional requirements was a catch-all, requiring that proposals meet the PAR and five criteria. A second requirement was a reiteration of the PAR requirement to achieve 100 Mbps throughput at the top of the MAC.

Furthermore, since it was expected that not all regulatory domains would allow a single device to use multiple 20 MHz channels (an easy way to achieve the throughput objective), the second requirement added a restriction that 100 Mbps throughput be achieved in a single 20 MHz channel. To enforce efficient use of spectrum, another requirement was added for a mode of operation with a spectral efficiency of at least 3 bps/Hz.

Four functional requirements addressed operational bands and backward compatibility. One of these requirements was that the protocol should support operation in the 5 GHz band due to the large availability of spectrum there. Another requirement was that at least some modes of operation be backward compatible with 802.11a systems. Noteworthy was the fact that there was no requirement to support operation in the 2.4 GHz band. However, if a proposal did support 2.4 GHz band operation, it was required that there be modes of operation that were backward compatible with 802.11g systems. In this context, some flexibility was given, allowing an 802.11n AP to be configured to accept or reject associations from legacy stations.

The 802.11e amendment to the standard, nearing completion at the time, added many features for improving the quality of service (QoS) in 802.11 systems. Many of the perceived applications for 802.11n involved real time voice and video which necessitate QoS. Therefore a functional requirement was included which mandated that a proposal allow for the implementation of 802.11e features within an 802.11n station.

The comparison criteria in Stephens (2004) outlined metrics and required disclosure of results which would allow for comparison between proposals under the same simulation setup and assumptions. The comparison criteria incorporated the simulation scenarios and usage models defined in Stephens *et al.* (2004). During the development of the comparison criteria, the task group realized that members of the task group did not always share the same definitions for common terms. Therefore definitions for goodput, backward compatibility, and signal-to-noise ratio (SNR) were provided. The comparison criteria covered four main categories: marketability, backward compatibility and coexistence with legacy devices, MAC related criteria, and PHY related criteria.

Under marketability, the proposal must provide goodput results for residential, enterprise, and hotspot simulation scenarios. Goodput is defined by totaling the number of bits in the MAC service data units (MSDU) indicated at the MAC service access point (SAP), and dividing by the simulation duration (Stephens, 2004). Two optional criteria included describing the PHY and MAC complexity. The PHY complexity was to be given relative to 802.11a.

To ensure backward compatibility and coexistence with legacy devices, a proposal was required to provide a summary of the means used to achieve backward compatibility with 802.11a and, if operating in 2.4 GHz, 802.11g. Simulation results demonstrating interoperability were also required. The goodput of a legacy device in an 802.11n network and the impact of a legacy device on the goodput of 802.11n devices were also to be reported.

The MAC related criteria included performance measurements and changes that were made to the MAC. In the residential, enterprise, and hotspot simulation scenarios a number of different metrics were to be captured and reported. These included the ability to support the service requirements of various applications, including QoS requirements. Measurements of aggregate goodput of the entire simulation scenario were required to indicate network capacity. MAC efficiency was to be provided, which is defined as the aggregate goodput divided by the average PHY data rate. To ensure reasonable range for the new modes of operation, throughput versus range curves were also to be provided.

The PHY related criteria included PHY rates and preambles, channelization, spectral efficiency, PHY performance, and PHY changes. In addition, the comparison criteria also defined PHY impairments to be used in combination with channel models for PHY simulations. Each proposal was required to generate simulation results for both additive white Gaussian noise (AWGN) and non-AWGN channels. Furthermore, simulation conditions to analyze the impact on packet error rate (PER) of carrier frequency offset and symbol clock offset were also defined.

1.2.3 Call for proposals

The TGn call for proposals was issued on May 17, 2004, with the first proposals presented in September 2004. Over the course of the process two main proposal teams emerged, TGn Sync and WWiSE (world wide spectral efficiency). The TGn Sync proposal team was founded by Intel, Cisco, Agere, and Sony with the objective of covering the broad range of markets these companies were involved in, including the personal computer (PC), enterprise, and consumer electronics markets. The WWiSE proposal team was formed by Airgo Networks, Broadcom, Conexant, and Texas Instruments. These semiconductor companies were interested in a simple upgrade to 802.11a for fast time to market. Many other companies were involved in the proposal process and most ended up joining one of these two proposal teams.

The key features of all the proposals were similar, including spatial division multiplexing and 40 MHz channels for increased data rate, and frame aggregation for improved MAC efficiency. The proposals differed in scope (TGn Sync proposed numerous minor improvements to the MAC while WWiSE proposed limiting changes) and support for advanced features such as transmit beamforming (initially absent from the WWiSE proposal).

A series of proposal down-selection and confirmation votes took place between September 2004 and May 2005. During that time, mergers between proposals and enhancements to proposals took place. The TGn Sync proposal won the final down-selection vote between it and WWiSE, but failed the confirmation vote in May 2005.

1.2.4 Handheld devices

During this period interest arose in a new emerging market of converged Wi-Fi and mobile handsets. The shipment of dual mode Wi-Fi/cellular handsets had grown significantly from 2005 to 2006. Some participants in the proposal process believed that handsets would be the dominant Wi-Fi platform within a few years (de Courville *et al.*, 2005). At the time, converged mobile devices were projected to grow worldwide at a compound annual growth rate of 30% (IDC, 2007).

A contentious issue for handheld proponents was the high throughput requirement for 100 Mbps throughput. This, in essence, would force all 802.11n devices to have multiple antennas. This is a difficult requirement for converged mobile devices, since they already contain radios and antennas for cellular 2G, 3G, Bluetooth, and in some cases GPS. Concern was raised that mandating 802.11n devices to have multiple antennas would force handset manufacturers to continue to incorporate single antenna 802.11a/g into handsets and not upgrade to 802.11n. Not only does this diminish the capabilities of the handset device, it burdens all future 802.11n deployments with continued coexistence with 802.11a/g embedded in these new handset devices.

For this reason an ad-hoc group was formed to create functional requirements supporting single antenna devices. Two new requirements were added to the functional requirements document in July 2005. The first requirement mandated that a proposal define single antenna modes of operation supporting at least 50 Mbps throughput in a 20 MHz channel. The second requirement dictated that an 802.11n AP or station interoperate with client devices that comply with 802.11n requirements but incorporate only a single antenna. This requirement resulted in 802.11n making mandatory at least two antennas in an AP, but only one antenna in a non-AP device.

1.2.5 Merging of proposals

After the failed confirmation vote, a joint proposal effort was started within the task group to merge the two competing proposals. Due to entrenched positions and the large membership of the group, the joint proposal effort proceeded very slowly. As a result, Intel and Broadcom formed the Enhanced Wireless Consortium (EWC) in October 2005 to produce a specification outside the IEEE that would bring products to market faster. With much of the task group membership ultimately joining the EWC, this effort had the effect of breaking the deadlock within the IEEE, and the EWC specification, which was essentially a merger of the TGn Sync and WWiSE proposals, was adopted as the joint proposal and submitted for confirmation to TGn where it was unanimously passed in January 2006.

1.2.6 802.11n amendment drafts

The joint proposal was converted to a draft 802.11 standard amendment for higher throughput (TGn Draft 1.0), and entered letter ballot. In letter ballot, IEEE 802.11

working group members (not just task group members) vote to either adopt the draft as is or reject it with comments detailing changes needed. The draft requires at least a 75% affirmative vote within the IEEE 802.11 working group in order to proceed to sponsor ballot where it is considered for adoption by the broader IEEE standards association. TGn Draft 1.0 entered letter ballot in March 2006 and, not unusually, failed to achieve the 75% threshold for adoption. Comment resolution began May 2006 on the roughly 6000 unique technical and editorial comments submitted along with the votes.

With resolution of the TGn Draft 1.0 comments, TGn Draft 2.0 went out for letter ballot vote in February 2007 and this time passed with 83% of the votes. However, there were still 3000 unique technical and editorial comments accompanying the letter ballot votes. It is typical for the task group to continue comment resolution until a minimum number of negative votes are received; thus comment resolution for TGn Draft 2.0 continued between March 2007 and September 2007, resulting in TGn Draft 3.0. Since TGn Draft 2.0 passed, TGn Draft 3.0 through TGn Draft 7.0 only required a recirculation ballot in which comments may only address clauses that changed between the drafts. Sponsor ballot began in January 2009 with completion of the 802.11n standard amendment based on Draft 11.0 in September 2009. The submissions contributed by the task group participants in the development of the standard are publicly available on the World Wide Web.[2] The final 802.11n standard amendment was published in 2009 and then incorporated into the 2012 revision of the IEEE 802.11 standard, both of which are available for purchase from the IEEE.[3]

Of great value to someone investigating the 802.11n PHY is the transmit waveform generator developed by Metalink. The description of the generator, developed in MATLAB®, is given in Anholt and Livshitz (2006). The actual source code is publicly available and is included in Anholt and Livshitz (2007). Most, if not all, transmit waveform features are supported by the generator.

1.3 Environments and applications for 802.11n

In the development of 802.11n, three primary environments were considered for studying system performance and capabilities: residential, enterprise, and hotspot. Within each of these environments a different mix of existing and new applications was envisioned. Use cases were defined (Stephens *et al.*, 2004) that describe how an end user uses an application in a specific WLAN environment. Examples include watching television remotely from the cable or set-top box within the home, or talking on the telephone remotely from one's desk at work. Additionally, usage models were developed for each environment which combined multiple use cases and applications.

Finally, a simulation scenario was created for each usage model and environment. These simulation scenarios were used to stress MAC capability when comparing proposals. Each simulation scenario includes a channel model associated with the particular environment. In addition, the location of the AP and stations were defined, giving a

[2] http://grouper.ieee.org/groups/802/11/ [3] http://standards.ieee.org/getieee802/

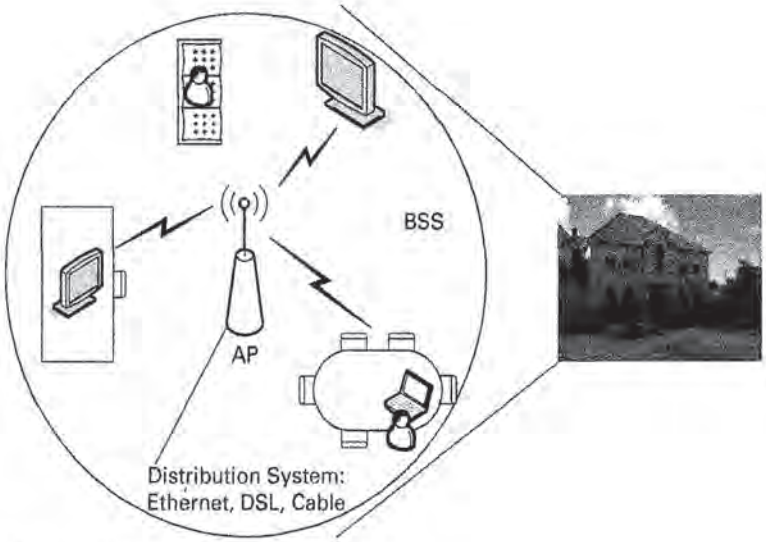

Figure 1.4 Residential usage model.

spatial component to the usage model in terms of the distance between the AP and the stations. For each application, system parameters were defined such as packet size, maximum packet loss rate tolerated by the application, maximum delay, network-layer protocol running (e.g. UDP or TCP), and offered load.

The residential usage model consists of a single BSS, as illustrated in Figure 1.4. This model typically includes only one AP and many client stations. In a typical AP-station configuration, applications include Internet access and streaming audio and video. Furthermore, user experience with applications like intra-networking for local file transfer, backups, and printing is enhanced with higher data rates. New applications such as voice over IP (VoIP) and video phones were also incorporated into the residential usage model.

The high throughput task group envisioned an AP that could also take the form of a wireless home media gateway. Such a device would distribute audio and video content throughout the home, such as DVD and standard and high definition TV. Other residential applications benefiting from higher wireless data rates include content download from a video camera or photo camera. Interactive gaming has recently begun to incorporate wireless technology. Gamers benefit from the freedom of not being tethered by wires when the connections between the controller and the console, the console and the display, and the console to internet access are made wireless.

The usage model for an enterprise environment emphasizes network connectivity supported by multiple BSSs to cover larger buildings and floor plans, as illustrated in Figure 1.5. The BSSs are interconnected via the distribution system, typically Ethernet, creating an extended service set (ESS). As in a cellular deployment, each additional AP increases the total network coverage and capacity.

Networking applications such as file transfer and disk backup will benefit greatly from the higher data rates of 802.11n. Higher data rates will increase network capacity providing support for a larger number of clients. Higher throughputs will also enable new applications such as remote display via a wireless connection between a laptop and

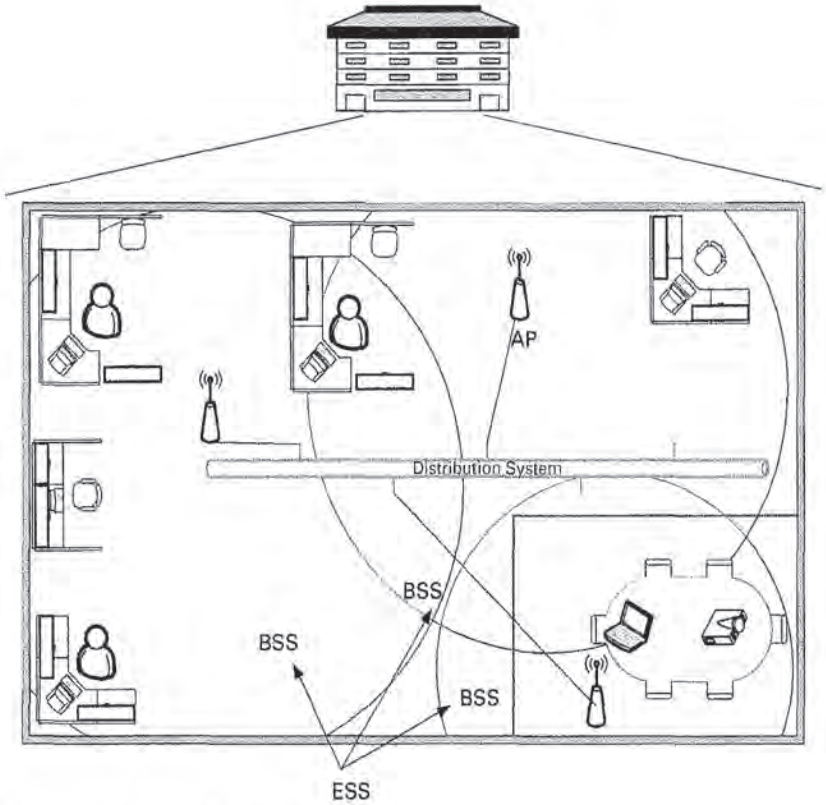

Figure 1.5 Enterprise usage model.

projector, simplifying presentations in conference rooms. Additionally, wireless video conferencing and VoIP may be supported (Stephens *et al.*, 2004).

The hotspot model envisions locations such as an airport lounge (illustrated in Figure 1.6), coffee shop, library, hotel, or convention center. Some municipalities have also blanketed downtown areas with Wi-Fi coverage. A hotspot could be located either indoors or outdoors and could cover a large open area. Therefore the propagation model could be substantially different from either residential or enterprise. In a hotspot, most traffic goes through the Internet and a session is typically limited to less than two hours (Stephens *et al.*, 2004). Applications include web browsing, Internet file transfer, and email. Also, new hotspot applications are envisioned such as the ability to watch a TV program or movie on a laptop or other display. This would involve the streaming of audio and video content over the Internet or the redistribution of standard or high definition TV signals.

1.4 Major features of 802.11n

PHY data rates in 802.11n are significantly improved over 802.11a and 802.11g primarily through the use of spatial multiplexing using MIMO and 40 MHz operation. To take

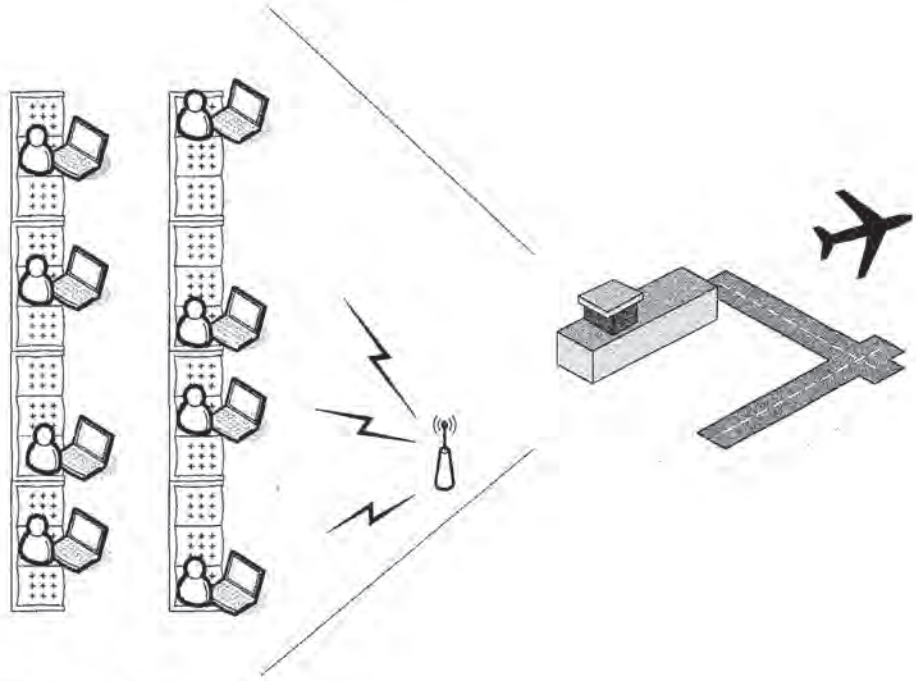

Figure 1.6 Hotspot usage model.

advantage of the much higher data rates provided by these techniques, MAC efficiency is also improved through the use of frame aggregation and enhancements to the block acknowledgement protocol. These features together provide the bulk of the throughput enhancement over that achievable with 802.11a and 802.11g.

Robustness is improved inherently through the increased spatial diversity provided by the use of multiple antennas. Space-time block coding (STBC) as an option in the PHY further improves robustness, as does fast link adaptation, a mechanism for rapidly tracking changing channel conditions. More robust channel codes are adopted in the form of low density parity check (LDPC) codes. The standard amendment also introduces transmit beamforming, with both PHY and MAC enhancements to further improve robustness.

A number of other enhancements provide further gains. In the PHY, these include a shorter guard interval, which may be used under certain channel conditions. The PHY also includes a Greenfield preamble, which is shorter than the mandatory mixed format preamble. However, unlike the mixed format, it is not backward compatible with existing 802.11a and 802.11g devices without MAC protection. In the MAC, the reverse direction protocol provides a performance improvement for certain traffic patterns, by allowing a station to sublease the otherwise unused portion of its allocated transmit opportunity to its remote peer and thus reducing overall channel access overhead. A reduced interframe space (RIFS) used when transmitting a burst of frames reduces overhead in comparison to the existing short interframe space (SIFS).

An overview of the mandatory and optional features of the 802.11n PHY is given in Figure 1.7. The first generation of products typically operate in the 2.4 GHz band only,

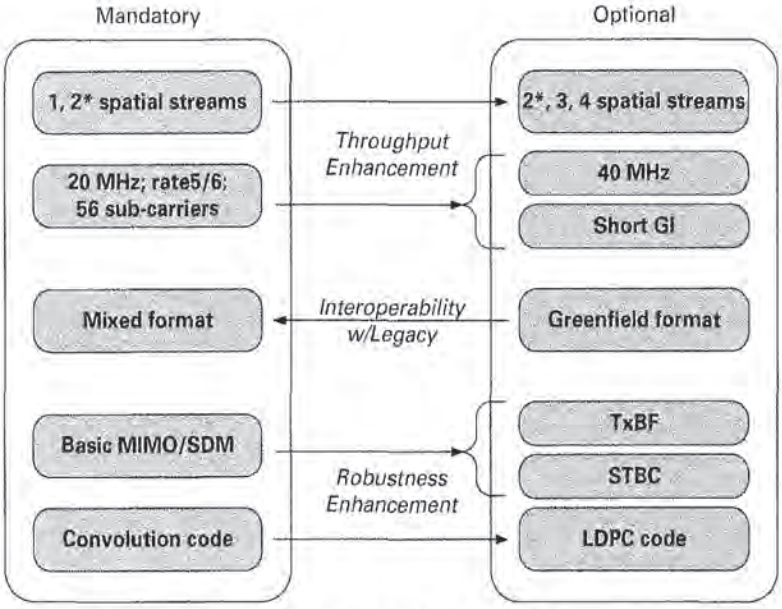

Figure 1.7 Mandatory and optional 802.11n PHY features. (* 2 spatial streams mandatory for AP only.)

with up to two spatial streams and 40 MHz channel width. In this book the term spatial streams is used to refer to one or more independent data streams transmitted from the antennas. A device requires at least as many antennas as spatial streams. When using the short guard interval, these initial products are able to achieve a PHY data rate of 300 Mbps. With second generation products, we begin to see dual-band 2.4 GHz and 5 GHz products. These products also achieve 300 Mbps, but several incorporate an extra receive antenna chain for additional receive diversity. Some products also support the Greenfield preamble format. Third generation devices added another transmit antenna chain to support three spatial streams and 450 Mbps. For robustness, devices began employing STBC. Due to the number of sub-options with TxBF, it was difficult to select a common set of sub-options to certify. This greatly limited the deployment of TxBF in third generation devices.

An overview of the features added to the MAC in 802.11n and 802.11ac is given in Figure 1.8. In addition to the throughput and robustness enhancing features already mentioned, the MAC is extended in a number of other areas.

The numerous optional features in 802.11n and 802.11ac mean that extensive signaling of device capability is required to ensure coexistence and interoperability. For example, whether a device supports certain PHY features such as the Greenfield format preamble or MAC features such as the ability to participate in a reverse direction protocol exchange.

The existence of wide channel operation (40 MHz or greater) also creates a number of coexistence issues. The AP needs to manage the wide channel BSS so that different channel width devices, both legacy and (very) high throughput, are able to associate with the BSS and operate. Because wide channel operation uses two or more 20 MHz channels, mechanisms are needed to mitigate the effect this might have on neighboring

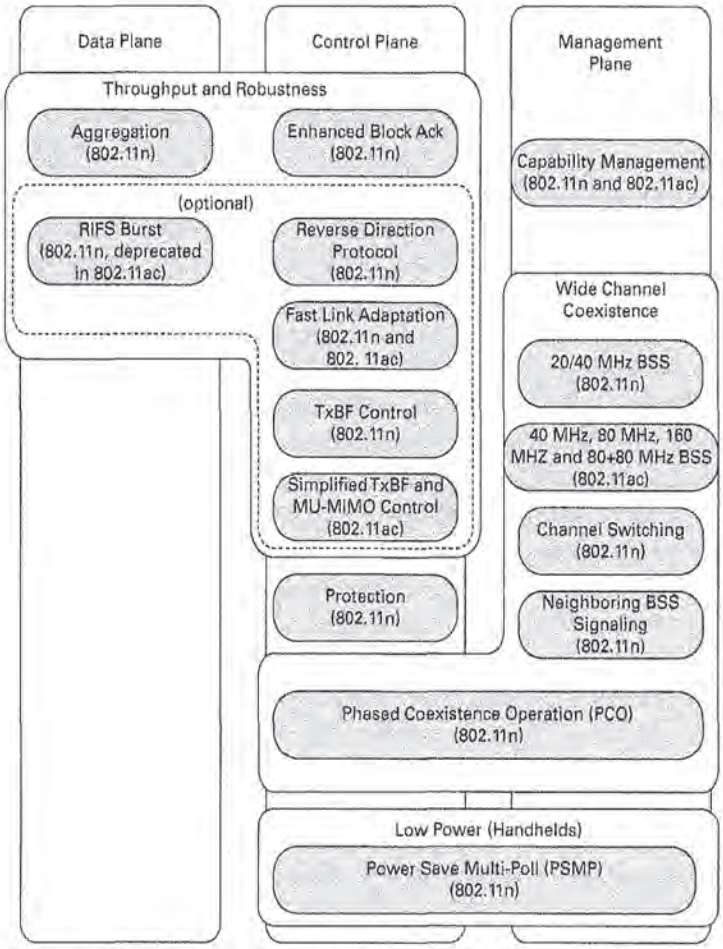

Figure 1.8 Summary of 802.11n and 802.11ac MAC enhancements.

20 MHz BSSs operating independently on any of these channels. Coexistence is primarily achieved through careful channel selection, i.e. choosing a pair of channels that have little or no active neighborhood traffic. To this end, the 802.11n and 802.11ac amendments add scanning requirements to detect the presence of active neighborhood BSSs as well as the ability to actively move the BSS to another pair of channels should a neighboring 20 MHz BSS become active.

In recognition of the growing importance of handheld devices, 802.11n added a channel access scheduling technique called power-save multi-poll (PSMP) to efficiently support a large number of stations.

1.5 History of Very High Throughput and 802.11ac

As the 802.11n standard amendment development matured and associated products became popular in the market, 802.11 initiated a new study group in May 2007 to

investigate Very High Throughput (VHT) technologies. Initially the study group was started to address IMT-advanced operation, in the hopes of such new spectrum in bands <6 GHz being allocated to unlicensed usage. However, this initial objective was dropped and the focus of the study group shifted to enhancing 802.11n in the 5 GHz band.

The Wi-Fi Alliance was solicited to provide usage models to help develop requirements (Myles and de Vegt, 2008). The general categories of the usage models included wireless display, distribution of high definition TV, rapid upload/download, backhaul, outdoor campus, auditorium, and manufacturing floor. Specific usages that will be most prevalent in the market place include compressed video streaming around a house, rapid sync-and-go, and wireless I/O. With streaming around the home, it is envisioned that TVs and DVRs around the home will have wireless capability and that 100+ Mbps aggregate of videos from a DVR can be displayed wirelessly on TVs in different rooms. This is similar to the 802.11n residential usage model illustrated in Figure 1.4, with emphasis on high resolution video with minimal interference in the 5 GHz band as opposed to the 2.4 GHz band. With rapid sync-and-go, users can quickly sync movies or pictures between mobile devices such as a phone, a laptop, or a tablet. With a 1 Gbps radio link, a 1 GB video file will take much less than a minute to transfer between devices. Data rates exceeding 1 Gbps will provide the capability for a wireless desktop, with wireless connections between a computer and peripherals such as monitors, printers, and storage devices.

With this input, the Very High Throughput study group developed two Project Authorization Requests (PARs), one for the 5 GHz band (802.11ac) and one for the 60 GHz band (802.11ad). The scope for 802.11ac includes: (1) single link throughput supporting at least 500 Mbps, (2) multi-station throughput of at least 1 Gbps, (3) exclusion of 2.4 GHz band, and (4) backward compatibility and coexistence with legacy 802.11 devices in the 5 GHz band. The PAR was approved in September 2008 and the 802.11ac task group began in November 2008.

The task group initially developed a specification framework document (Stacey *et al.*, 2011), a functional requirements and evaluation methodology document (Loc and Cheong, 2011), an amendment to 802.11n channel model document (Breit *et al.*, 2010), and a usage model document (De Vegt, 2009). This process was purposely different than the proposal down-selection process of 802.11n. After the challenging experience in 802.11n, the group opted for the less contentious approach of developing a specification as a group based on a specification framework. Through its various revisions, the specification framework document built a list of features that would be included in the draft specification, with detail added to the features as the document evolved.

An initial Draft 0.1 was developed based on the specification framework and approved by the task group in January 2011. This draft went through an internal task group comment and review cycle, resulting in a Draft 1.0 released to the 802.11 working group for letter ballot in May 2011. The task group addressed the comments on Draft 1.0 coming out of the letter ballot to produce Draft 2.0 which was released in January 2012. Comment resolution on Draft 2.0 completed in May 2012, resulting in Draft 3.0. Comment resolution on Draft 3.0 completed in September 2012, resulting in Draft 4.0.

At the time this book went to press, the standard amendment was in recirculation letter ballot on Draft 3.0 and would continue there until a minimum number of negative votes and comments were received. It will then proceed to sponsor ballot. Whereas letter ballot includes only voting members in IEEE 802.11, the sponsor ballot pool may include members from all of the IEEE 802 Standard Association, providing a broader review of the draft.

It is expected that sponsor ballot will begin in March 2013. Final approval of the 802.11ac standard amendment is expected in December 2013.[4] However, as was the case with 802.11n, initial products with basic 802.11ac features based on a draft will be certified and emerge on the market well before final approval.

The submissions contributed by the task group participants in the development of the standard are publicly available on the World Wide Web.[5] The drafts of the standard are only available to voting members of 802.11, but, Draft 3.0 of 802.11ac was released to the public. Draft 3.0 is currently available for purchase from the IEEE.[6] Once approved, the final standard amendment would be available there as well.

A transmit waveform generator was also implemented for 802.11ac, this time by CSR. The description of the generator, developed in MATLAB®, is given in Tong and Popescue (2011). The actual source code is publicly available and is embedded in the document. Most, if not all, 802.11ac transmit waveform features are supported by the generator.

The new PHY enhancements in 802.11ac to increase the data rate include channel bandwidth expansion to 80 and 160 MHz. In addition, a new feature in 802.11ac is the use of non-contiguous channels, whereby two non-adjacent 80 MHz channels may be used to form a 160 MHz transmission, termed 80+80 MHz. This allows more flexible channel assignment with the wider bandwidth to avoid heavily occupied channels or even to avoid radars. Furthermore, the number of spatial streams is increased to eight, double that of 802.11n. Modulation size is increased to 256-QAM for a 33% increase in data rate, when link quality permits. Lastly, 802.11ac expands on MIMO in 802.11n to enable multi-user MIMO (MU-MIMO). By allowing simultaneous transmissions to multiple devices, network capacity improves.

The techniques introduced in 802.11n to improve robustness, TxBF, STBC, and LDPC code are also employed in 802.11ac. However, modifications have been made to each of the techniques to simplify operation and reduce the number of sub-options, which should result in increased adoption of these features in the market.

As opposed to 802.11n, 802.11ac has only one preamble. Like the 802.11n mixed format preamble, the VHT preamble contains a legacy compatible portion of the preamble for compatibility with 802.11a/n devices. In addition, the VHT preamble supports both single user and multi-user operation.

An overview of the mandatory and optional features of the 802.11ac PHY is given in Figure 1.9. It is expected that the first generation 802.11ac devices will have one, two,

[4] The reader is referred to http://grouper.ieee.org/groups/802/11/Reports/802.11_Timelines.htm for the latest update on the timeline of 802.11n.

[5] http://grouper.ieee.org/groups/802/11/ [6] http://standards.ieee.org/getieee802/

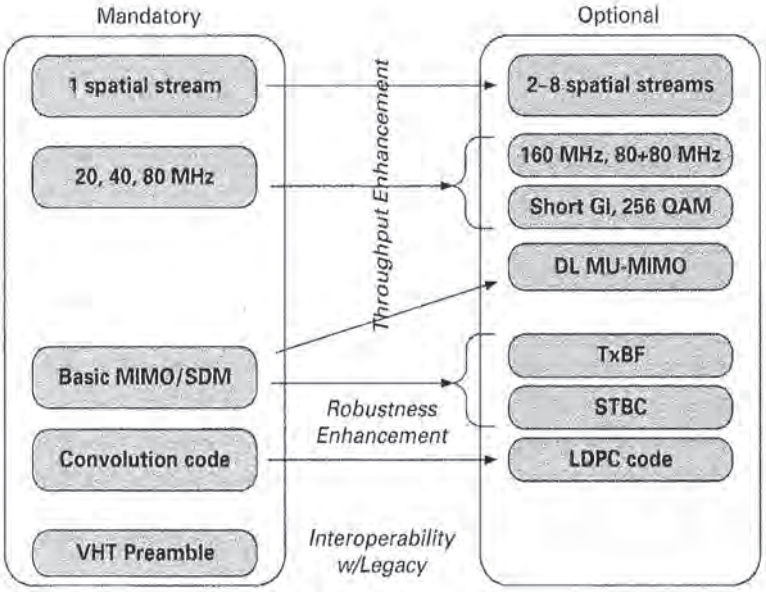

Figure 1.9 Mandatory and optional 802.11ac PHY features.

or three spatial streams, as with current 802.11n devices. The major enhancement in data rate enhancement in these devices will be 80 MHz. It is also expected that most devices will include 256-QAM. With the simplification of TxBF in 802.11ac, this feature may be included in first generation 802.11ac devices. Some of these devices may also employ STBC and LDPC. Features like more than three spatial streams, 160 MHz, and MU-MIMO will only see prominence in future generation devices.

With 802.11ac, the MAC includes enhancements in aggregation, and improved wide channel operation in the presence of hidden nodes through a dynamic and static RTC/CTS bandwidth signaling mechanism. An enhanced power save operation with the presence of a station identifier in the PHY header is included, as well as a mechanism for signaling a station's operating mode (channel bandwidth and number of active receive chains).

A new sounding protocol is introduced to support TxBF and MU-MIMO. Significantly, there are a minimal number of implementation options with this protocol, which should promote industry adoption.

Since the wider channel width could occupy a significant potion of the available spectrum in the 5 GHz band, there are new scanning rules for detecting overlapping BSS operation with requirements and recommendation for channel selection when establishing a VHT BSS.

1.6 Outline of chapters

The book is divided into three parts. The first part, Chapters 2–6, covers the PHY and provides a comprehensive review of all mandatory and optional PHY features in

802.11n. Chapter 7 covers the 802.11ac PHY features. The second part, Chapters 8–12, covers the MAC, an overview of existing MAC features, and a detailed review of the new features introduced in 802.11n and 802.11ac. The last part, Chapters 13–15, covers transmit beamforming, MU-MIMO, and fast link adaptation.

Chapter 2 gives a brief overview of orthogonal frequency division multiplexing (OFDM). Chapter 3 begins with a description of multiple-input multiple-output (MIMO) basics and spatial division multiplexing (SDM). This is followed by a discussion of the MIMO environment and the 802.11n MIMO multipath fading channel and propagation models. The chapter concludes with an explanation of linear receiver design and highlights of maximum likelihood estimation. Included in the discussion of MIMO and receiver design are capacity based performance curves.

Chapter 4 details the design of the mixed format (MF) preamble used for interoperability with legacy 802.11a/g OFDM devices. The chapter begins with a review of 802.11a preamble design. Included in the review are illustrations of the waveform. A description of the 802.11a/g packet encoding process and receive procedure is presented, which includes a receiver block diagram. This leads into a discussion of the legacy part of the MF preamble. Next, the high throughput (HT) portion of the preamble is described. Following this, the encoding of the Data field is presented. The chapter ends with a discussion of the receive procedure and a block diagram for basic modes of operation. Tables of parameters of the modulation and coding scheme (MCS) for basic modes of operation are given in an appendix.

Chapter 5 outlines all the PHY techniques employed in the 802.11n specification to increase the data rate. The first section of the chapter details the new 40 MHz channel and waveform. This includes a plot illustrating throughput as a function of range. This is followed by a brief discussion of the extra subcarriers which were added to the 802.11n 20 MHz waveform. The next part of the chapter gives the MCS definitions. This includes several waterfall curves illustrating the packet error rate (PER) versus SNR performance in additive white Gaussian noise (AWGN) and in the 802.11n MIMO multipath fading channel models. A description of the shorter Greenfield (GF) preamble is also provided in this chapter. This also includes discussion on the debate of how much the GF preamble actually improves performance. The last topic covered in this chapter is on the short guard interval (GI).

Chapter 6 covers the subject of improving the robustness of the system. Four techniques are described. The first method is receive diversity, where PER versus SNR waterfall curves are provided along with throughput curves to demonstrate the gain achieved from receive diversity in a MIMO system. The next technique is a straightforward one involving spatial expansion (SE), which provides a small amount of transmit diversity gain. Waterfall curves are provided for SE as well. This is followed by a detailed description of space-time block coding (STBC). Transmit antenna configurations are presented, along with an approach for implementing a receiver and equalizer. Again performance curves are presented that illustrate which system configurations benefit the most from STBC. In the last part of the chapter, low density parity check (LDPC) codes are discussed. The specific characteristics of the LDPC encoding process in the 802.11n standard amendment are detailed. Waterfall curves for LDPC are provided to compare performance with the mandatory binary convolutional code.

The new VHT PHY is described in Chapter 7. The new channelization for 802.11ac is illustrated. This chapter focuses on the SU aspects of the new VHT format preamble and data field.

The MAC section begins in Chapter 8 with a functional description of the 802.11 MAC as background for the remaining chapters. This chapter covers the basic contention-based access protocol including the 802.11e quality of service (QoS) extensions, channel access timing, the concept of a transmit opportunity, and the basic acknowledgement and block acknowledgement protocols.

Chapter 9 describes why changes are necessary in the MAC to improve throughput and then details the two key throughput enhancing features: aggregation and enhancements to the block acknowledgement protocol.

Beyond the basic contention-based access protocol, the 802.11 MAC includes additional channel access mechanisms. Chapter 10 provides an overview of these mechanisms, including the point coordination function (PCF) from the original 802.11 specification and the hybrid coordinated channel access (HCCA) function from the 802.11e amendment. The chapter then provides details on the power-save multi-poll (PSMP) channel access technique and the reverse direction protocol, both of which are new in 802.11n.

Coexistence and interoperability is a critical issue with 802.11n and 802.11ac and Chapter 11 provides details on this broad topic. The chapter covers capability signaling and BSS control. The chapter then covers wider channel operation, managing HT and VHT BSS operation, and maintaining interoperability with narrower bandwidth devices. The critical topic of coexistence between neighboring BSSs occupying each other's secondary channel is also discussed. Finally, the chapter covers protection mechanisms.

To round out the MAC section, Chapter 12 provides details on MAC frame formats. This chapter is intended as a reference for the discussions in the other chapters.

The final part of the book deals with the complex topics of transmit beamforming, MU-MIMO, and fast link adaptation. Chapter 13 provides details on both the PHY and MAC aspects of single user transmit beamforming for both 802.11n and 802.11ac. Chapter 14 covers both PHY and MAC aspects of MU-MIMO. Lastly, Chapter 15 describes fast link adaptation for both 802.11n and 802.11ac.

References

ABIresearch (2007). *Wi-Fi IC Market Analysis and Forecasts*. 2008-12-31.

ABIresearch (2012). *Wireless Connectivity Market Data*. 2012-03-14.

Anholt, M. and Livshitz, M. (2006). *Waveform Generator*, IEEE 802.11-06/1714r1.

Anholt, M. and Livshitz, M. (2007). *Waveform Generator Source Code*, IEEE 802.11-07/0106r0.

Breit, G., Sampath, H., Vermani, S., *et al.* (2010). *TGac Channel Model Addendum*, IEEE 802.11-09/0308r12.

de Courville, M., Muck, M., van Waes, N., *et al.* (2005). *Handset Requirements for TGn*, IEEE 802.11-05/0433r0.

De Vegt, R., (2009). *802.11ac Usage Models Document*, IEEE 802.11-09/0161r2.

Erceg, V., Schumacher, L., Kyritsi, P., *et al.* (2004). *TGn Channel Models*, IEEE 802.11-03/940r4.

Foschini, G. J. (1996). Layered space-time architecture for wireless communication in a fading environment when using multi-element antennas. *Bell Labs Technical Journal*, Autumn, 41–59.

IDC (2007). *Worldwide Converged Mobile Device 2007–2011 Forecast and Analysis, IDC #206585*. 2007-05-01.

IEEE (2006) *IEEE 802.11n Project Authorization Request, 26 May 2006* available at: http://standards.ieee.org/board/nes/projects/802-11n.pdf.

ISO/IEC 7498-1:1994, Information technology – Open Systems Interconnection – Basic Reference Model: The Basic Model.

Jones, V. K., De Vegt, R., and Terry, J. (2002), *Interest for HDR Extension to 802.11a*, IEEE 802.11-02/081r0.

Loc, P. and Cheong, M., (2011). *TGac Functional Requirements and Evaluation Methodology*, IEEE 802.11-09/0451r16.

Myles, A. and de Vegt, R. (2008). *Wi-Fi Alliance (WFA) VHT Study Group Usage Models*, IEEE 802.11-07/2988r4.

Rosdahl, J. (2003). *Criteria for Standards Development*, IEEE 802.11-02/799r6.

Stacey, R., Perahia, E., Stephens, A., *et al.* (2011). *Specification Framework for TGac*, IEEE 802.11-09/0992r21.

Stephens, A. (2004), *IEEE 802.11 TGn Comparison Criteria*, IEEE 802.11-03/814r31.

Stephens, A. (2005). *802.11 TGn Functional Requirements*, IEEE 802.11-03/813r13.

Stephens, A., Bjerke, B., Jechoux, B., *et al.* (2004). *Usage Models*, IEEE 802.11-03/802r23.

Tong, F. and Popescue, A. (2011). *User Guide for 802.11ac Waveform Generator*, IEEE 802.11-11/0517r7.

4 PHY interoperability with 11a/g legacy OFDM devices

One of the functional requirements in the development of the 802.11n standard was that some modes of operation must be backward compatible with 802.11a (and 802.11g if 2.4 GHz was supported) as described in Stephens (2005). Furthermore, the 802.11n standard development group also decided that interoperability should occur at the physical layer. This led to the definition of a mandatory mixed format (MF) preamble in 802.11n. In this chapter, we first review the 802.11a packet structure, transmit procedures, and receive procedures to fully understand the issues in creating a preamble that is interoperable between 802.11a and 802.11n devices. For further details regarding 802.11a beyond this review, refer to clause 18 in IEEE (2012). Following this overview, the mixed format preamble, which is part of 802.11n, is discussed.

4.1 11a packet structure review

The 802.11a packet structure is illustrated in Figure 4.1.

The Short Training field (STF) is used for start-of-packet detection and automatic gain control (AGC) setting. In addition, the STF is also used for initial frequency offset estimation and initial time synchronization. This is followed by the Long Training field (LTF), which is used for channel estimation and for more accurate frequency offset estimation and time synchronization. Following the LTF is the Signal field (SIG), which contains the rate and length information for the packet. Example rates are BPSK, rate ½ encoding and 64-QAM, rate ¾ encoding. Following this is the Data field. The first 16 bits of the Data field contain the Service field. An example of an 802.11a transmit waveform is given in Figure 4.2.

4.1.1 Short Training field

The STF is 8 μs in length. In the time domain, the STF contains ten repetitions of a 0.8 μs symbol. The STF is defined based on the frequency domain sequence given in Eq. (4.1) (IEEE, 2012):

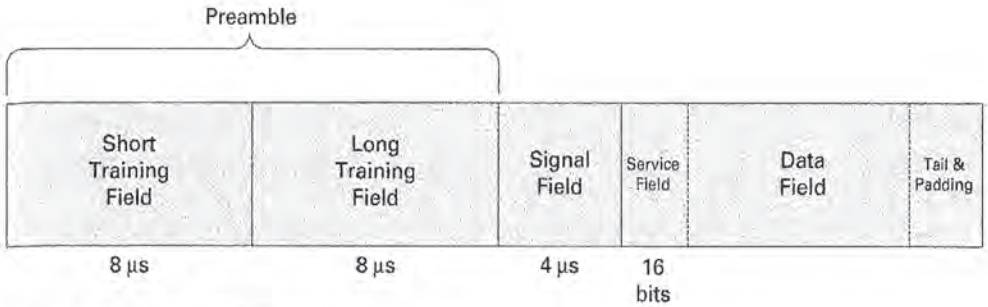

Figure 4.1 802.11a packet structure.

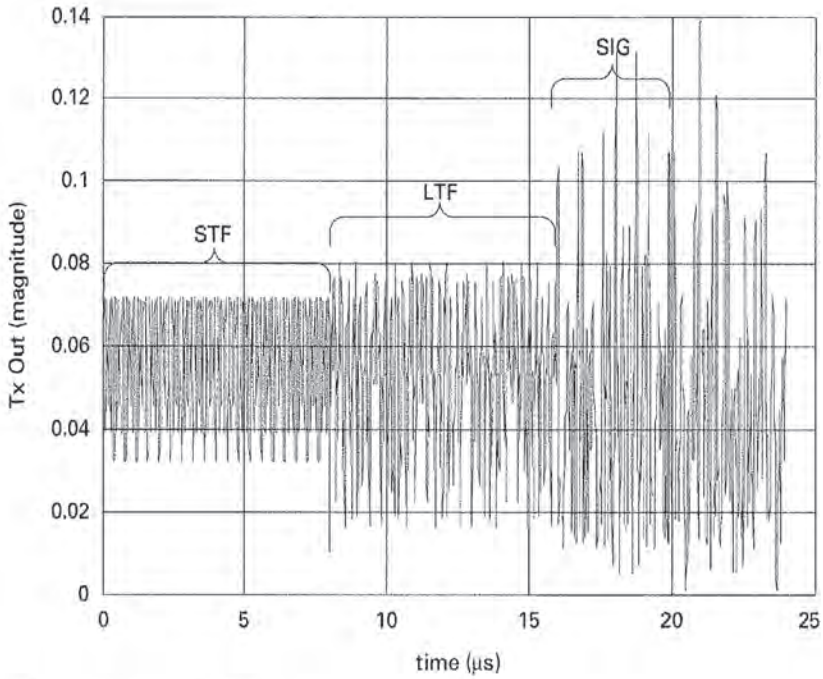

Figure 4.2 802.11a transmit waveform.

$$S_{-26,26} = \sqrt{13/6}\,\{0,\ 0,\ 1+j,\ 0,\ 0,\ 0,\ -1-j,\ 0,\ 0,\ 0,\ 1+j,\ 0,\ 0,\ 0,\ -1-j,\ 0,\ 0,\ 0,\ -1-j,\ 0,\ 0,\ 0,\ 1+j,\ 0,\ 0,\ 0,\ 0,\ 0,\ 0,\ 0,\ -1-j,\ 0,\ 0,\ 0,\ -1-j,\ 0,\ 0,\ 0,\ 1+j,\ 0,\ 0,\ 0,\ 1+j,\ 0,\ 0,\ 0,\ 1+j,\ 0,\ 0,\ 0,\ 1+j,\ 0,\ 0\} \tag{4.1}$$

The sequence uses 12 of the 52 subcarriers. A 64-point IFFT creates a 3.2 μs time domain sequence with a pattern which repeats four times (resulting in 0.8 μs periodicity). This is illustrated in Figure 4.3, with a sampling rate of 20 Msamples/s. This sequence may then be repeated two and a half times to create ten short symbol repetitions.

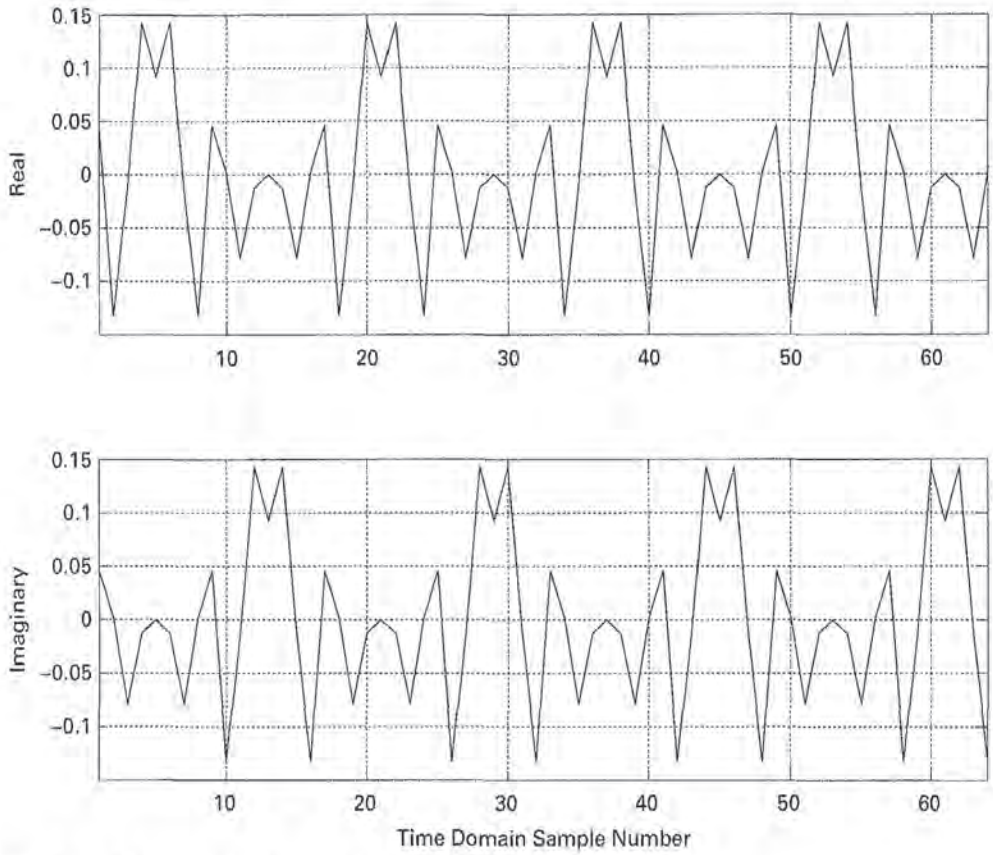

Figure 4.3 Construction of short training symbols.

The sequence was chosen to have good correlation properties and a low peak-to-average power so that its properties are preserved even after clipping or compression by an overloaded analog front end. The cross-correlation between the STF and one short training symbol is illustrated in Figure 4.4. There is a separation of over 10 dB between a correlation peak and a correlation sidelobe.

The correlation peaks may be used to derive an initial time estimate in a time domain based timing acquisition method. It is important to note that the cross-correlation properties of the STF are degraded by delayed responses in the channel. In Figure 4.5, we give an example of the cross-correlation with a channel modeled by two taps. The curve represented by the solid line depicts the channel with the second tap delayed by 50 ns. The curve represented by the dashed line depicts the channel with the second tap delayed by 400 ns. With 50 ns, the cross-correlation peak is a bit wider than the peak illustrated in Figure 4.4. However, with 400 ns, extra correlation peaks arise which may degrade timing acquisition. This issue had a major impact on the design of the MF preamble in 802.11n and is further discussed in Section 4.2.1.

The repetitive nature of the STF can also be used by correlating a 0.8 μs short symbol with the previous symbol (commonly termed autocorrelation since the received signal is

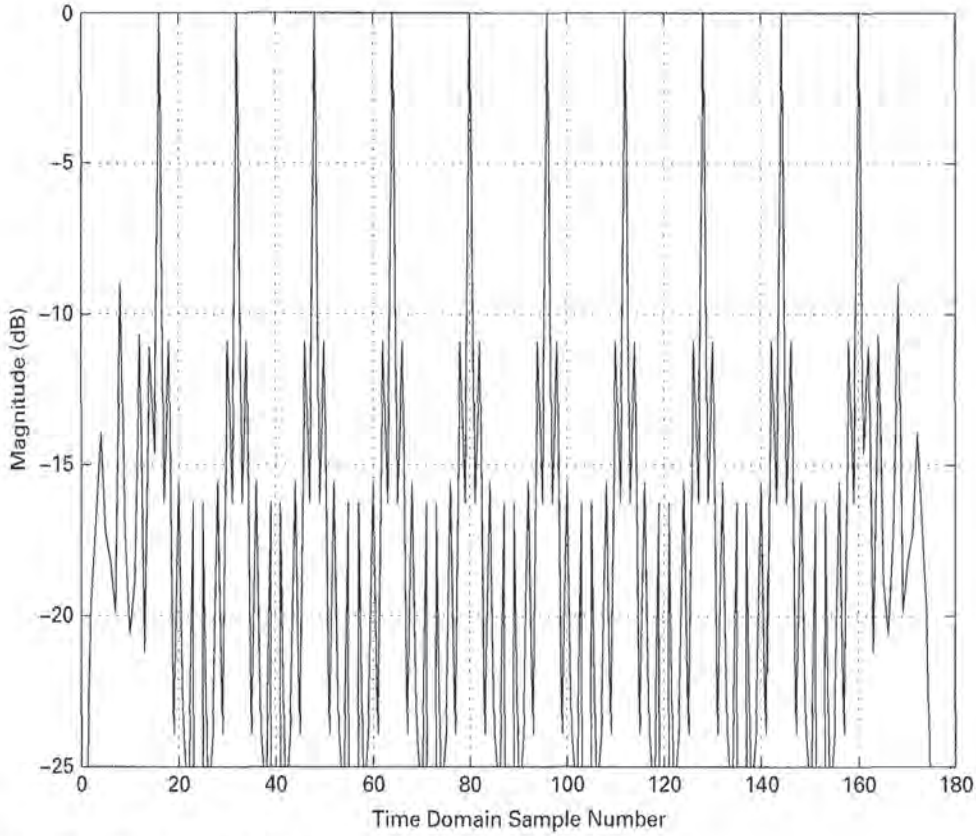

Figure 4.4 Short Training field correlation.

correlated with a delayed version of itself). This technique may be used for packet detection, whereby the correlation value exceeding a threshold indicates a packet detect. Additionally, this correlation value may be used to set the AGC. This approach proved less sensitive to longer delay spreads as compared to the cross-correlation; however, it is potentially less effective in noisier conditions.

The STF is also used for initial frequency offset estimation. Due to the symbol repetition, the difference in phase between two samples in the STF separated by 0.8 μs (or 16 samples if sampling at 20 MHz) allows an estimate of the frequency offset. This operation can resolve a frequency offset between the transmitting device and receiving device of up to ±625 kHz (±1/0.8 μs/2).

4.1.2 Long Training field

The LTF is also 8 μs in length, and is composed of two 3.2 μs long training symbols prepended by a 1.6 μs cyclic prefix. The cyclic prefix is comprised of the second half of the long training symbol. The long training symbol is a 64-point IFFT of the frequency domain sequence given in Eq. (4.2) (IEEE, 2012). Numbering the subcarrier locations ranging from −32, −31,. . .,−1,0,1,. . ., 31, the populated subcarriers are located from −26,

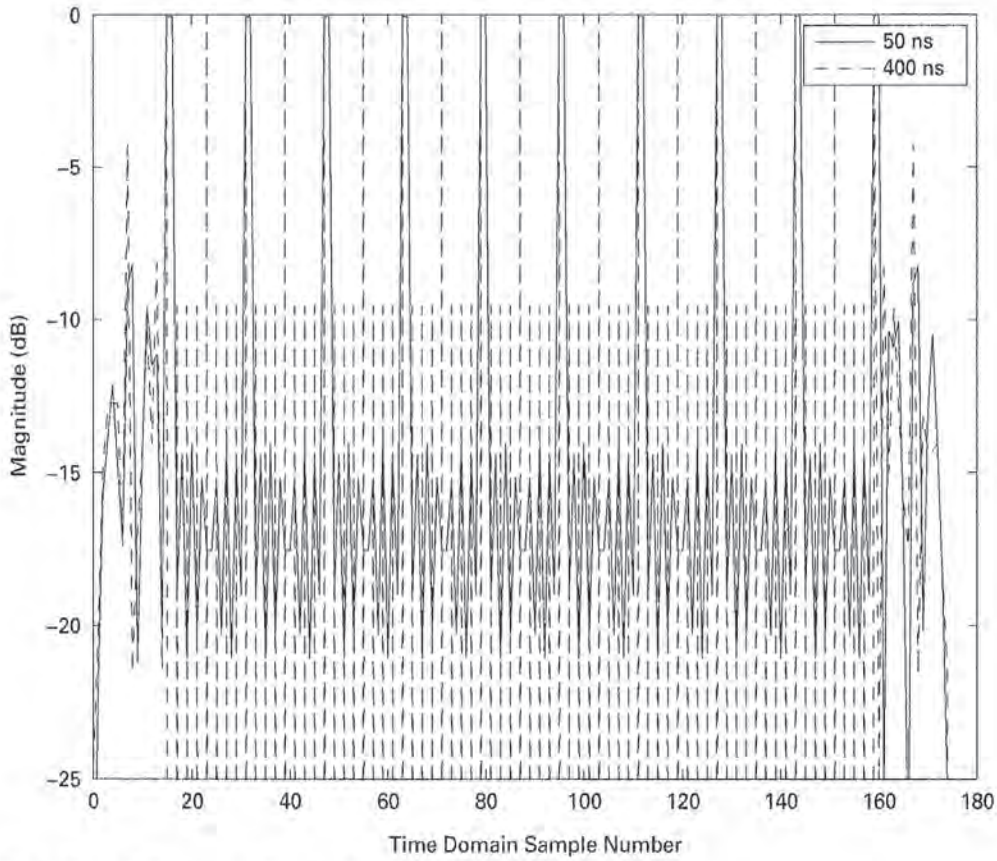

Figure 4.5 STF cross-correlation with a delayed response.

$-25, \ldots, -2, -1, 1, 2, \ldots, 25, 26$. All the populated subcarriers have the value of +1 or −1. The subcarrier at DC, L_0, is not populated.

$$L_{-26,26} = \{1, 1, -1, -1, 1, 1, -1, 1, -1, 1, 1, 1, 1, 1, 1, -1, -1, 1, 1, -1, 1, -1, 1, 1, 1, 1, 0, 1, -1, -1, 1, 1, -1, 1, -1, 1, -1, -1, -1, -1, -1, 1, 1, -1, -1, 1, -1, 1, -1, 1, 1, 1, 1\} \tag{4.2}$$

The cross-correlation between the entire preamble and the long training symbol is illustrated in Figure 4.6, with a sampling rate of 20 Msamples/s. The correlation peaks may be used to derive a more accurate time estimate in a time domain based timing acquisition method. Alternatively, the 1.6 μs cyclic prefix of the LTF may be used for correlation, with either cross-correlation or autocorrelation. Additionally, the transition between the STF and LTF may be used for more accurate time acquisition, e.g. by determining when the STF autocorrelation subsides.

Due to the symbol repetition, the difference in phase between two samples in the LTF separated by 3.2 μs (or 64 samples if sampling at 20 MHz) allows a more accurate estimate of the carrier frequency offset. This operation can resolve a frequency offset of

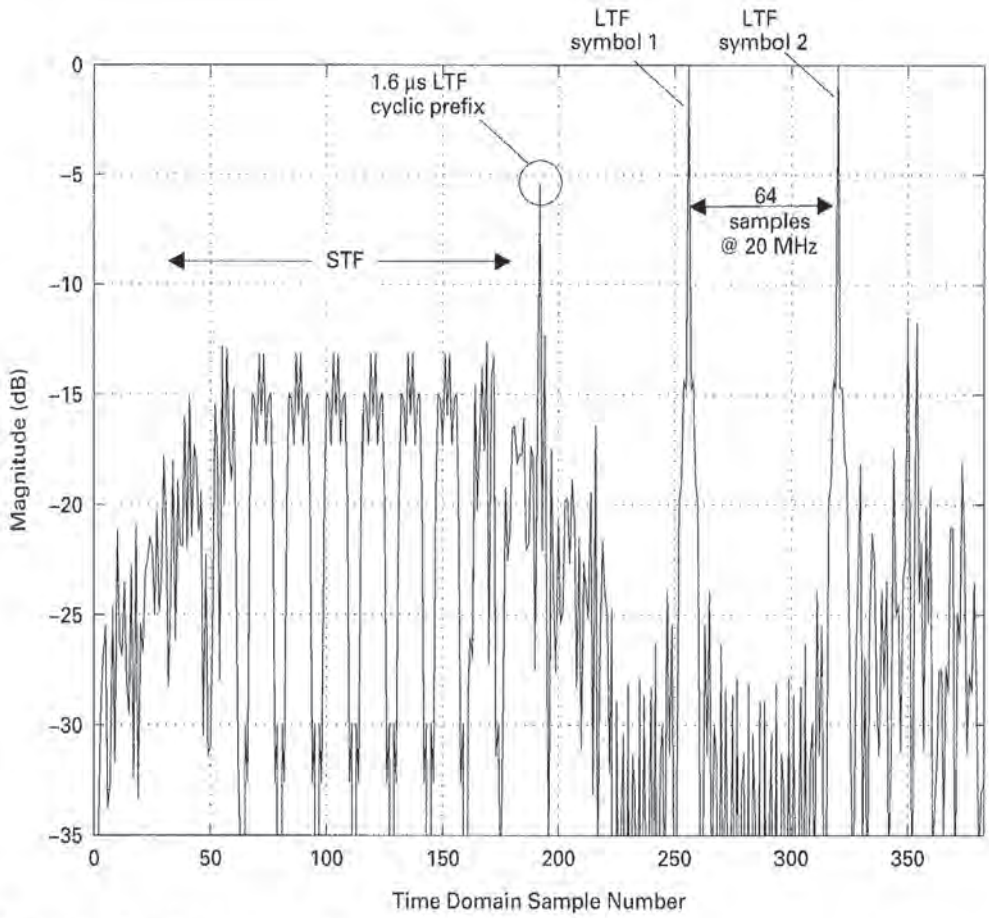

Figure 4.6 Correlation of the preamble with long training symbol.

up to ±156.25 kHz (±1/3.2 μs/2), so it should be used in conjunction with the STF frequency offset estimate.

The other main purpose of the LTF is for channel estimation. The receiver extracts the two long training symbols from the LTF. An FFT is performed on the symbols and the training subcarriers are extracted. The subcarriers from the first long training symbol are averaged with the subcarriers from the second symbol to reduce the effect of noise by 3 dB. Subsequently for each subcarrier k we have the basic communication system equation, $y_k = h_k \cdot L_k + z_k$. The values for L_k are given in Eq. (4.2). The known training symbol information is divided out of the received signal leaving the channel estimate for each subcarrier k, $\hat{h}_k = y_k / L_k$.

Since the channel estimate is used to equalize the subsequent OFDM symbols, noise on the channel estimate propagates through the packet during data detection. To reduce the noise on the channel estimate, subcarrier smoothing may be employed. A simple approach is to perform a weighted average of the channel estimate at subcarrier k with its adjacent neighbors, as shown in Eq. (4.3):

$$\tilde{h}_k = \frac{a \cdot \hat{h}_{k-1} + b \cdot \hat{h}_k + a \cdot \hat{h}_{k+1}}{2 \cdot a + b} \tag{4.3}$$

The nature of the channel must be taken into consideration with subcarrier smoothing. In a low delay spread, flat fading channel, channel taps on adjacent subcarriers are highly correlated and subcarrier smoothing provides a significant noise reduction benefit. However, in a highly frequency selective fading channel, adjacent channel taps may not be correlated and more sophisticated smoothing algorithms must be applied otherwise improper averaging degrades the channel estimate.

4.1.3 Signal field

The Signal field (SIG) consists of 24 information bits, illustrated in Figure 4.7. The SIG itself is transmitted using BPSK modulation and rate ½ binary convolution code (BCC) (followed by interleaving) to maximize the probability of reception. The BCC is described in Section 4.1.5. Not only is it important for the intended receiver to correctly decode the SIG, but also nearby stations need to correctly decode the SIG in order to properly defer the channel access.

The SIG consists of a single 4 μs symbol (a 3.2 μs OFDM symbol prepended by a 0.8 μs cyclic prefix). The waveform uses 52 subcarriers, as in the LTF. The 48 coded bits are BPSK modulated on to 48 subcarriers. Four additional subcarriers are used as pilots for phase and frequency tracking and training. Numbering the subcarrier locations ranging from −32, −31,. . ., −1, 0, 1,. . ., 31, the populated subcarriers are located at −26, −25,. . ., −2, −1, 1, 2,. . ., 25, 26. The pilot subcarriers are −21, −7, 7, 21. The remaining 48 subcarriers are populated with the coded SIG bits.

The SIG contains packet information to configure the receiver: rate (modulation and coding) and length (amount of data being transmitted in octets). The details of the rate field are given in Table 4.1. The reserved bit was intended for future use. The parity bit gives the even parity over the first 17 bits. The tail bits are set to zero and used to flush the encoder and decoder, since the SIG is separately encoded from the data field.

The parity and reserve bits played a large role in the development of the 11n mixed format (MF) preamble structure. A single parity bit in the SIG proved to be problematic in lower SNR conditions. In very noisy conditions, the probability of a false positive with a single parity bit approaches 50%. This happens especially when no signal is present at the receiver. A false positive incorrectly indicates a valid SIG, which leads the receiver to use the length and rate values to defer transmission. In a noisy environment or when no packet is present, these fields are random bits, and the device cannot receive or transmit a valid packet for potentially a long period of time. This significantly reduces throughput.

Rate 4 bits	Reserved 1 bit	Length 12 bits	Parity 1 bit	Tail 6 bits

Figure 4.7 Signal field.

Table 4.1 Rate information

Rate bit field	Data rate (Mbps)	Modulation	Code rate
1101	6	BPSK	1/2
1111	9	BPSK	3/4
0101	12	QPSK	1/2
0111	18	QPSK	3/4
1001	24	16-QAM	1/2
1011	36	16-QAM	3/4
0001	48	64-QAM	2/3
0011	54	64-QAM	3/4

This problem is partially mitigated by first measuring the received signal level and only processing signals which exceed a threshold. However, some manufacturers additionally used the reserve bit as extra parity. To maintain backward compatibility with devices in the field, it was decided not to use the reserve bit in the SIG to indicate a new 802.11n MF packet. This then required an auto-detection between 802.11a and 802.11n MF packets, which is discussed further in Section 4.2.2.1.

4.1.4 Data field

The Data field consists of the Service field, data bits, tail bits, and, if necessary, pad bits. The first 16 bits of the Data field contain the Service field. The first 7 bits of the Service field are the scrambler initialization bits. They are used to synchronize the descrambler and are set to zero to enable estimation of the initial state of the scrambler in the receiver. The remaining 9 bits are reserved and also set to zero.

Following the Service field are the data bits, which in turn are followed by six tail bits which are set to zero. Pad bits (also zeros) are added to the end of the packet so the resulting length fills up the last data symbol.

A length-127 frame synchronous scrambler is used in 802.11a which uses the generator polynomial $G(D) = D^7 + D^4 + 1$. The 127-bit sequence generated repeatedly by the scrambler is (leftmost used first), 00001110 11110010 11001001 00000010 00100110 00101110 10110110 00001100 11010100 11100111 10110100 00101010 11111010 01010001 10111000 1111111, if the all ones initial state is used (IEEE, 2012). When transmitting, the initial state of the scrambler is actually set to a pseudo-random non-zero state for each packet. Scrambling with a different sequence provides peak-to-average protection via retransmission. After the scrambling operation on the Data field, the six tail bits are replaced by six unscrambled zero bits. Pad bits are stripped off at the receiver.

The Data field consists of a stream of symbols, each data symbol 4 μs in length. A data symbol is comprised of a 3.2 μs OFDM symbol prepended by a 0.8 μs cyclic prefix. The waveform uses 52 subcarriers, as in the LTF and SIG. The data bits are encoded and modulated on to 48 subcarriers, as per the rate information in the SIG. Four additional subcarriers are used as pilots for phase and frequency tracking and training. Numbering the subcarrier locations −32, −31,..., −1, 0, 1,..., 31, the populated subcarriers are

located at −26, −25,..., −2, −1, 1, 2,..., 25, 26. The pilot subcarriers are located on subcarriers −21, −7, 7, 21 with values as follows:

$$P_K = \begin{cases} 1 & k = -21, -7, 7 \\ -1 & k = 21 \\ 0 & \text{otherwise} \end{cases} \tag{4.4}$$

The polarity of the pilot subcarriers is controlled by the sequence, p_n, which is a cyclic extension of the following 127 element sequence (IEEE, 2012):

$$\begin{aligned} p_{0\ldots126v} = \{&1, 1, 1, 1, -1, -1, -1, 1, -1, -1, -1, -1, 1, 1, -1, 1, -1, -1, 1, \\ &1, -1, 1, 1, -1, 1, 1, 1, 1, 1, 1, -1, 1, 1, 1, -1, 1, 1, -1, -1, 1, 1, 1, \\ &-1, 1, -1, -1, -1, 1, -1, 1, -1, -1, 1, -1, -1, 1, 1, 1, 1, 1, -1, \\ &-1, 1, 1, -1, -1, 1, -1, 1, -1, 1, 1, -1, -1, -1, 1, 1, -1, -1, -1, \\ &-1, 1, -1, -1, 1, -1, 1, 1, 1, 1, -1, 1, -1, 1, -1, 1, -1, -1, -1, \\ &-1, -1, 1, -1, 1, 1, -1, 1, -1, 1, 1, 1, -1, -1, 1, -1, -1, -1, 1, \\ &1, 1, -1, -1, -1, -1, -1, -1, -1\} \end{aligned} \tag{4.5}$$

The sequence p_n can be generated by the scrambler. The remaining 48 subcarriers are populated with the coded data bits.

4.1.5 Packet encoding process

The packet encoding process begins by creating the STF and LTF as described in Sections 4.1.1 and 4.1.2. The SIG is produced based on the selected rate and length, following the description in Section 4.1.3. The encoding of the Data field follows the block diagram in Figure 4.8.

The data bits are prepended by the Service field and appended by six tail zero bits. If necessary, additional pad zero bits are also appended to the Data field. The extended sequence is then scrambled. The initial state of the scrambler is set to a non-zero random value. At the receiver, the first seven bits of the Service field give the initial state of the scrambler. The same scrambler is used at the receiver to descramble the received data. After the scrambler, the six scrambled tail bits are replaced by unscrambled zero bits. This causes the convolution encoder, which follows, to return to the zero state.

The scrambled data is encoded with a rate ½ binary convolutional encoder (BCC). The encoder has a constraint length of 7 and a generator polynomial of [133, 171] octal. If necessary, the sequence is punctured to the selected code rate if a higher rate is chosen. Further detail is provided in IEEE (2012, Clause 18.3.5.5) and van Nee and Prasad (2000).

The coded data is grouped into a number of bits per symbol and each group is block interleaved with two permutations. The first permutation maps adjacent coded bits onto non-adjacent subcarriers. In this manner, adjacent coded bits are not impacted by the same frequency selective fade. The second permutation ensures that adjacent coded bits are distributed between less and more significant bits of the modulation constellation.

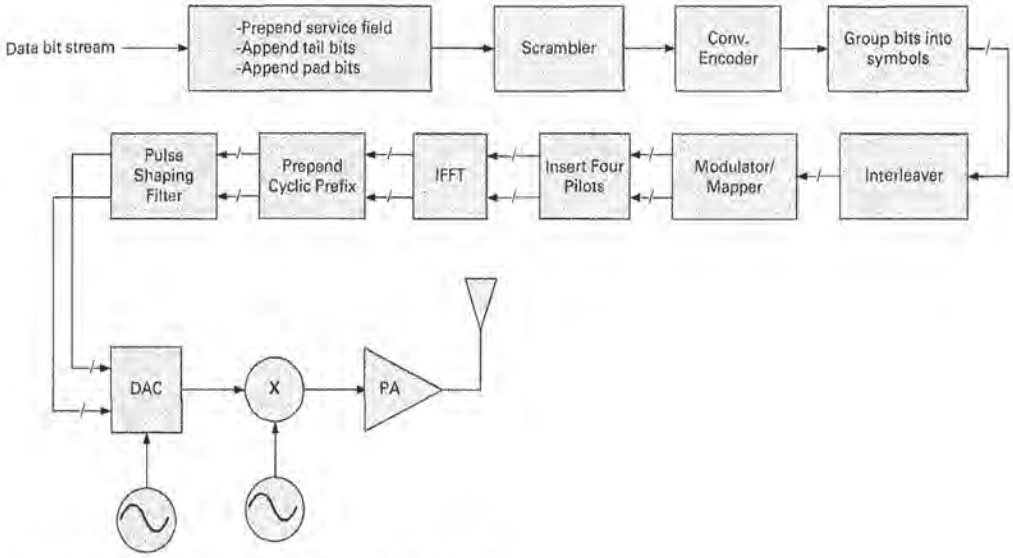

Figure 4.8 Transmitter block diagram for Data field.

This ensures that long strings of bits are not mapped to the lower reliability, less significant constellation bits.

Following the interleaver, the groups of bits are modulated according to the selected rate and mapped onto the corresponding subcarriers. There are four modulation formats possible: BPSK, QPSK, 16-QAM, and 64-QAM. At this stage, the modulated data are complex numbers. For each symbol, the pilot subcarriers are inserted into their corresponding subcarriers. Subcarrier locations for data and pilots are given in Section 4.1.4.

Each symbol group of subcarriers is transformed into the time domain by an IFFT. A cyclic prefix is prepended to the symbol. A pulse shaping function may be applied to each symbol to smooth transitions between symbols. Smoothing transitions between symbols reduces the spectral sidelobes and may be necessary to meet the spectral mask. A pulse shaping function is not specified in the standard; however, the following example is given in IEEE (2012) for 802.11a:

$$w_T(t) = \begin{cases} \sin^2\left(\frac{\pi}{2}\left(0.5 + \frac{t}{T_{TR}}\right)\right) & -\frac{T_{TR}}{2} < t < \frac{T_{TR}}{2} \\ 1 & \frac{T_{TR}}{2} \le t < T - \frac{T_{TR}}{2} \\ \sin^2\left(\frac{\pi}{2}\left(0.5 - \frac{t-T}{T_{TR}}\right)\right) & T - \frac{T_{TR}}{2} \le t < T + \frac{T_{TR}}{2} \end{cases} \tag{4.6}$$

where T_{TR} is the transition time of the windowing function, which creates an overlap between adjacent symbols to smooth the transition. With a sampling rate of 20 Msamples/s, symbol duration of 4 μs, and T_{TR} = 100 ns, the windowing function is given by Eq. (4.7) (IEEE, 2012):

$$w_T(n) = \begin{cases} 1 & 1 < n < 79 \\ 0.5 & 0.80 \\ 0 & \text{otherwise} \end{cases} \tag{4.7}$$

An alternative approach is to use a 40 MHz IFFT with additional windowing.

Lastly, each of the OFDM symbols is appended one after another. The digital baseband signal is converted to analog with a DAC, which is then followed by an up-converter to RF and a power amplifier.

Further details on the encoding process are given in IEEE (2012, Clause 18) (otherwise known as 802.11a), van Nee and Prasad (2000) and Halford (2001). An example of data bits encoded into an 802.11a packet is given in IEEE (2012, Annex L).

4.1.6 Receive procedure

Typically, the receiver waits for a signal to exceed a threshold before initiating the packet reception procedure. The minimum requirement in 802.11a is to detect the start of a valid transmission received at a power level of at least −82 dBm within 4 μs with a probability greater than 90%. Due to competitive pressures, most products exceed this specification by 5–10 dB.

The short training symbols are processed to set the AGC, initial frequency correction, and initial timing acquisition. This is followed by processing the long training symbols for fine frequency correction and fine timing adjustment. The LTF is also used to generate the channel estimate.

The next 4 μs symbol is the SIG. The receiver follows the same symbol processing as the data, except for the de-scrambler. The bits in the SIG are not scrambled. Once the SIG bits are extracted, the receiver evaluates the parity bit for errors in the SIG. If the parity indicates an error, the receiver returns to an idle state. Upon no errors being detected by the parity bit, the receiver is configured based on rate and length information. The rate determines the modulation type and coding rate. The length determines the duration of the data stream in octets.

Following the SIG is the Data field, for which a receiver block diagram is illustrated in Figure 4.9. For each 4 μs symbol, the 0.8 μs GI is removed and an FFT is performed. Using the channel estimate from the LTF, the subcarrier data is equalized as described in Section 3.6. The four pilot subcarriers are used for phase rotation correction, and may be used for further frequency offset and symbol timing correction.

Trellis coded modulation (TCM), which combines modulation and coding, was generally accepted as the best approach for improved performance. However, with the commercial availability and popularity of Viterbi decoders, researchers began investigating schemes for maximizing performance with separate modulation and coding entities to enable reuse of the Viterbi decoder. In Zehavi (1992) it was shown that in a fading channel the code diversity is improved by bit-wise interleaving at the encoder output. The analysis in Caire *et al.* (1998) goes further and demonstrates that on some channels there is a downside to combining demodulation and decoding. For this reason, the 802.11a system is based on bit interleaved coded modulation (BICM). Therefore, the subcarrier

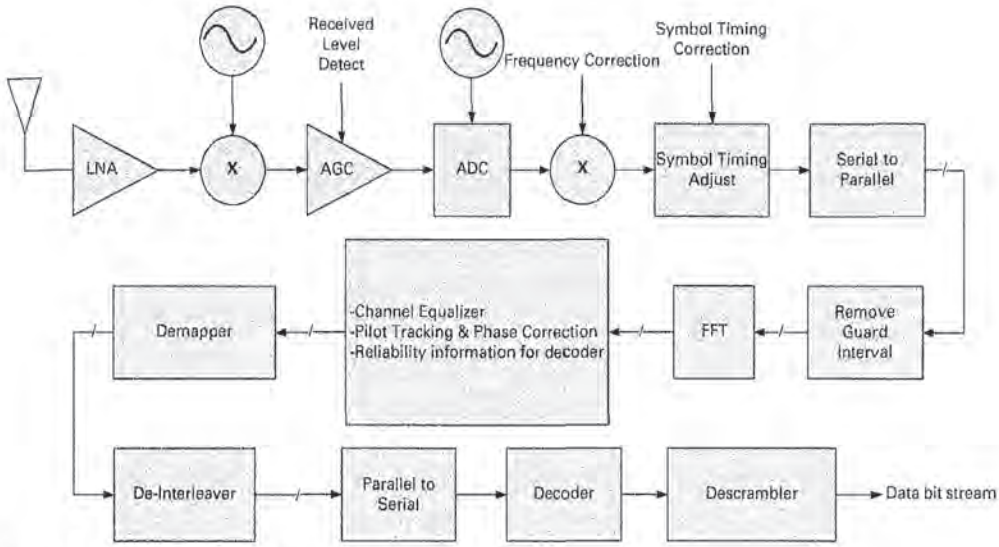

Figure 4.9 Receiver block diagram for Data field.

data is then demapped by finding bit probabilities from the closest constellation points to the equalized signal. This is followed by the deinterleaver, which is the inverse of the interleaver function. A comprehensive presentation of BICM is given in Caire *et al.* (1998), and further information on low-complexity demapping of BICM is given in van Nee and Prasad (2000) and Akay and Ayanoglu (2004a).

After the parallel to serial conversion (see Figure 4.9), the data is treated as a stream rather than symbol blocks. In a conventional receiver with ZF or MMSE, the output of the demapper and deinterleaver is passed directly to the decoder, typically a Viterbi decoder. If the code rate is higher than ½, zero metrics are inserted into the decoder in place of the puncture bits.

However, with a frequency selective channel, decoding performance substantially improves by using the channel estimates to weight the decoder metrics (Akay and Ayanoglu, 2004b). The bits associated with subcarriers that are faded are de-weighted (less reliable). This forces the portions of the decoder trellis for which the SNR is low due to the channel fade to have lower branch metrics and have a smaller contribution to the path metric. The subcarriers with high SNR are larger branch metrics and are emphasized in the path metric. Based on the maximum likelihood estimator, we can mathematically demonstrate the benefit of applying channel estimates to weight the decoder metrics.

The maximum likelihood estimation was discussed in Section 3.7 and given in Eq. (3.37). For soft-decision decoding in an AWGN channel with fading, the probability density function of the demodulator output is given by Eq. (4.8) (Proakis, 1989):

$$p(y \mid x_i) = \frac{1}{\sqrt{2\pi}} \exp\left[\frac{(y - h \cdot x_i)^2}{2\sigma^2}\right] \tag{4.8}$$

Extrapolating from this, the maximum likelihood estimate of the transmitted data is given by Eq. (4.9) (Akay and Ayanoglu, 2004b):

$$\hat{X} = \min_i \left| \frac{Y - H \cdot X_i}{\sigma} \right|^2 \tag{4.9}$$

where Y is the received signal, σ^2 is the variance of the noise, H and $\tilde{H}$ are the channel tap and channel estimate, respectively, and X_i is the set of possible transmitted data. By factoring, we arrive at the expression for the ML estimator given in Eq. (4.10) (Akay and Ayanoglu, 2004b):

$$\hat{X} = \min_i \frac{|\tilde{H}|^2}{\sigma^2} \left| \frac{Y}{\tilde{H}} - X_i \right|^2 \tag{4.10}$$

The $Y/\tilde{H}$ term in Eq. (4.10) is the expression for a ZF receiver. The demapping operation is given by the $|Y/\tilde{H} - X_i|$ term. Therefore, to approach ML performance with a ZF receiver, we simply need to include the extra weighting step, given by the $|\tilde{H}|^2/\sigma^2$ term. Since with BPSK there is no coupling between bits in the constellation, whose information is lost in a low-complexity BICM demapping operation, Eq. (4.10) provides ML with a ZF receiver.

As illustrated in Figure 4.9, the final step in the receive procedure is descrambling the Data field. The first seven bits of the Service field give the initial state of the descrambler. The same scrambler is used to descramble the data stream. Bits received after the data length indicated by the SIG are discarded.

Further details on the 802.11a packet reception process are given in IEEE (2012, Clause 18) (otherwise known as 802.11a), van Nee and Prasad (2000), and Halford (2001).

4.2 Mixed format high throughput packet structure

New high throughput (HT) packet formats are used to transmit multiple spatial streams. The mixed format (MF) HT preamble begins with legacy (802.11a) fields to ensure backward compatibility with 802.11a and OFDM 802.11g. These are followed by high throughput training fields. An overview of the fields is given in Figure 4.10. The MF preamble may be used for either 20 MHz or 40 MHz channel width. However, this section focuses on the general functionality of the MF preamble, and only describes the mandatory 20 MHz waveform. The optional 40 MHz waveform is covered in Section 5.1. In addition, other optional features such as sounding packets, short guard interval, STBC, and LDPC and their impact on the waveform design are addressed in Sections 13.6, 5.5, 6.3, and 6.4, respectively.

A plot of a full 802.11n MF waveform with two spatial streams is given in Figure 4.11. The legacy part of the preamble comprises the first 20 μs. The HT part of the preamble comprises the next 20 μs, with two spatial streams. This is then followed by the HT data field.

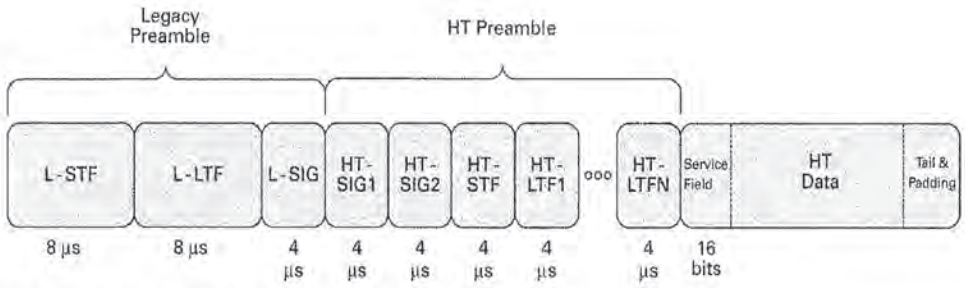

Figure 4.10 Mixed format preamble.

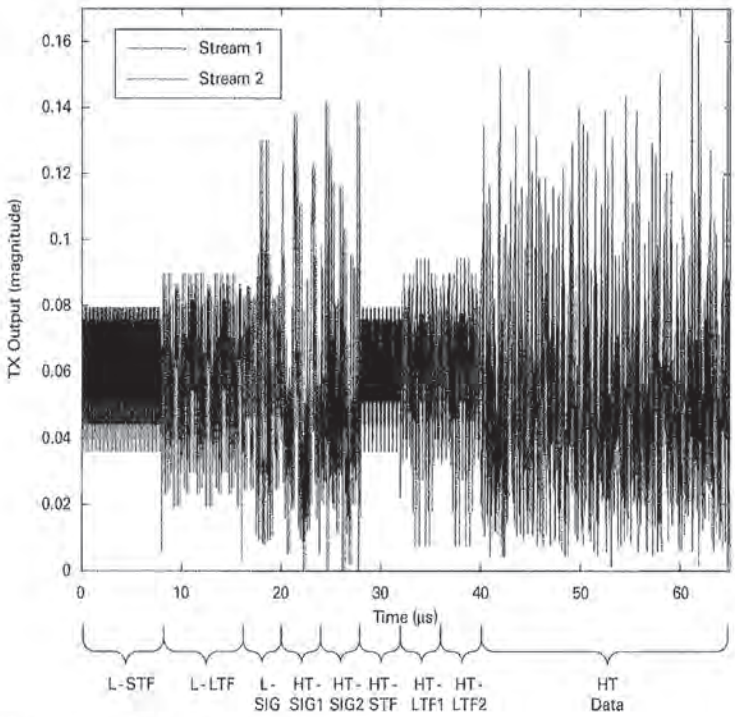

Figure 4.11 802.11n MF with two spatial streams.

The following sections describe the fields of the MF preamble in detail.

4.2.1 Non-HT portion of the MF preamble

The first part of the MF preamble consists of non-HT (legacy) training fields identical to 802.11a, as illustrated in Figure 4.10. It contains a Non-HT Short Training field (L-STF), non-HT Long Training field (L-LTF), and Non-HT Signal field (L-SIG) such that legacy devices can detect the preamble. However, as discussed below, an 802.11n HT device also needs to use these fields for training and mandatory demodulation of the L-SIG.

Referring to Section 4.1.1, the L-STF is used for start-of-packet detection, AGC setting, initial frequency offset estimation, and initial time synchronization by legacy

devices. The L-LTF is used for further fine frequency offset estimation and time synchronization. The L-LTF is also used to generate channel estimates for receiving and equalizing the L-SIG. With proper decoding of the L-SIG, legacy 802.11a/g devices extract the rate and length information and are able to determine the proper time to remain off air. This is discussed in more detail in Section 11.5.9.

Since HT devices perform similar acquisition functions as legacy devices using the L-STF and L-LTF, the issue arises of how to transmit the legacy part of the MF preamble that is a single spatial stream with 802.11n devices that in most cases have multiple transmit antennas. To understand the issue, consider a single antenna legacy device with 17 dBm output transmit power. To maintain similar cost and complexity, a comparable two transmit antenna HT device has two power amplifiers each with 14 dBm output power for the same total output power. If the legacy part of the MF preamble is transmitted from a single antenna of the HT device, the maximum power and range during legacy training is reduced by 3 dB. Moreover, with four antennas, the power on a single transmit RF chain and antenna drops by 6 dB.

To alleviate this transmit power disparity, it is necessary to transmit the legacy training from all antennas of an HT device. However, since the legacy preamble is single stream, transmitting the same signal from each antenna may cause unintentional and undesirable beamforming effects. Since the L-STF is used for AGC setting, large variations in the power of the L-STF also results in saturation or quantization errors.

4.2.1.1 Cyclic shifts

During development of the 802.11n standard, several approaches for how to transmit the legacy training from all antennas were investigated. One approach that was considered was transmitting a subset of subcarriers on each antenna. However, with four transmit antennas, the L-STF, which consists of only twelve active subcarriers, would consist of only three active subcarriers per antenna. This is a very small number of subcarriers per antenna and this approach also suffers from legacy compatibility issues.

Hence, to decorrelate the signals transmitted from different antennas with a single spatial stream and alleviate undesirable beamforming effects, different cyclic shifts (T_{CS}) are applied to each of the signals on the different antennas. Consider an OFDM symbol $s(t)$ over a symbol period T. Replace $s(t)$ with $s(t - T_{CS})$ when $0 \le t < T + T_{CS}$, and with $s(t - T_{CS} - T)$ when $T + T_{CS} \le t \le T$. The cyclic shifted signal is defined as

$$s_{CS}(t;\ T_{CS})|_{T_{CS}<0} = \begin{cases} s(t - T_{CS}) & 0 \le t < T + T_{CS} \\ s(t - T_{CS} - T) & T + T_{CS} \le t \le T \end{cases} \tag{4.11}$$

The cyclic shift is applied to each OFDM symbol in the packet separately. Equivalently, in the frequency domain, where $S(f)$ is the Fourier transform of $s(t)$, the cyclic shifted symbol can be described as

$$S_{CS}(f) = S(f)e^{-j2\pi f T_{CS}} \tag{4.12}$$

A two antenna example is given in Figure 4.12, with a −200 ns cyclic shift applied to the signal on the second antenna.

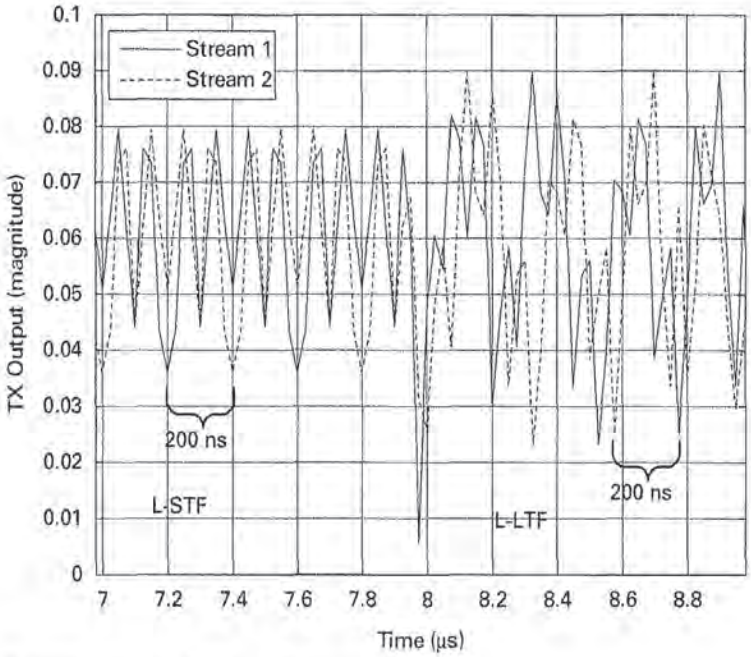

Figure 4.12 Example of cyclic shift applied to second antenna.

The L-STF is used for AGC setting. Thus, in order to properly adjust the gain setting in the receiver, the power of the STF needs to match the power of the Data field. The ratio between the power of the L-STF and the power of the Data field as measured by the receiver with the propagation modeled by channel model D is given in Figure 4.13. The top graph demonstrates two transmit antennas, and the bottom graph demonstrates four transmit antennas. Several combinations of cyclic shifts are given. For both graphs, the legend gives the cyclic shift on the signals transmitted on each antenna.

With both two and four transmit antennas, having no cyclic shifts on any of the signals results in large variation between the power of the L-STF and Data field, as illustrated by the dash-dotted lines. When the power of the L-STF is smaller than the Data field, the gain is set too high causing saturation or clipping of the data. When the power of the L-STF is larger than the Data field, the gain is set too low causing quantization of the data. With two antennas, the power variation between L-STF and Data field diminishes as the cyclic shift exceeds –200 ns. However, with four antennas, cyclic shifts of up to –600 ns are required to minimize variation.

4.2.1.2 Legacy compatibility

Legacy OFDM devices receive the HT packet with MF preamble and process the L-STF, L-LTF, and L-SIG. As discussed in Section 4.1.1 and illustrated in Figure 4.5, the performance of legacy OFDM devices that employ a cross-correlation receiver is degraded by delayed responses. The MF preamble with cyclic shifts applied to the signals on the additional antennas appears to the legacy OFDM devices as a signal

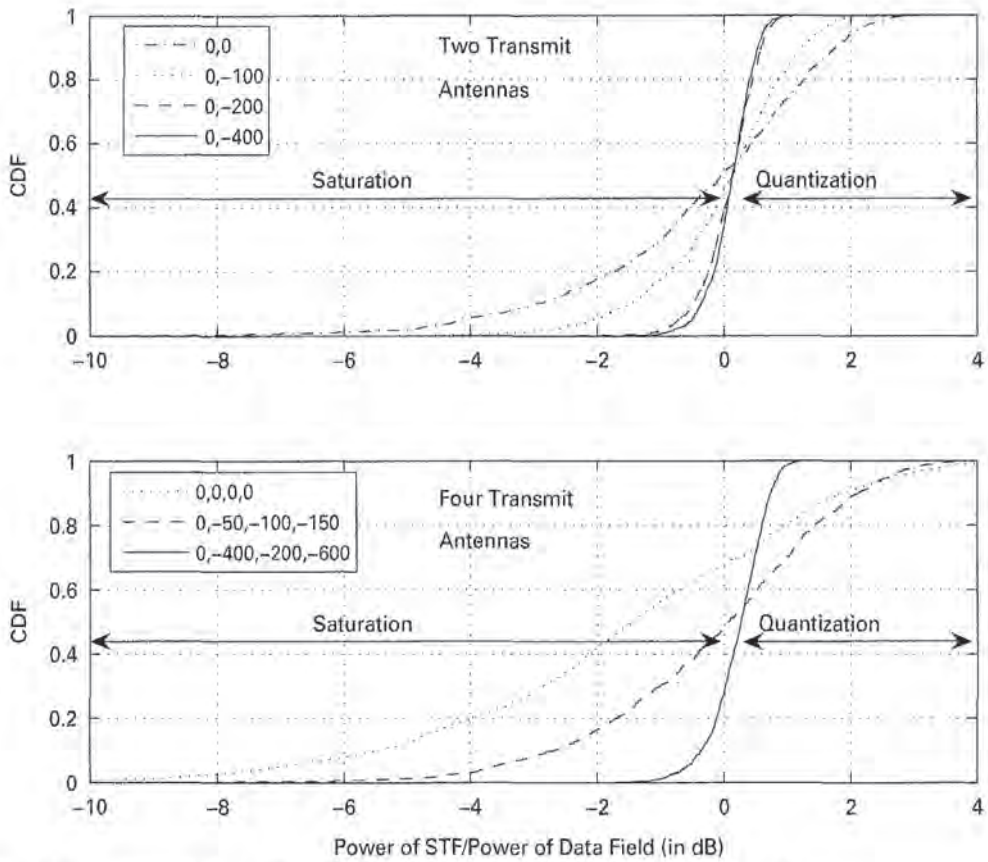

Figure 4.13 Power of the L-STF relative to power of the Data field for channel model D.

convolved with a channel with a delayed response. The larger the cyclic shift, the larger the delay spread, and the more the legacy receiver is degraded.

During development of the standard, measurements were made by Aoki and Takeda (2005) with 802.11a devices with cross-correlation receivers to test the sensitivity to cyclic shifts. Figure 4.14 illustrates the results of their experiment. Since the legacy device is only able to process up to the L-SIG in the MF preamble, only the SIG error rate was measured. The line marked with diamonds (♦) is the performance of the receiver when receiving an 802.11a transmission, to which we are comparing. The line marked with squares (■) demonstrates the legacy performance when receiving a two antenna transmission with 50 ns cyclic shift on the second antenna. The line marked with triangles (▲) demonstrates the legacy performance when receiving a two antenna transmission with 400 ns cyclic shift on the second antenna. As seen from the results, with 50 ns cyclic shift the SIG error rate is comparable to 802.11a performance. However, with 400 ns cyclic shift the SIG error rate degrades substantially. A compromise was reached to define a maximum magnitude of 200 ns cyclic shift on the non-HT part of the MF preamble.

Table 4.2 gives the values of the cyclic shifts that are applied to the L-STF, L-LTF, L-SIG, and the HT-SIG of the MF preamble.

Table 4.2 Cyclic shift for non-HT portion of the packet (IEEE, 2012). IEEE Std 802.11-2012, © 2012 IEEE. All rights reserved

Number of Tx chains	Cyclic shift for Tx chain 1 (ns)	Cyclic shift for Tx chain 2 (ns)	Cyclic shift for Tx chain 3 (ns)	Cyclic shift for Tx chain 4 (ns)
1	0	–	–	–
2	0	−200	–	–
3	0	−100	−200	–
4	0	−50	−100	−150

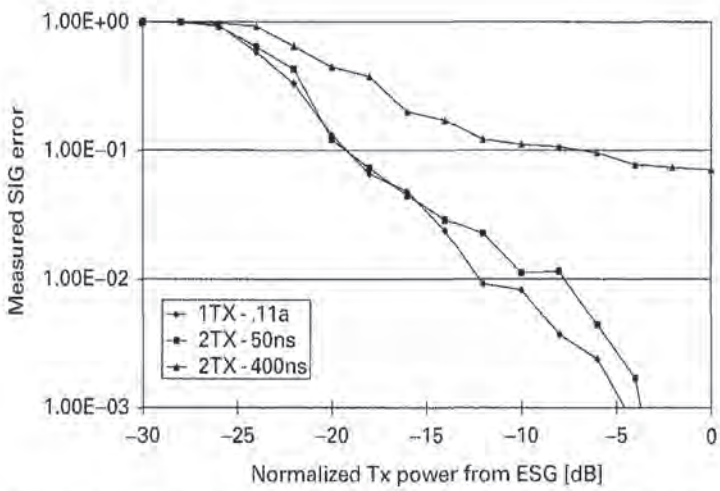

Figure 4.14 Preamble performance with cross-correlation 802.11a receiver in channel model D. Reproduced with permission from Aoki and Takeda (2005).

With more than four transmit antenna chains, specific values for the cyclic shifts on the additional transmit chains are not given. However, the standard states that the shifts on the additional antennas must be between −200 ns and 0 ns.

4.2.1.3 Non-HT Short Training field

In 802.11a, the scaling of the Short Training field was set to make the power of the symbol equal to that of the Long Training field. In 802.11n, the scaling of the symbol is set to make the total power of the time domain signal (summed over all transmit chains) equal to one. Thus, the L-STF frequency domain sequence S_k for the 20 MHz channel is identical to that of 802.11a, given by Eq. (4.1), except as above, the scaling of the sequence for L-STF is $\sqrt{1/2}$ rather than $\sqrt{13/6}$. The time domain L-STF waveform for the 20 MHz channel bandwidth for each transmit chain i_{TX} is defined by the equation below:

$$r_{\text{L-STF}}^{(i_{TX})}(t) = \frac{1}{\sqrt{N_{TX} \cdot 12}} \sum_{k=-26}^{26} S_k \exp\left(j2\pi\, k\Delta_F \left(t - T_{CS}^{i_{TX}}\right)\right) \qquad (4.13)$$

where $\Delta_F = 312.5$ kHz (20 MHz/64); $T_{cs}^{i_{TX}}$ represents the cyclic shift for transmit chain i_{TX} with values given by Table 4.2; and N_{TX} is the number of transmit chains.

As described in Section 4.1.1, the L-STF may be created by performing a 64-point IFFT over the frequency domain sequence resulting in a 3.2 μs time domain sequence, which is repeated two and a half times to create the 8 μs L-STF waveform. A windowing function may be applied to the L-STF waveform to smooth transitions between it and the L-LTF (refer to Section 4.1.5, and Eqs. (4.6) and (4.7)).

4.2.1.4 Non-HT Long Training field

The L-LTF frequency domain sequence for the 20 MHz channel is identical to that of 802.11a, given by Eq. (4.2). The time domain L-LTF waveform for the 20 MHz channel bandwidth for each transmit chain i_{TX} is defined by the equation below:

$$r_{L-LTF}^{(i_{TX})}(t) = \frac{1}{\sqrt{N_{TX} \cdot 52}} \sum_{k=-26}^{26} L_k \exp\left(j2\pi\, k\Delta_F \left(t - T_{GI2} - T_{CS}^{i_{TX}}\right)\right) \qquad (4.14)$$

where $\Delta_F = 312.5$ kHz (20 MHz/64); $T_{cs}^{i_{TX}}$ represents the cyclic shift for transmit chain i_{TX} with values given by Table 4.2; T_{GI2} is the 1.6 μs guard interval; and N_{TX} is the number of transmit chains.

As described in Section 4.1.2, the resulting long training symbol created by performing a 64-point IFFT over the frequency domain sequence is a 3.2 μs time domain sequence. The 8 μs L-LTF waveform may be created by repeating the long training symbol twice and prepended by a 1.6 μs cyclic prefix. A windowing function may be applied to the L-LTF waveform to smooth transitions between it and the L-STF and L-SIG (refer to Section 4.1.5, and Eqs. (4.6) and (4.7)).

4.2.1.5 Non-HT Signal field

The construction of the Non-HT Signal field is identical to the Signal field in 802.11a and described in Section 4.1.3. Although some fields have been co-opted to protect 802.11n from 802.11a devices, e.g. the rate field is always set to 6 Mbps and the length field is set so that 802.11a devices correctly defer transmission for at least the entire duration of the HT packet.

Furthermore, the waveform derived from the 48 complex data d_k, $k = 0, \ldots, 47$, may need to be transmitted over multiple antennas. Legacy cyclic shifts are applied to each signal on each transmit antenna chain i_{TX} as described in Section 4.2.1.1. The L-SIG waveform for each transmit antenna chain i_{TX} is given below:

$$r_{L-SIG}^{(i_{TX})}(t) = \frac{1}{\sqrt{N_{TX} \cdot 52}} \sum_{k=-26}^{26} (D_k + p_0 P_k) \exp\left(j2\pi k\Delta_F \left(t - T_{GI} - T_{CS}^{i_{TX}}\right)\right) \qquad (4.15)$$

where D_k and $M'(k)$, given by

$$D_k = \begin{cases} 0 & k = 0, \pm 7, \pm 21 \\ d_{M'(k)} & \text{otherwise} \end{cases}$$

$$M^{r}(k) = \begin{cases} k+26 & -26 \le k \le -22 \\ k+25 & -20 \le k \le -8 \\ k+24 & -6 \le k \le -1 \\ k+23 & 1 \le k \le 6 \\ k+22 & 8 \le k \le 20 \\ k+21 & 22 \le k \le 26 \end{cases}$$

are the mapping of complex data values to subcarrier locations while leaving space for pilots, DC, and guard band; $T_{CS}^{i_{TX}}$ represents the non-HT cyclic shift for transmit chain i_{TX} with values given by Table 4.2; T_{GI} is the 0.8 μs guard interval; P_k is the same as legacy OFDM and is given by Eq. (4.4); and p_0 is the same as legacy OFDM and is given by Eq. (4.5).

As described in Section 4.1.3, the resulting waveform is a 3.2 μs time domain OFDM symbol. A 0.8 μs cyclic prefix is prepended, resulting in a 4.0 μs symbol. A windowing function may be applied to the L-SIG waveform to smooth transitions between it and the L-LTF and HT-SIG (refer to Section 4.1.5, and Eqs. (4.6) and (4.7)). The transmitter block diagram for L-SIG is illustrated in Figure 4.15.

4.2.2 HT portion of the MF preamble

As illustrated in Figure 4.10, the HT portion of the MF preamble consists of the High Throughput Signal field (HT-SIG), High Throughput Short Training field (HT-STF), and High Throughput Long Training field (HT-LTF). The two OFDM symbols of the HT-SIG, HT-SIG$_1$ and HT-SIG$_2$, contain new signaling information and are also used for auto-detection between HT MF and legacy OFDM packets. The HT-STF is used to redo

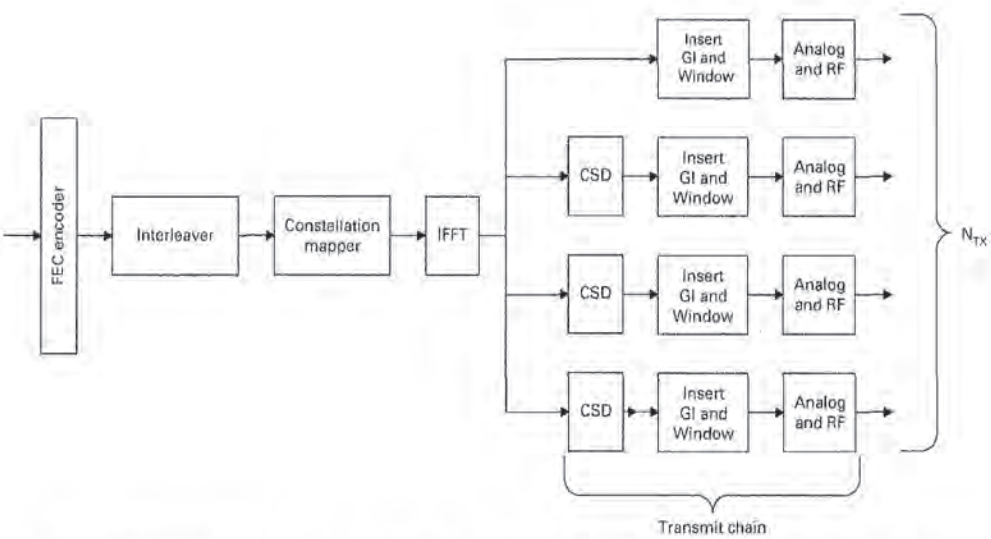

Figure 4.15 Transmitter block diagram for L-SIG and HT-SIG of the HT mixed format packet. Reproduced with permission from IEEE (2012), IEEE Std 802.11–2012, © 2012 IEEE. All rights reserved.

the AGC setting. The HT-LTFs are used for MIMO channel estimation. The HT Data field follows the HT-LTFs.

4.2.2.1 High Throughput Signal field

The HT-SIG contains 48 information bits, divided into two symbols, HT-SIG$_1$ and HT-SIG$_2$, each containing 24 information bits. We require 32 bits to signal the new HT information and modes. In addition, the HT-SIG includes an 8-bit CRC for strong error detection, as opposed to the single parity in the L-SIG. As in the L-SIG, the last 6 bits are tail bits (set to zero) to terminate the trellis of the convolution code since the HT-SIG is also encoded with a rate ½ BCC. The HT-SIG is illustrated in Figure 4.16.

In HT-SIG$_1$, the first 7 bits are used to signal which of the modulation coding schemes (MCS) 0 to 76 is used for transmission of the Data field. The MCSs consist of BPSK, QPSK, 16-QAM, and 64-QAM, identical to 802.11a. The coding rates include 1/2, 2/3, and 3/4 the same as 802.11a, and a new rate 5/6. MCS 0 to 7 consist of single stream, MCS 8 to 15 consist of two streams, MCS 16 to 23 consist of three streams, and MCS 24 to 31 consist of four streams. MCS 0 to 31 have equal modulation on each stream. MCS 32 only applies to 40 MHz operation and is discussed in Chapter 5. MCS 33 to 76 have unequal modulation on each stream and are discussed in Chapter 13. The MCS parameters and data rates for 20 MHz, equal modulation, and 800 ns guard interval are defined in Tables 4.7–4.10. Values 77 to 127 are reserved.

The CBW 20/40 bit is used to indicate whether the transmission has 20 MHz or 40 MHz bandwidth. This information is useful to allow a 20 MHz receiver to determine

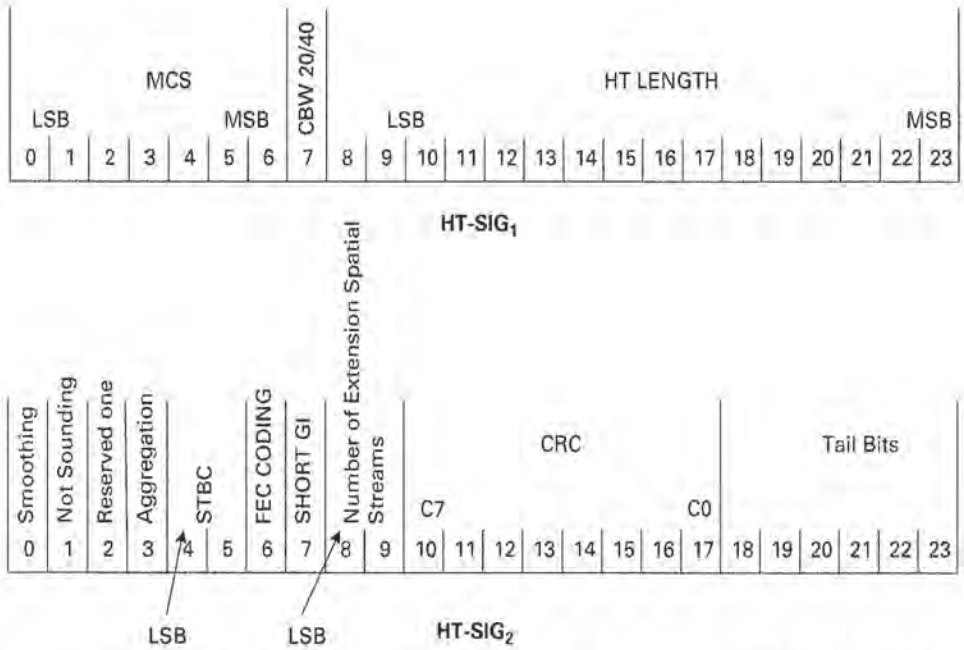

Figure 4.16 Format of HT-SIG$_1$ and HT-SIG$_2$. Reproduced with permission from IEEE (2012). IEEE Std 802.11–2012, © 2012 IEEE. All rights reserved.

that it is not capable of receiving the transmission and to terminate reception early, reducing power consumption. Sixteen bits are used for the Length field to allow for long packets in the range of 0 to 65 535 bytes. Longer packets than 802.11a are needed to improve efficiency at higher data rates.

In HT-SIG$_2$, the Smoothing bit, Not Sounding bit, and Number of Extension Spatial Streams bits are all related to Tx beamforming. With Tx beamforming or spatial expansion, the resulting channel between the transmitter and receiver could exceed 800 ns. High delay spread results in the decorrelation of adjacent subcarriers. In addition, with certain methods of Tx beamforming, a phase discontinuity could exist between adjacent subcarriers. Both of these conditions degrade the channel estimate when subcarrier smoothing is used (refer to Section 4.1.2 for a discussion on subcarrier smoothing). Under these conditions, the transmitter should set the Smoothing bit to 0 to inform the receiver that only per-carrier (unsmoothed) channel estimation should be employed.

When the Not Sounding bit is set to 0, the transmission is a sounding packet. A sounding packet is used to gather channel state information for Tx beamforming and link adaptation. To sound extra spatial dimensions, beyond that of the Data field, the Number of Extension Spatial Streams field is set to greater than zero. Further detail on sounding packets is found in Section 13.6.

The aggregate bit indicates whether the payload contains a single MPDU (aggregate bit set to 0) or an aggregate of MPDUs (A-MPDU) (aggregate bit set to 1). An A-MPDU contains delimiters between the individual MPDUs. The PHY reports to the MAC that the packet contains an A-MPDU immediately after decoding the HT-SIG. The MAC requires this information in order to extract the individual MPDUs; refer to Section 9.2.2.

The two STBC bits indicate the dimensionality of the STBC operation. When the bits have a value of 0, there is no STBC. The value of 3 is reserved. Other values are discussed in detail in Section 6.3.

The remaining three informational bits include a bit for FEC Coding that is set to 0 to indicate that the data is BCC encoded, or set to 1 to indicate LDPC encoding. The other bit is the Short GI bit, which is set to 1 to indicate that a 400 ns short guard interval is used, rather than the standard 800 ns length guard interval. These features are presented in Chapter 6. The last bit is a reserved bit that is always set to 1.

The CRC protects bits 0 to 33 of the HT-SIG (bits 0 to 23 of HT-SIG$_1$ and bits 0 to 9 of HT-SIG$_2$) (IEEE, 2012). The generator polynomial is $G(D) = D^8 + D^2 + D + 1$. Figure 4.17 shows the operation of the CRC. First, the shift register is reset to all ones. The HT-SIG bits are then passed sequentially through the exclusive-or operation (XOR) at the input. When the last bit has entered, the output is generated by shifting the bits out of the shift register, c7 first, through an inverter.

As an example, if bits [m0...m33] are given by

$$\{1111000100100110000000001110000000\}$$

the resulting CRC bits {c7...c0} are {10101000}.

The 48 HT-SIG bits are BCC encoded with rate ½ resulting in 96 bits. These are split into two symbols. Each symbol is interleaved, BPSK mapped, and has pilot subcarriers

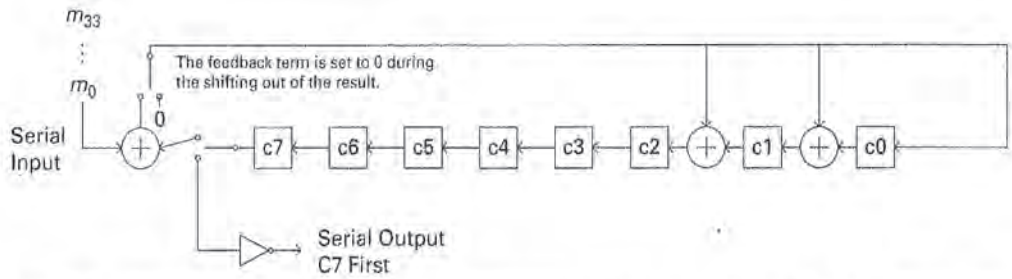

Figure 4.17 HT-SIG CRC calculation. Reproduced with permission from IEEE (2012). IEEE Std 802.11-2012, © 2012 IEEE. All rights reserved.

inserted as described in Section 4.1.3. The complex numbers generated by these steps are denoted as d_k, $k = 0, \ldots, 47$. The resulting time domain waveform for the two HT-SIG OFDM symbols is given in Eq. (4.16). Cyclic shifts are applied to the additional transmit antennas as with the L-SIG. To complete the waveform, a cyclic prefix is prepended to each OFDM symbol.

$$r^{i_{TX}}_{HT-SIG}(t) = \frac{1}{\sqrt{N_{TX} \cdot 52}} \sum_{n=0}^{1} \sum_{k=-26}^{26} \left(\mathrm{j}\, D_{k,n} + p_{n+1} P_k\right) \times \exp\left(\mathrm{j}\, 2\pi\, k \Delta_F \left(t - nT_{SYM} - T_{GI} - T^{i_{TX}}_{CS}\right)\right) \tag{4.16}$$

where D_k is the mapping of complex data values to subcarrier locations, as for L-SIG defined by Eq. (4.15); $T_{SYM} = 4$ μs symbol time composed of 3.2 μs OFDM symbol time and 0.8 μs guard interval; $T^{i_{TX}}_{CS}$ is the non-HT cyclic shift for transmit chain i_{TX} with values given by Table 4.2; $T_{GI} = 0.8$ μs guard interval; P_k denotes the pilot subcarriers defined to be the same as legacy OFDM and given by Eq. (4.4); and p_{n+1} is the pilot polarity defined to be the same as legacy OFDM and given by Eq. (4.5) – since the first value of the sequence is used for L-SIG, HT-SIG uses the next two values.

A windowing function may be applied to each of the HT-SIG symbols to smooth transitions between it and adjacent symbols (refer to Section 4.1.5, and Eqs. (4.6) and (4.7)). The transmitter block diagram for the HT-SIG symbols is illustrated in Figure 4.15.

Note that in Eq. (4.16) the data D_k are rotated by 90 degrees (multiplication by j). Since both the L-SIG and HT-SIG are BPSK modulated, the HT-SIG is rotated by 90 degrees relative to L-SIG, as illustrated in Figure 4.18.

The rotation allows for robust auto-detection between L-SIG and HT-SIG$_1$ to differentiate between legacy OFDM packets and HT MF packets.

An example auto-detection algorithm is as follows. For each symbol that is processed, compute a metric based on the power of the real part of the data subcarriers averaged over the 48 data subcarriers minus the power of the imaginary part of the data subcarriers averaged over the 48 data subcarriers. Figure 4.19 illustrates the relative timing of the preamble fields between legacy and HT MF. During the time spanning 16 μs to 20 μs, the symbol corresponds to the SIG in a legacy OFDM packet or the L-SIG in the HT MF packet. For both packet formats, the metric is a large positive number. During the time

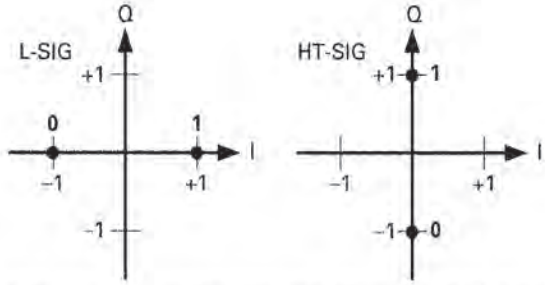

Figure 4.18 Data subcarrier constellations of L-SIG and HT-SIG. Reproduced with permission from IEEE (2012). IEEE Std 802.11-2012, © 2012 IEEE. All rights reserved.

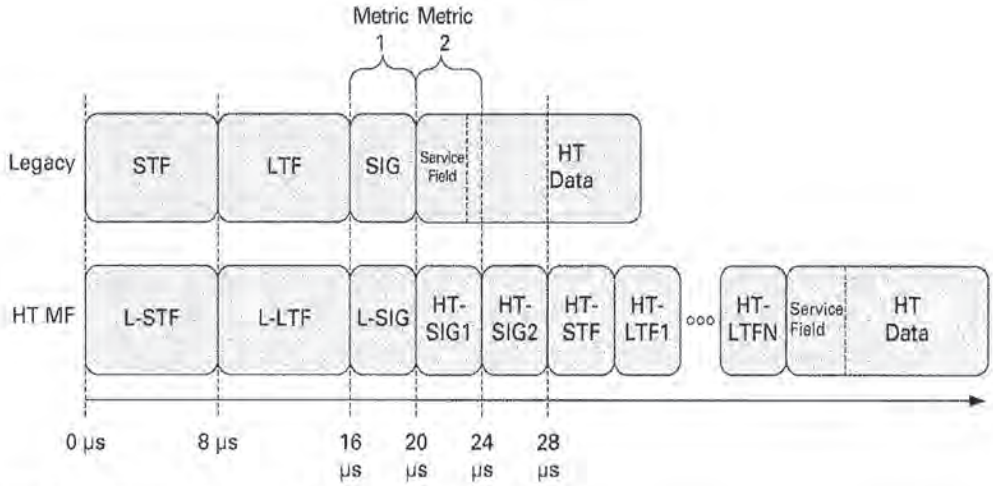

Figure 4.19 Timing of the preamble fields in legacy and HT MF.

spanning 20 μs to 24 μs, the symbol corresponds to the first data symbol in a legacy OFDM packet or HT-SIG$_1$ in the HT MF packet. For the first data symbol in a legacy OFDM packet, the metric ranges from large positive with BPSK modulation to 0 for QAM modulation. (Moreover, in the case of QAM modulation the packet cannot be HT, yet due to pipelining this knowledge is not yet available.) For the HT-SIG$_1$ of the HT MF packet, the metric is a large negative number. Finally, the metric from the time spanning 16 μs to 20 μs is compared with the metric from the time spanning 20 μs to 24 μs. With an appropriate threshold, we can differentiate between a legacy OFDM packet and an HT MF packet.

4.2.2.2 High Throughput Short Training field

As was discussed in Section 4.2.1.1, large cyclic shifts are required to decorrelate the signals when the same spatial stream is sent on the different transmit antenna chains. This was illustrated in Figure 4.13, where, with four transmit antennas, cyclic shifts with a magnitude of 600 ns are required for the STF to have comparable power to the Data field. However, for backward compatibility with legacy OFDM devices, a cyclic shift with

Table 4.3 Cyclic shift for values for HT-STF, HT-LTF, and Data field (IEEE, 2012). IEEE Std 802.11-2012, © 2012 IEEE. All rights reserved

Number of spatial streams	Cyclic shift for spatial stream 1 (ns)	Cyclic shift for spatial stream 2 (ns)	Cyclic shift for spatial stream 3 (ns)	Cyclic shift for spatial stream 4 (ns)
1	0	–	–	–
2	0	–400	–	–
3	0	–400	–200	–
4	0	–400	–200	–600

only a maximum magnitude of 200 ns is needed for L-STF as discussed in Section 4.2.1.2. Therefore, an additional field is added after HT-SIG to enable accurate power estimates for AGC (automatic gain control) setting required for MIMO. The HT-STF allows for a more accurate AGC setting than L-STF and reduces the dynamic range requirement on the ADC. The values of the cyclic shifts for different numbers of spatial streams are given in Table 4.3.

The time domain HT-STF waveform for 20 MHz channel bandwidth for each spatial stream i_{SS} is defined by Eq. (4.17). The subcarrier sequence S_k for the HT-STF is identical to that of the L-STF, defined in Eq. (4.13). For simplicity, we assume that the number of spatial streams is equal to the number of transmit antennas (direct mapping). Spatial mapping, which maps fewer spatial streams to more transmit antennas, is discussed in Section 4.2.3.8.

$$r^{i_{SS}}_{\text{HT-STF}}(t) = \frac{1}{\sqrt{N_{SS} \cdot 12}} \sum_{k=-26}^{26} S_k \exp\left(\mathrm{j}\, 2\pi k \Delta_F \left(t - T^{i_{SS}}_{CS}\right)\right) \tag{4.17}$$

where $\Delta_F = 312.5$ kHz (20 MHz/64); $T^{i_{SS}}_{CS}$ represents the cyclic shift for spatial stream i_{SS} with values given by Table 4.3; and N_{SS} is the number of spatial streams.

The HT-STF symbol is 4.0 μs in length. A windowing function may be applied to the HT-STF symbol to smooth transitions between it and adjacent symbols (refer to Section 4.1.5, and Eqs. (4.6) and (4.7)).

4.2.2.3 High Throughput Long Training field

A new HT Long Training field is provided in the HT MF preamble for MIMO channel estimation. A 4 μs HT long training symbol is transmitted for each spatial stream indicated by the selected MCS, except in the case of three spatial streams where four long training symbols are transmitted. An orthogonal mapping matrix is used to generate the HT-LTF. In order to permit non-complex mapping matrix for three spatial streams, the extra long training symbol was added. The same cyclic shifts as used for HT-STF, defined in Table 4.3, are applied to the long training symbols to accurately match the power variation of the Data field.

The HT-LTF is illustrated in Figure 4.20. The HT long training frequency sequence is multiplied by a value (+1 or −1) from the orthogonal mapping matrix. Each long training symbol is cyclic shifted with values given in Table 4.3.

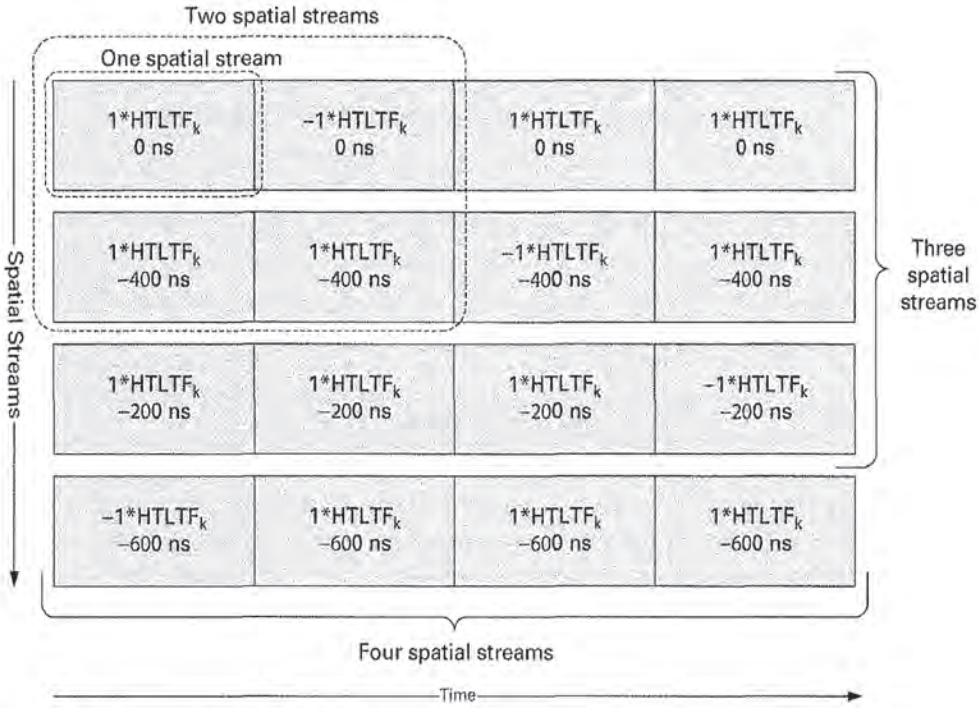

Figure 4.20 Construction of the HT-LTF.

The HT long training symbol for 20 MHz operation is defined based on the frequency domain sequence given in Eq. (4.18) (IEEE, 2012). This sequence is an extension of the legacy long training symbol (defined by Eq. (4.2)), where two additional subcarriers, −28 and −27, are filled with +1 and two additional subcarriers, 27 and 28, are filled with −1:

$$\mathrm{HTLTF}_{-28:28} = \begin{bmatrix} 1,1,1,1,-1,-1,1,1,-1,1,-1,1,1,1,1,1,1,-1,-1,1,1,-1,1,-1, \\ 1,1,1,1,0,1,-1,-1,1,1,-1,1,-1,1,-1,-1,-1,-1,-1,1,1,-1, \\ -1,1,-1,1,-1,1,1,1,1,-1,-1 \end{bmatrix} \tag{4.18}$$

The time domain HT-LTF waveform for 20 MHz channel bandwidth for each spatial stream i_{SS} and for each long training symbol n, $1 \le n \le N_{LTF}$, is defined by Eq. (4.19). For simplicity, we assume that the number of spatial streams is equal to the number of transmit antennas (direct mapping). Spatial mapping, which maps fewer spatial streams to more transmit antennas, is discussed in Section 4.2.3.8.

$$r_{\mathrm{HT-LTF}}^{n,i_{SS}}(t) = \sqrt{\frac{1}{N_{SS} \cdot 56}} \cdot \sum_{k=-28}^{28} [P_{\mathrm{HTLTF}}]_{i_{SS},n} \mathrm{HTLTF}_k \times \exp\left(\mathrm{j}\, 2\pi\, k \Delta_F \left(t - T_{GI} - T_{CS}^{i_{SS}}\right)\right) \tag{4.19}$$

where T_{GI} is the 0.8 μs guard interval; $\Delta_F = 312.5$ kHz (20 MHz/64); $T_{CS}^{i_{SS}}$ represents the cyclic shift for spatial stream i_{SS} with values given by Table 4.3; and N_{SS} is the number of spatial streams.

The orthogonal mapping matrix is given in Eq. (4.20) (IEEE, 2012):

$$P_{HTLTF} = \begin{pmatrix} 1 & -1 & 1 & 1 \\ 1 & 1 & -1 & 1 \\ 1 & 1 & 1 & -1 \\ -1 & 1 & 1 & 1 \end{pmatrix} \tag{4.20}$$

The number of long training symbols is given in Eq. (4.21):

$$N_{LTF} = \begin{cases} N_{SS} & \text{if } N_{SS} = 1, 2, 4 \\ 4 & \text{if } N_{SS} = 3 \end{cases} \tag{4.21}$$

To complete the waveform, a 0.8 μs cyclic prefix is prepended to each 3.2 μs OFDM symbol. A windowing function may be applied to each long training symbol to smooth transitions between it and adjacent symbols (refer to Section 4.1.5, and Eqs. (4.6) and (4.7)).

4.2.3 Data field

Many of the steps in the encoding process of the Data field are the same as 802.11a, a description of which will not be repeated. For an explanation of the 802.11a functions, refer to Section 4.1.5. The transmitter block diagram for the HT Data field is given in Figure 4.21.

The following sections describe the encoding process when using the mandatory binary convolutional code (BCC). Refer to Section 6.4 for the encoding steps when using the optional low density parity check (LDPC) code. In addition, refer to Section 6.3 for the waveform design when using the optional space-time block code (STBC).

4.2.3.1 Bit string

As in 802.11a, the Service field consisting of 16 zero bits is prepended to the data bits. With BCC, six (all zeros) tail bits are appended to the data bits. If necessary, the bit string is extended with pad bits (all zeros) such that the resulting length can be divided equally into an integer multiple of OFDM symbols. The encoding process for the optional LDPC code is described in Section 6.4.

The number of OFDM symbols in the Data field is as follows:

$$N_{SYM} = \left\lceil \frac{8 \cdot \text{length} + 16 + 6}{N_{DBPS}} \right\rceil \tag{4.22}$$

where length is the value of the Length field in octets in the HT-SIG field illustrated in Figure 4.16; and N_{DBPS} is the number of data bits per OFDM symbol determined by the selected MCS.

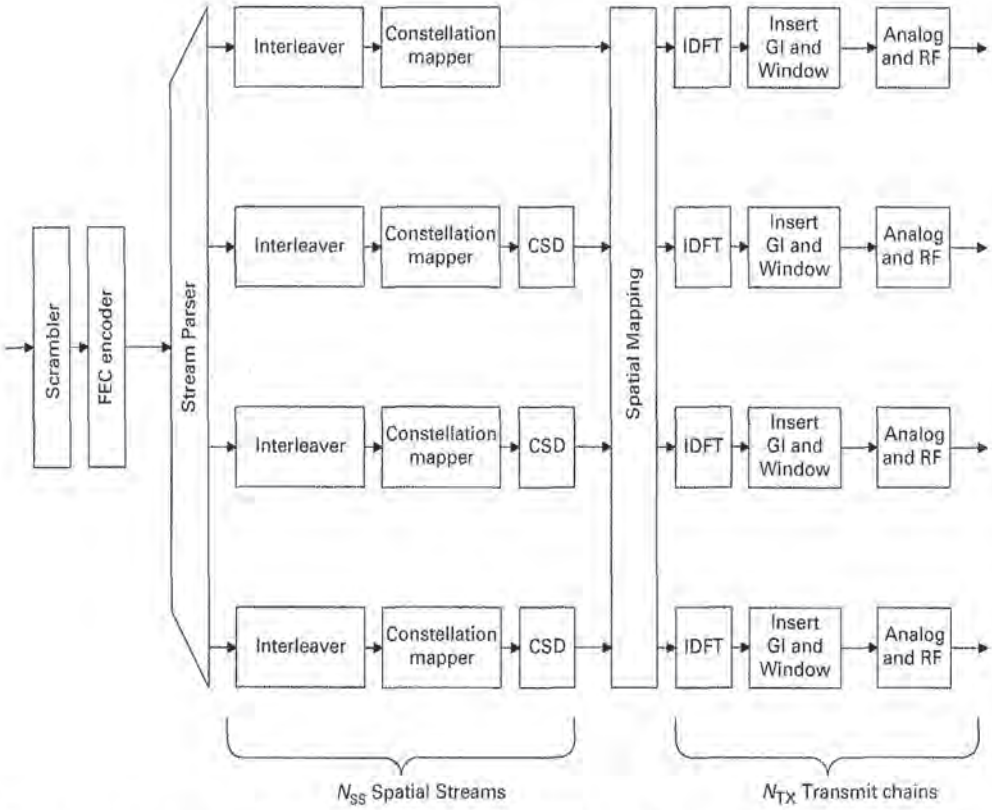

Figure 4.21 Transmitter block diagram for HT Data field. Reproduced with permission from IEEE (2012). IEEE Std 802.11-2012, © 2012 IEEE. All rights reserved.

The symbol $\lceil x \rceil$ denotes the smallest integer greater than or equal to x, corresponding to the *ceiling* function. The number of pad bits is therefore $N_{SYM} \cdot N_{DBPS} - 8 \cdot \text{length} - 16 - 6$.

4.2.3.2 Scrambling and encoding

The resulting data bit string is scrambled with the same scrambler as in 802.11a, described in Section 4.1.4. The six scrambled zero bits that served as tail bits following the data are replaced with the same number of non-scrambled zero bits. This returns the convolutional encoder to the zero state, and is described further in IEEE (2012, Clause 18.3.5.2).

The scrambled bit string is encoded with the rate ½ BCC. After encoding, the bit string is punctured to the selected data rate. Both encoding and puncturing are the same as in 802.11a and are described in Section 4.1.5.

4.2.3.3 Stream parsing

After encoding and puncturing, the bit string is re-arranged into a new set of bit strings equal to the number of spatial streams (N_{SS}). To simplify the description, this section only describes the stream parsing function for equal MCSs. For unequal MCSs, refer to

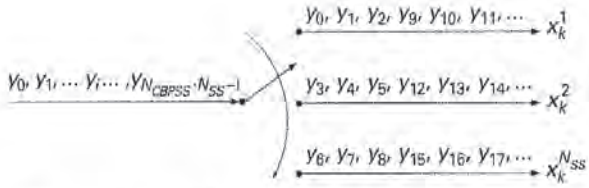

Figure 4.22 Stream parser for single encoder and equal MCS.

Section 13.4. The output of the stream parser is N_{SS} bit strings, each of length N_{CBPSS} (coded bits per spatial stream).

A block of s bits is alternately assigned to different spatial streams in a round robin fashion. Figure 4.22 illustrates an example of 64-QAM ($s = 3$) and three spatial streams.

The size of a block of s bits is determined from a single axis (real or imaginary) of a constellation point, defined in the equation below:

$$s = \max\left\{1, \frac{N_{BPSCS}}{2}\right\} \tag{4.23}$$

where N_{BPSCS} is the number of coded bits per single subcarrier for each spatial stream, or equivalently the modulation order. The output of the stream parser, $x_k^{i_{SS}}$, is a function of the input, y_i, and is defined as follows:

$$\begin{aligned} x_k^{i_{SS}} &= y_i \\ i &= (i_{SS} - 1) \cdot s + s \cdot N_{SS} \cdot \left\lfloor \frac{k}{s} \right\rfloor + k \bmod s \end{aligned} \tag{4.24}$$

where $1 \le i_{SS} \le N_{SS}$ and $k = 0, 1, \ldots, N_{CBPSS} - 1$.

The symbol $\lfloor x \rfloor$ denotes the largest integer less than or equal to x, corresponding to the *floor* function. $k \bmod s$ is defined as the remainder from the division of the integer k by the integer s.

4.2.3.4 Interleaving

After the stream parser, each of the N_{SS} bit strings is interleaved using three permutations if BCC encoding was used. The first two interleaver permutations are based on the interleaver for 802.11a. The first permutation ensures that adjacent coded bits are mapped onto non-adjacent subcarriers (IEEE, 2012). The second permutation ensures that adjacent coded bits are mapped alternately onto less and more significant bits of the constellation, avoiding long runs of low reliability bits (IEEE, 2012). If more than one spatial stream exists, the third operation is applied, which performs a frequency rotation to the additional spatial streams.

In this section, we limit the description of the interleaver to 20 MHz operation and equal MCS to simplify the explanation. Interleaver design for 40 MHz is addressed in Section 5.1.4 and unequal MCS is addressed in Section 13.4.

The output of the first interleaver permutation, $w_k^{i_{SS}}$, is a function of the output of the stream parser, $x_i^{i_{SS}}$, and is defined as follows:

$$w_k^{i_{SS}} = x_k^{i_{SS}}$$
$$i = 4 \cdot N_{BPSCS} \cdot (k \bmod 13) + \left\lfloor \frac{k}{13} \right\rfloor \tag{4.25}$$

where $1 \le i_{SS} \le N_{SS}$, $k = 0,1, \ldots, N_{CBPSS} - 1$.

Comparing the first permutation to that of 802.11a, the modulus and floor function use a factor of 16 because 802.11a consists of 48 data subcarriers, which is divisible by 16. In 802.11n 20 MHz operation, there are 52 data subcarriers, which is divisible by 13.

The output of the second interleaver permutation, $y_k^{i_{SS}}$, is a function of the output of the first interleaver permutation, $w_i^{i_{SS}}$, and is defined as follows:

$$y_k^{i_{SS}} = w_j^{i_{SS}}$$
$$j = s \cdot \left\lfloor \frac{k}{s} \right\rfloor + \left(k + N_{CBPSS} - \left\lfloor \frac{13 \cdot k}{N_{CBPSS}} \right\rfloor \right) \bmod s \tag{4.26}$$

where $1 \le i_{SS} \le N_{SS}$, $k = 0,1, \ldots, N_{CBPSS} - 1$, and s is the same block size as with the stream parser, defined by Eq. (4.23).

If there is more than one spatial stream, the third permutation is performed. The output of the third interleaver permutation, $z_k^{i_{SS}}$, is a function of the output of the second interleaver permutation, $y_r^{i_{SS}}$, and is defined as follows:

$$z_k^{i_{SS}} = y_r^{i_{SS}}$$
$$r = \left(k - \left(((i_{SS} - 1) \cdot 2) \bmod 3 + 3 \cdot \left\lfloor \frac{i_{SS} - 1}{3} \right\rfloor \right) \cdot 11 \cdot N_{BPSCS} \right) \bmod N_{CBPSS} \tag{4.27}$$

where $1 \le i_{SS} \le N_{SS}$, and $k = 0,1, \ldots, N_{CBPSS} - 1$.

4.2.3.5 Modulation mapping

The subcarriers in 802.11n are BPSK, QPSK, 16-QAM, or 64-QAM modulated based on the selected MCS in the same method as in 802.11a (refer to IEEE (2012, Clause 18.3.5.8) or van Nee and Prasad (2000) for further details). The bit streams at the output of the interleaver are accordingly mapped to complex constellation points, with the notation shown in Eq. (4.28) for the data streams. Each 20 MHz HT OFDM symbol consists of 52 complex data values for each stream indexed by k.

$$d_{k,l,n},\ k = 0, 1, \ldots, 51,\ l = 1, \ldots, N_{SS},\ n = 0, 1, \ldots, N_{SYM} - 1 \tag{4.28}$$

where N_{SYM} is the number of OFDM symbols defined in Eq. (4.22), and N_{SS} is the number of spatial streams.

4.2.3.6 Pilot subcarriers

In 802.11n 20 MHz operation, the pilot subcarriers are located in the same subcarriers as in 802.11a, −21, −7, 7, and 21, as given in Eq. (4.29) (IEEE, 2012):

Table 4.4 Pilot subcarrier values for 20 MHz transmission (IEEE, 2012). IEEE Std 802.11-2012, © 2012 IEEE. All rights reserved

N_{ss}	i_{ss}	$\Psi_{i_{ss},0}^{(N_{ss})}$	$\Psi_{i_{ss},1}^{(N_{ss})}$	$\Psi_{i_{ss},2}^{(N_{ss})}$	$\Psi_{i_{ss},3}^{(N_{ss})}$
1	1	1	1	1	−1
2	1	1	1	−1	−1
2	2	1	−1	−1	1
3	1	1	1	−1	−1
3	3	1	−1	1	−1
3	3	−1	1	1	−1
4	1	1	1	1	−1
4	2	1	1	−1	1
4	3	1	−1	1	1
4	4	−1	1	1	1

$$P_{(i_{ss},n)}^{-28,28} = \Big\{0,0,0,0,0,0,0,\Psi_{i_{ss},n\oplus 4}^{(N_{ss})},0,0,0,0,0,0,0,0,0,0,0,0,0, \\ \Psi_{i_{ss},(n+1)\oplus 4}^{(N_{ss})},0,0,0,0,0,0,0,0,0,0,0,0,0,\Psi_{i_{ss},(n+2)\oplus 4}^{(N_{ss})}, \\ 0,0,0,0,0,0,0,0,0,0,0,0,0,\Psi_{i_{ss},(n+3)\oplus 4}^{(N_{ss})},0,0,0,0,0,0,0\Big\} \tag{4.29}$$

where $n \oplus a$ indicates symbol number modulo integer a and the patterns $\Psi_{i_{ss},n}^{(N_{ss})}$ are defined in Table 4.4.

For each spatial stream there is a different pilot subcarrier pattern. In addition, for each number of spatial streams, the set of pilot subcarrier patterns is different. And finally, the pattern is cyclically shifted from symbol to symbol due to the modulo indexing operation of $\Psi_{i_{ss},n\oplus 4}^{(N_{ss})}$ in Eq. (4.29).

4.2.3.7 Transmission in 20 MHz HT format

The 52 data subcarriers and the four pilot subcarriers for each spatial stream are combined and an IFFT is performed to generate the OFDM data symbol. For simplicity, we assume the number of spatial streams is equal to the number of transmit antennas (direct mapping). Spatial mapping, which maps fewer spatial streams to more transmit antennas, is discussed further in Section 4.2.3.8. The resulting time domain waveform for the OFDM data symbols is given by Eq. (4.30). To complete the waveform, a cyclic prefix is prepended to each OFDM symbol:

$$r_{\text{HT-DATA}}^{n,i_{ss}}(t) = \sqrt{\frac{1}{N_{SS}\cdot 56}}\cdot \sum_{n=0}^{N_{SYM}-1}\sum_{k=-28}^{28}\left(D_{k,i_{ss},n} + p_{n+3}P_{(i_{ss},n)}^{k}\right) \\ \times \exp\left(j2\pi k\Delta_F\left(t - nT_{SYM} - T_{GI} - T_{CS}^{i_{ss}}\right)\right) \tag{4.30}$$

where $D_{k,l,n}$ is defined as

$$D_{k,l,n} = \begin{cases} 0 & k = 0, \pm 7, \pm 21 \\ d_{M^r(k),l,n} & \text{otherwise} \end{cases}$$

and

$$M^r(k) = \begin{cases} k + 28 & -28 \le k \le -22 \\ k + 27 & -20 \le k \le -8 \\ k + 26 & -6 \le k \le -1 \\ k + 25 & 1 \le k \le 6 \\ k + 24 & 6 \le k \le 20 \\ k + 23 & 22 \le k \le 28 \end{cases}$$

is the mapping of complex data values to subcarrier locations; T_{GI} is the 0.8 μs guard interval; T_{SYM} is the 4 μs symbol time, composed of 3.2 μs OFDM symbol time and 0.8 μs guard interval; Δ_F = 312.5 kHz (20 MHz/64); $T_{CS}^{i_{SS}}$ represents the cyclic shift for spatial stream i_{SS} with values given by Table 4.3; N_{SS} is the number of spatial streams; N_{SYM} is the number of OFDM symbols defined in Eq. (4.22); p_n is the pilot polarity defined the same as legacy OFDM and given by Eq. (4.5) since the first three values of the sequence are used for L-SIG and HT-SIG, indexing into the pilot polarity sequence is offset by three; and $P^k_{(i_{SS},n)}$ denotes the pilot subcarriers, defined by Eq. (4.29).

A windowing function may be applied to each data symbol to smooth transitions between it and adjacent symbols (refer to Section 4.1.5, and Eqs. (4.6) and (4.7)).

4.2.3.8 Spatial expansion

Consider a device with four antennas wanting to transmit two spatial streams. One reason for the usefulness of this type of configuration is if the current channel environment does not support additional spatial streams. To maximize the output power, each transmit chain needs to be utilized for transmitting the signal. The question arises of how to map fewer spatial streams to more transmit antenna chains without causing unintentional beamforming and making the best use of the available power amplifiers and transmit chains.

Continuing the two spatial stream example, we have complex data for an individual subcarrier and OFDM symbol,

$$\begin{bmatrix} d_1 \\ d_2 \end{bmatrix}$$

After applying the cyclic shift defined for two spatial streams, the complex data is given by

$$\begin{bmatrix} d_1 \\ d_2 \exp(-\mathrm{j}\, 2\pi\, k\Delta_F\, (-400\text{ ns})) \end{bmatrix}$$

As a first step we can repeat the two streams over the additional antennas, as follows:

$$\frac{1}{\sqrt{2}} \begin{bmatrix} d_1 \\ d_2 \exp(-\mathrm{j}\, 2\pi\, k\Delta_F(-400\text{ ns})) \\ d_1 \\ d_2 \exp(-\mathrm{j}\, 2\pi\, k\Delta_F(-400\text{ ns})) \end{bmatrix}$$

However, if such a signal was transmitted, simultaneous transmission of the same signals has undesired beamforming effects. To decorrelate the signals we multiply the signals by a cyclic shift. An example is given below:

$$\frac{1}{\sqrt{2}}\begin{bmatrix} d_1 & \times & \exp(-\mathrm{j}2\pi k\Delta_F(0\mathrm{ns})) \\ d_2\exp(-\mathrm{j}2\pi k\Delta_F(-400\mathrm{ns})) & \times & \exp(-\mathrm{j}2\pi k\Delta_F(0\mathrm{ns})) \\ d_1 & \times & \exp(-\mathrm{j}2\pi k\Delta_F(-200\mathrm{ns})) \\ d_2\exp(-\mathrm{j}2\pi k\Delta_F(-400\mathrm{ns})) & \times & \exp(-\mathrm{j}2\pi k\Delta_F(-200\mathrm{ns})) \end{bmatrix}$$
$$= \frac{1}{\sqrt{2}}\begin{bmatrix} d_1\exp(-\mathrm{j}2\pi k\Delta_F(0\mathrm{ns})) \\ d_2\exp(-\mathrm{j}2\pi k\Delta_F(-400\mathrm{ns})) \\ d_1\exp(-\mathrm{j}2\pi k\Delta_F(-200\mathrm{ns})) \\ d_2\exp(-\mathrm{j}2\pi k\Delta_F(-600\mathrm{ns})) \end{bmatrix}$$

With this selection of cyclic shifts we only attain a 200 ns separation between copies of the same signal. One might be tempted to use a set of cyclic shifts consisting of [0 ns; 0 ns; −400 ns; +400 ns] which would result in an overall cyclic shift on the data of [0 ns; −400 ns; 0 ns; −400 ns] separating the same signals by 400 ns. However, in order for the HT-STF and the HT-LTF to match the data, the same spatial mapping matrix applied to the data must be applied to those fields. In the first case, the spatial mapping applied to the short training symbol would result in

$$\frac{1}{\sqrt{2}}\begin{bmatrix} S\cdot\exp(-\mathrm{j}\,2\pi\,k\Delta_F(0\text{ ns})) \\ S\cdot\exp(-\mathrm{j}\,2\pi\,k\Delta_F(-400\text{ ns})) \\ S\cdot\exp(-\mathrm{j}\,2\pi\,k\Delta_F(-200\text{ ns})) \\ S\cdot\exp(-\mathrm{j}\,2\pi\,k\Delta_F(-600\text{ ns})) \end{bmatrix}$$

which matches the cyclic shifts in Table 4.3. In the second case, the spatial mapping applied to the short training symbol would result in

$$\frac{1}{\sqrt{2}}\begin{bmatrix} S\cdot\exp(-\mathrm{j}\,2\pi\,k\Delta_F(0\text{ ns})) \\ S\cdot\exp(-\mathrm{j}\,2\pi\,k\Delta_F(-400\text{ ns})) \\ S\cdot\exp(-\mathrm{j}\,2\pi\,k\Delta_F(0\text{ ns})) \\ S\cdot\exp(-\mathrm{j}\,2\pi\,k\Delta_F(-400\text{ ns})) \end{bmatrix}$$

Since the same short training symbol is used over all streams, and subsequently all antennas, the resulting cyclic shift must be different for each transmit antenna chain. To summarize, the selection of the spatial mapping matrix must consider the properties of the HT-DATA as well as the HT-STF and HT-LTF.

The 802.11n standard does not specify spatial mapping matrices, though a few examples are given. Table 4.5 gives mapping matrices which result in cyclic shifts on the HT-STF and HT-LTF for each transmit antenna chain that match those in Table 4.3 for the equivalent number of spatial streams. In matrix notation, the resulting signal is $Q_k X_k$, where Q_k is the spatial expansion matrix of dimension $N_{TX} \times N_{SS}$ and X_k is the signal vector of dimension $N_{SS} \times 1$.

Table 4.5 Spatial expansion matrices

N_{TX}	N_{SS}	Q_k
2	1	$\frac{1}{\sqrt{2}}\begin{bmatrix} 1 \\ \exp(-j2\pi\, k\Delta_F(-400\text{ns})) \end{bmatrix}$
3	1	$\frac{1}{\sqrt{3}}\begin{bmatrix} 1 \\ \exp(-j2\pi\, k\Delta_F(-400\text{ns})) \\ \exp(-j2\pi\, k\Delta_F(-200\text{ns})) \end{bmatrix}$
4	1	$\frac{1}{2}\begin{bmatrix} 1 \\ \exp(-j2\pi\, k\Delta_F(-400\text{ns})) \\ \exp(-j2\pi\, k\Delta_F(-200\text{ns})) \\ \exp(-j2\pi\, k\Delta_F(-600\text{ns})) \end{bmatrix}$
3	2	$\frac{\sqrt{2}}{3}\begin{bmatrix} 1 & 0 \\ 0 & 1 \\ \exp(-j2\pi\, k\Delta_F(-200\text{ns})) & 0 \end{bmatrix}$
4	2	$\frac{1}{\sqrt{2}}\begin{bmatrix} 1 & 0 \\ 0 & 1 \\ \exp(-j2\pi\, k\Delta_F(-200\text{ns})) & 0 \\ 0 & \exp(-j2\pi\, k\Delta_F(-200\text{ns})) \end{bmatrix}$
4	3	$\frac{\sqrt{3}}{2}\begin{bmatrix} 1 & 0 & 0 \\ 0 & 1 & 0 \\ 0 & 0 & 1 \\ \exp(-j2\pi\, k\Delta_F(-600\text{ns})) & 0 & 0 \end{bmatrix}$

The waveform equations for HT-STF, HT-LTF, and HT-DATA defined by Eqs. (4.17), (4.19), and (4.30) are modified to incorporate the spatial mapping the matrix Q which maps the N_{SS} spatial streams to the i_{TX} transmit antenna chain, as follows:

$$r_{\text{Field}}^{(i_{TX})}(t) = \frac{1}{\sqrt{N_{SS} \cdot N_{\text{Field}}^{\text{Tone}}}} \sum_{k=-N_{SR}}^{N_{SR}} \sum_{i_{SS}=1}^{N_{SS}} [Q_k]_{i_{TX},i_{SS}} X_k^{i_{SS}} \times \exp\left(j\, 2\pi\, k\Delta_F \left(t - T_{GI}^{\text{Field}} - T_{CS}^{i_{SS}}\right)\right) \tag{4.31}$$

where T_{GI}^{Field} is the 0.8 μs guard interval for HT-LTF and HT-DATA, 0 for HT-STF; $N_{\text{Field}}^{\text{Tone}} =$ 56 for HT-LTF and HT-DATA, 12 for HT-STF; $N_{SR} = 28$ for HT-LTF and HT-DATA, 26 for HT-STF; N_{SS} is the number of spatial streams; $T_{CS}^{i_{SS}}$ represents the cyclic shift for spatial stream i_{SS} with values given by Table 4.3; and $X_k^{i_{SS}} = S_k$ for HT-STF, $[P_{\text{HTLTF}}]_{i_{SS},n}$ HTLTF_k for HT-LTF, and $\left(D_{k,i_{ss},n} + P_{n+3}\, P_{i_{SS},n}^k\right)$ for HT-DATA.

As a final note, transmit beamforming is also used to map spatial streams to transmit antenna chains and is addressed in Chapter 13.

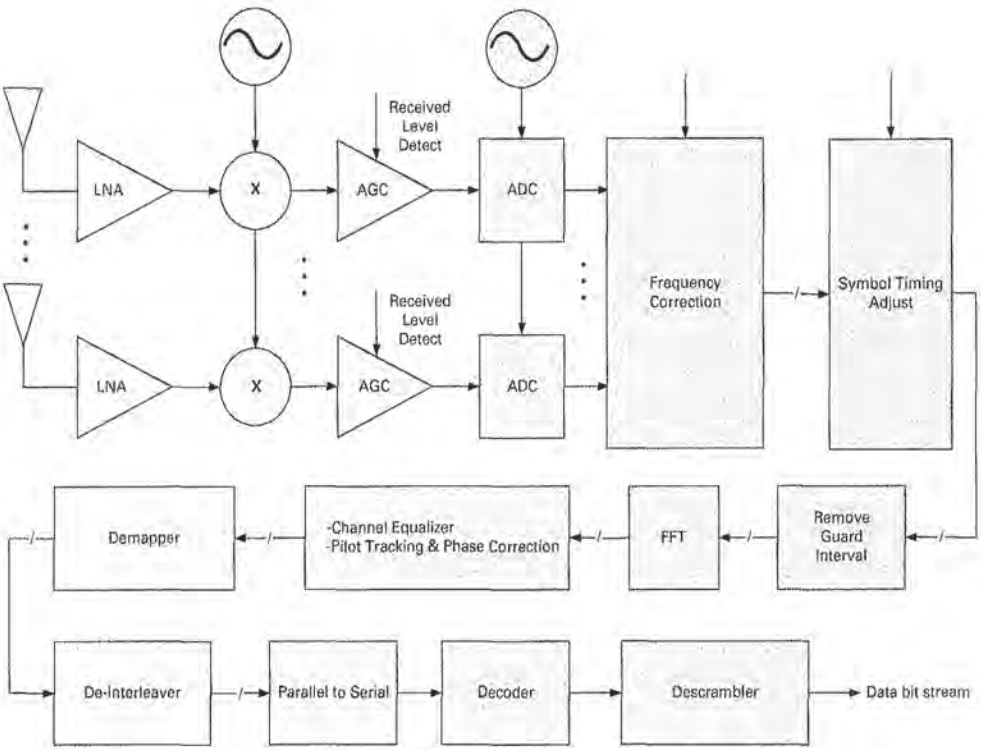

Figure 4.23 Receiver block diagram for MIMO.

4.2.4 HT MF receive procedure

This section describes the receive procedure for the basic modes of operation for 20 MHz. Special conditions due to optional features are addressed in their corresponding sections. Such features include GF preamble, sounding packet, short guard interval, LDPC, and STBC described in Sections 5.4, 13.6, 5.5, 6.4, and 6.3, respectively.

4.2.4.1 RF front end

A basic block diagram for a MIMO receiver is illustrated in Figure 4.23. A MIMO receiver design has multiple receive antenna chains each consisting of an antenna, LNA, down converter, AGC, and ADC. To maximize the dynamic range on each antenna branch, typically each AGC in each receive chain is individually adjusted.

Since the MF packet begins with the legacy preamble, the use of the L-STF for AGC, initial frequency correction, and initial time acquisition is similar to that of 802.11a, described in Section 4.1.6. However, 802.11n devices typically have multiple receive antennas, therefore correlation functions for start-of-packet detection and coarse timing should be summed over all the antennas to maximize detection performance. The coarse time adjustment is applied to all receive signals. Similarly, if in the transmitter all the transmit chains use the same oscillator, and in the receiver all the receive chains use the same oscillator, the frequency estimation described in Section 4.1.1 may also be

summed over all receive antenna chains and applied to all received signals. Since the 802.11n standard mandates that the transmit center frequency and the symbol clock frequency for all transmit antennas is to be derived from the same reference oscillator, the requirement of common oscillator source is not onerous. Further description of time synchronization and frequency estimation for MIMO systems is given in van Zelst and Schenk (2004).

4.2.4.2 Legacy part of the preamble

Processing of the L-LTF and L-SIG follows next as described in Section 4.1.6. However, with the multiple receive antennas of a MIMO receiver, more robust processing may be performed on the single stream transmission of the L-SIG than with a single antenna legacy receiver. Reception of a single stream transmission by multiple receive antennas is generally described in Section 3.2. Furthermore, the benefits of maximal ratio combining are described in Section 6.1.

With a legacy packet, a check of the SIG parity bit to determine the validity of the packet would occur. However, if the packet is an HT packet, it is not necessary to fail the packet upon an invalid L-SIG parity bit. Therefore, the check of the L-SIG parity bit only needs to occur if it has been determined based on auto-detection that the packet is a legacy packet. The auto-detection between legacy and HT MF packets occurs during the next symbol following the L-SIG, which is the HT-SIG for an HT MF packet as described in Section 4.2.2.1.

4.2.4.3 High Throughput Signal field (HT-SIG)

Except for the 90 degree phase rotation, the HT-SIG field is modulated and encoded similarly to the L-SIG and the receive processing steps are the same as that of the L-SIG. With regard to decoding, the HT-SIG data are encompassed by two OFDM symbols and are treated as a single block when decoded. Since the frequency correction and time synchronization were computed based on L-STF and L-LTF, it advisable that phase rotation correction computed during the L-SIG and HT-SIG be used for further frequency offset and symbol timing correction before processing the HT-LTF. This minimizes the error in the channel estimates computed from the HT-LTF.

If signal loss occurs at any point during processing during the legacy part of the preamble and the HT-SIG, the receiver terminates reception. However, the device must not access the medium (defer) for as long as the received signal level remains above −62 dBm (for 20 MHz operation). This ensures that even if the receiver is not able to process the signal, the fundamental nature of carrier sense multiple access is still maintained. This basic operation is termed clear channel assessment (CCA).

In the next step of the receive procedure, the HT-SIG CRC is checked for validity. With a valid determination of the HT-SIG CRC, the information bits in the HT-SIG (described in Section 4.2.2.1) are used to configure the receiver for reception of the packet. At this point even following signal loss, the device refrains from accessing the medium until the transmit time (TXTIME) computed based on the HT-SIG values has expired:

$$\text{TXTIME} = T_{\text{L-STF}} + T_{\text{L-LTF}} + T_{\text{L-SIG}} + T_{\text{HT-SIG}} + T_{\text{HT-STF}} + N_{\text{LTF}} \cdot T_{\text{HT-LTF}} + T_{\text{SYM}} \cdot N_{\text{SYM}} \tag{4.32}$$

where $T_{\text{L-STF}}$, $T_{\text{L-LTF}}$, $T_{\text{HT-SIG}}$ = 8 μs duration; $T_{\text{L-SIG}}$, $T_{\text{HT-LTF}}$, $T_{\text{HT-STF}}$ = 4 μs duration; T_{SYM} = 4 μs duration for 800 ns guard interval operation; N_{SYM} is the number of OFDM symbols in the Data field defined by Eq. (4.22); and N_{LTF} is the number of long training symbols, determined from the MCS – the number of long training symbols is based on the number of spatial streams indicated by the MCS (excluding a sounding packet).

The computation of TXTIME changes for GF preamble, short guard interval, sounding packet, LDPC, and STBC. The modifications for TXTIME are described in Section 5.4.4, 5.5, 13.6, 6.4, and 6.3, respectively.

TXTIME must be computed even if the indicated rate or mode is not supported. An exception to the TXTIME computation is if the reserved bit is decoded as 0. If the HT-SIG CRC is valid, then a reserved bit value of 0 indicates an invalid condition or a false positive of the CRC computation. Furthermore, if the MCS field is in the range 77–127 or the STBC field has a value of 3, TXTIME can not be computed. In these conditions, the device must not access the medium for as long as the received signal level remains above −62 dBm (for 20 MHz operation), rather than based on the TXTIME computation.

One further note on proper CCA, even though the GF preamble is optional, an HT device not capable of receiving such preamble type must still properly defer. Rules regarding CCA of a GF packet received by an HT non-GF capable device are discussed in Section 5.4.4.

4.2.4.4 High Throughput Training fields and MIMO channel estimation

Following the HT-SIG fields is the HT-STF that is used to readjust the AGC, as described in Section 4.2.2.2. The subsequent symbols comprise the HT-LTF used for MIMO channel estimation. To explain the steps to compute the channel estimates for the MIMO channel, we begin with a two stream, two transmit and two receive antenna example. The receiver processes each 3.2 μs long training symbol by removing the cyclic prefix from the HT-LTF and performs an FFT to extract the training subcarriers. For the first symbol in time, indicated by t_1, the frequency domain representation for each training subcarrier k at the receiver is represented by Eq. (4.33). Note that z is AWGN. Refer to Figure 3.4 in Section 3.3 for a general illustration of the MIMO system.

$$\begin{aligned} y_{1,t_1}^k &= h_{11}^k \cdot \text{HTLTF} \cdot e^{-j\,2\pi k \Delta_F T_{CS}^1} + h_{12}^k \cdot \text{HTLTF} \cdot e^{-j\,2\pi k \Delta_F T_{CS}^2} + z_{1,t_1}^k \\ y_{2,t_1}^k &= h_{21}^k \cdot \text{HTLTF} \cdot e^{-j\,2\pi k \Delta_F T_{CS}^1} + h_{22}^k \cdot \text{HTLTF} \cdot e^{-j\,2\pi k \Delta_F T_{CS}^2} + z_{2,t_1}^k \end{aligned} \tag{4.33}$$

Then at the second symbol in time, t_2,

$$\begin{aligned} y_{1,t_2}^k &= h_{11}^k \cdot \text{HTLTF} \cdot (-1) \cdot e^{-j\,2\pi k \Delta_F T_{CS}^1} + h_{12}^k \cdot \text{HTLTF} \cdot e^{-j\,2\pi k \Delta_F T_{CS}^2} + z_{1,t_2}^k \\ y_{2,t_2}^k &= h_{21}^k \cdot \text{HTLTF} \cdot (-1) \cdot e^{-j\,2\pi k \Delta_F T_{CS}^1} + h_{22}^k \cdot \text{HTLTF} \cdot e^{-j\,2\pi k \Delta_F T_{CS}^2} + z_{2,t_2}^k \end{aligned} \tag{4.34}$$

we see the effect of the orthogonal mapping matrix in Eq. (4.20). The "−1" term is from the first row and second column of the matrix. To simplify the expressions, we combine the channel tap h with the cyclic shift, $\tilde{h}_{i,m} = h_{i,m} e^{-j\,2\pi k \Delta_F T_{CS}^{m}}$. As a note, the cyclic shifts applied to the long training symbols are also applied to the data symbols. Redefining the channel taps to incorporate the cyclic shift has the added advantage of automatically removing the effect of the cyclic shift when equalizing the data with the channel estimate, since the channel estimate is the combination of the channel tap and the cyclic shift. The simplification for Eqs. (4.33) and (4.34) is given in the equation below:

$$\begin{aligned} y_{1,t_1}^k &= \tilde{h}_{11}^k \cdot \mathrm{HTLTF} + \tilde{h}_{12}^k \cdot \mathrm{HTLTF} + z_{1,t_1}^k \\ y_{2,t_1}^k &= \tilde{h}_{21}^k \cdot \mathrm{HTLTF} + \tilde{h}_{22}^k \cdot \mathrm{HTLTF} + z_{2,t_1}^k \\ y_{1,t_2}^k &= \tilde{h}_{11}^k \cdot \mathrm{HTLTF} \cdot (-1) + \tilde{h}_{12}^k \cdot \mathrm{HTLTF} + z_{1,t_2}^k \\ y_{2,t_2}^k &= \tilde{h}_{21}^k \cdot \mathrm{HTLTF} \cdot (-1) + \tilde{h}_{22}^k \cdot \mathrm{HTLTF} + z_{2,t_2}^k \end{aligned} \tag{4.35}$$

Once the two symbols are processed and the subcarriers are extracted, the subcarriers from symbol one are combined with the subcarriers from symbol two to derive the channel estimates. First the symbols from antenna one are combined, as follows. The subcarriers from the first symbol are subtracted by the subcarriers from the second symbol to derive the channel estimate for $\tilde{h}_{11}^k$. This cancels out the $\tilde{h}_{12}^k$ term. Then the subcarriers from the first symbol are added with the subcarriers from the second symbol to derive the channel estimate for $\tilde{h}_{12}^k$. This cancels out the $\tilde{h}_{11}^k$ term. This is expressed in the equation below:

$$\begin{aligned} \hat{h}_{11}^k &= \frac{y_{1,t_1}^k - y_{1,t_2}^k}{2 \cdot \mathrm{HTLTF}} \\ \hat{h}_{12}^k &= \frac{y_{1,t_1}^k + y_{1,t_2}^k}{2 \cdot \mathrm{HTLTF}} \end{aligned} \tag{4.36}$$

Using the subcarriers from the second antenna, we similarly derive the channel estimate for $\tilde{h}_{21}^k$ and $\tilde{h}_{22}^k$, as follows:

$$\begin{aligned} \hat{h}_{21}^k &= \frac{y_{2,t_1}^k - y_{2,t_2}^k}{2 \cdot \mathrm{HTLTF}} \\ \hat{h}_{22}^k &= \frac{y_{2,t_1}^k + y_{2,t_2}^k}{2 \cdot \mathrm{HTLTF}} \end{aligned} \tag{4.37}$$

Combining the subcarriers from the two symbols to extract the channel estimate is possible due to the orthogonal mapping matrix.

The derivation of the channel estimates can be generalized to an arbitrary number of spatial streams and receive antennas. First we define the received signal vector Y_{tn} with the number of elements equal to the number of receive antennas (N_{RX}), and the Long Training field index n, $1 \le n \le N_{LTF}$. The received signal vector from each symbol is combined into a single matrix, $[Y_{t_1}|Y_{t_2}| \cdots |Y_{t_{N_{LTF}}}]$ having the dimensions $N_{RX} \times N_{LTF}$, similarly with the noise vector Z; given in the equation below:

$$[Y^k_{t_1}|Y^k_{t_2}|\cdots|Y^k_{t_{N_{\mathrm{LTF}}}}] = \begin{bmatrix} \tilde{h}^k_{11} & \tilde{h}^k_{12} & \cdots & \tilde{h}^k_{1N_{\mathrm{SS}}} \\ \tilde{h}^k_{21} & \tilde{h}^k_{22} & \cdots & \tilde{h}^k_{2N_{\mathrm{SS}}} \\ \vdots & \vdots & \ddots & \vdots \\ \tilde{h}^k_{N_{\mathrm{RX}}1} & \tilde{h}^k_{N_{\mathrm{RX}}2} & \cdots & \tilde{h}^k_{N_{\mathrm{RX}}N_{\mathrm{SS}}} \end{bmatrix} \cdot \tilde{P} \cdot \mathrm{HTLTF}_k + [Z^k_{t_1}|Z^k_{t_2}|\cdots|Z^k_{t_{N_{\mathrm{LTF}}}}] \tag{4.38}$$

where $\tilde{P}$ is an $N_{\mathrm{SS}} \times N_{\mathrm{LTF}}$ subset of the orthogonal mapping matrix P_{HTLTF}. For example, with three spatial streams and four long training symbols,

$$\tilde{P} = \begin{pmatrix} 1 & -1 & 1 & 1 \\ 1 & 1 & -1 & 1 \\ 1 & 1 & 1 & -1 \end{pmatrix}$$

To compute the channel estimate matrix we multiply the received signal vector matrix by the transpose of $\tilde{P}$ and normalize, as follows:

$$\begin{bmatrix} \hat{h}^k_{11} & \hat{h}^k_{12} & \cdots & \hat{h}_{1N^k_{\mathrm{SS}}} \\ \hat{h}^k_{21} & \hat{h}_{22} & \cdots & \hat{h}^k_{2N_{\mathrm{SS}}} \\ \vdots & \vdots & \ddots & \vdots \\ \hat{h}^k_{N_{\mathrm{RX}}1} & \hat{h}^k_{N_{\mathrm{RX}}2} & \cdots & \hat{h}^k_{N_{\mathrm{RX}}N_{\mathrm{SS}}} \end{bmatrix} = \left[Y^k_{t_1}|Y^k_{t_2}|\cdots|Y^k_{t_{N_{\mathrm{LTF}}}}\right] \cdot \tilde{P}^T \cdot \frac{1}{N_{\mathrm{LTF}} \cdot \mathrm{HTLTF}_k} \tag{4.39}$$

4.2.4.5 Data field

Following the HT-LTF is the Data field, which is processed as illustrated in Figure 4.23. For each 4 μs symbol, the 0.8 μs GI is removed and an FFT is performed. The data may be equalized by a linear equalizer as described in Section 3.6, using the channel estimates from the HT-LTF (Eq. (4.39)).

In processing the pilot subcarriers to track the phase rotation, we again highlight the advantage of the receiver using a common oscillator for all the receive chains. A particular pilot subcarrier in the transmitted OFDM symbol in the frequency domain is described by the equation below:

$$\begin{bmatrix} y_1 \\ y_2 \\ \vdots \\ y_N \end{bmatrix} = \begin{bmatrix} h_{11} & h_{12} & \cdots & h_{1M} \\ h_{21} & h_{22} & \cdots & h_{2M} \\ \vdots & \vdots & \ddots & \vdots \\ h_{N1} & h_{N2} & \cdots & h_{NM} \end{bmatrix} \begin{bmatrix} p_1 \\ p_2 \\ \vdots \\ p_M \end{bmatrix} + \begin{bmatrix} z_1 \\ z_2 \\ \vdots \\ z_N \end{bmatrix}$$

or, in vector notation,

$$Y = HP + Z$$

If a common oscillator is employed, the received signal is described by

$$R = e^{j\phi}Y = HPe^{j\phi} + Ze^{j\phi}$$

Extracting the pilot subcarriers and equalizing with the channel estimate results in

$$H^{-1}R = Pe^{j\phi} + H^{-1}Ze^{j\phi}$$

for a ZF receiver. We may further enhance the estimation of the phase rotation by averaging over the spatial streams. As described in Akay and Ayanoglu (2004b), a weighted average using the channel estimates improves performance by de-weighting the subcarriers which are faded.

When a common oscillator is not employed, the received signal is described by the equation below:

$$\begin{bmatrix} r_1 \\ r_2 \\ \vdots \\ r_N \end{bmatrix} = \begin{bmatrix} e^{j\phi_1} & 0 & \cdots & 0 \\ 0 & e^{j\phi_2} & \cdots & 0 \\ \vdots & \vdots & \ddots & \vdots \\ 0 & 0 & \cdots & e^{j\phi_N} \end{bmatrix} \begin{bmatrix} y_1 \\ y_2 \\ \vdots \\ y_N \end{bmatrix}$$

or, in vector notation,

$$R = \Phi Y = \Phi HP + \Phi Z$$

In this case, it is difficult to separate the phase rotation from the channel. Such implementations result in inferior pilot tracking performance.

4.2.4.6 Demapping, deinterleaving, decoding, and descrambling

The demapping operation on each spatial stream is the same for an 802.11a receiver. The deinterleaver uses the following operations to perform the inverse of the interleaving described in Section 4.2.3.4.

The index of the bit in the received block (per spatial stream i_{ss}) is denoted by k. The first permutation reverses the third (frequency rotation) permutation of the interleaver (defined in Eq. (4.27)) if there is more than one spatial stream:

$$\begin{aligned} y_r^{i_{ss}} &= z_k^{i_{ss}} \\ r &= \left(k + \left(((i_{ss} - 1) \cdot 2) \bmod 3 + 3 \cdot \left\lfloor \frac{i_{ss} - 1}{3} \right\rfloor\right) \cdot 11 \cdot N_{BPSCS}\right) \bmod N_{CBPSS} \end{aligned} \tag{4.40}$$

where $1 \le i_{SS} \le N_{SS}$, $k = 0,1, \ldots, N_{CBPSS} - 1$. N_{BPSCS} is the number of coded bits per single subcarrier for each spatial stream, or equivalently the modulation order, and N_{CBPSS} is the coded bits per spatial stream.

The second permutation in the deinterleaver reverses the second permutation in the interleaver (defined in Eq. (4.26)) for each spatial stream:

$$w_j^{i_{SS}} = y_k^{i_{SS}}$$
$$j = s \cdot \text{floor}\,(k/s) + \left(k + \left\lfloor \frac{13 \cdot k}{N_{CBPSS}} \right\rfloor\right) \bmod s \tag{4.41}$$

where $1 \le i_{SS} \le N_{SS}$, $k = 0,1, \ldots, N_{CBPSS} - 1$, and s is defined in Eq. (4.23).

The third permutation in the deinterleaver reverses the first permutation of the interleaver (defined in Eq. (4.25)) for each spatial stream:

$$x_i^{i_{SS}} = w_k^{i_{SS}}$$
$$i = 13 \cdot k - (N_{CBPSS} - 1) \cdot \left\lfloor \frac{k}{4 \cdot N_{BPSCS}} \right\rfloor \tag{4.42}$$

where $1 \le i_{SS} \le N_{SS}$, $k = 0,1, \ldots, N_{CBPSS} - 1$.

As the final step in the deinterleaving process, the stream parsing operation (described in Section 4.2.3.3) is reversed by taking blocks of s bits from each spatial stream in a round robin fashion to create a single bit stream for the decoder.

The resulting convolutional coded data stream is decoded typically with a Viterbi decoder. If the MCS indicates a rate higher than ½, depuncturing is performed at the input of each decoder. Decoder performance can be substantially improved by using the MIMO channel estimates to weight the decoder metrics. Decoding is similar to 802.11a and described further in Section 4.1.6.

The first seven bits of the Service field give the initial state of the descrambler. The same scrambler used in 802.11a is used to descramble the data stream. Bits received after the data length, indicated by the HT-SIG, are discarded.

References

Akay, E. and Ayanoglu, E. (2004a). Low complexity decoding of bit-interleaved coded modulation for M-ary QAM. *International Conference on Communcations*, June 20–24, Paris, France, 901–5.

Akay, E. and Ayanoglu, E. (2004b). High performance Viterbi decoder for OFDM systems. *Vehicular Technology Conference*, May 17–19, Milan, Italy, 323–7.

Aoki, T. and Takeda, D. (2005). *Backward Compatibility of CDD Preambles*, IEEE 802.11-05/0006r1.

Caire, G., Taricco, G., and Biglieri, E. (1998). Bit-interleaved coded modulation. *IEEE Transactions on Information Theory*, **44**(3), 927–46.

Halford, S. (2001). Implementing OFDM in wireless designs. *Communications Design Conference*, October 1, San Jose, CA.

IEEE (2012). *IEEE Standard for Information Technology – Telecommunications and Information Exchange Between Systems – Local and Metropolitan Area Networks – Specific Requirements. Part 11: Wireless LAN Medium Access Control (MAC) and Physical Layer (PHY) Specifications.* IEEE Std 802.11™-2012 (Revision of IEEE Std 802.11-2007).

Proakis, J. G. (1989). *Digital Communications*. New York: McGraw-Hill.

Stephens, A. (2005). *802.11 TGn Functional Requirements*, IEEE 802.11-03/813r13.

van Nee, R. and Prasad, R. (2000). *OFDM for Wireless Multimedia Communications*. Boston, MA: Artech House.

van Zelst, A. and Schenk, T. C. W. (2004). Implementation of a MIMO OFDM-based wireless LAN system. *IEEE Transactions on Signal Processing*, **52**(2), 483–94.

Zehavi, E. (1992). 8-PSK trellis codes for a Rayleigh channel. *IEEE Transactions on Communications*, **40**, 873–84.

Appendix 4.1: 20 MHz basic MCS tables

The following tables consist of the MCSs for 20 MHz "basic" rates. As defined herein, the basic rates include equal modulation and the mandatory 800 ns guard interval. 40 MHz MCSs are described in Section 5.1.4, unequal modulation is described in Section 13.4, and short guard interval is described in Section 5.5.

For 20 MHz, there are 52 data subcarriers and four pilot subcarriers in an OFDM symbol in an individual spatial stream.

Table 4.6 describes the symbols used in the subsequent tables.

Table 4.7 defines the 20 MHz MCS parameters and data rates for single spatial stream transmission. The data rate is calculated by dividing N_{DBPS} by the symbol time of 4 μs (3.2 μs OFDM symbol plus 0.8 μs guard interval).

Table 4.6 Symbols used for MCS parameters (IEEE, 2012). IEEE Std 802.11-2012, © 2012 IEEE. All rights reserved

Symbol	Explanation
R	Code rate
N_{BPSCS}	Number of coded bits per single carrier for each spatial stream (or modulation order)
N_{CBPS}	Number of coded bits per OFDM symbol
N_{DBPS}	Number of data bits per OFDM symbol

Table 4.7 20 MHz MCS parameters for single spatial stream (IEEE, 2012). IEEE Std 802.11-2012, © 2012 IEEE. All rights reserved

MCS index	Modulation	R	N_{BPSCS}	N_{CBPS}	N_{DBPS}	Data rate (Mbps)
0	BPSK	1/2	1	52	26	6.5
1	QPSK	1/2	2	104	52	13.0
2	QPSK	3/4	2	104	78	19.5
3	16-QAM	1/2	4	208	104	26.0
4	16-QAM	3/4	4	208	156	39.0
5	64-QAM	2/3	6	312	208	52.0
6	64-QAM	3/4	6	312	234	58.5
7	64-QAM	5/6	6	312	260	65.0

Table 4.8 defines the 20 MHz MCS parameters and data rates for two spatial stream transmission.

Table 4.9 defines the MCS parameters and data rates for three spatial stream transmission.

Table 4.10 defines the MCS parameters and data rates for four spatial stream transmission.

Table 4.8 20 MHz MCS parameters for two spatial streams (IEEE, 2012). IEEE Std 802.11-2012, © 2012 IEEE. All rights reserved

MCS index	Modulation	R	N_{BPSCS}	N_{CBPS}	N_{DBPS}	Data rate (Mbps)
8	BPSK	1/2	1	104	52	13.0
9	QPSK	1/2	2	208	104	26.0
10	QPSK	3/4	2	208	156	39.0
11	16-QAM	1/2	4	416	208	52.0
12	16-QAM	3/4	4	416	312	78.0
13	64-QAM	2/3	6	624	416	104.0
14	64-QAM	3/4	6	624	468	117.0
15	64-QAM	5/6	6	624	520	130.0

Table 4.9 20 MHz MCS parameters for three spatial streams (IEEE, 2012). IEEE Std 802.11-2012, © 2012 IEEE. All rights reserved

MCS index	Modulation	R	N_{BPSCS}	N_{CBPS}	N_{DBPS}	Data rate (Mbps)
16	BPSK	1/2	1	156	78	19.5
17	QPSK	1/2	2	312	156	39.0
18	QPSK	3/4	2	312	234	58.5
19	16-QAM	1/2	4	624	312	78.0
20	16-QAM	3/4	4	624	468	117.0
21	64-QAM	2/3	6	936	624	156.0
22	64-QAM	3/4	6	936	702	175.5
23	64-QAM	5/6	6	936	780	195.0

Table 4.10 20 MHz MCS parameters for four spatial streams (IEEE, 2012). IEEE Std 802.11-2012, © 2012 IEEE. All rights reserved

MCS index	Modulation	R	N_{BPSCS}	N_{CBPS}	N_{DBPS}	Data rate (Mbps)
24	BPSK	1/2	1	208	104	26.0
25	QPSK	1/2	2	416	208	52.0
26	QPSK	3/4	2	416	312	78.0
27	16-QAM	1/2	4	832	416	104.0
28	16-QAM	3/4	4	832	624	156.0
29	64-QAM	2/3	6	1248	832	208.0
30	64-QAM	3/4	6	1248	936	234.0
31	64-QAM	5/6	6	1248	1040	260.0

7 Very High Throughput PHY

The major new PHY features and enhancements for Very High Throughput (VHT) in 802.11ac include wider bandwidth, modulation/coding/spatial streams, and downlink multi-user (MU) MIMO. The channel bandwidth in 802.11ac was expanded to include 80 MHz and 160 MHz waveforms. With 80 MHz and four spatial streams the maximum data rate is 1733.3 Mbps and with 160 MHz and four spatial streams the maximum data rate is 3466.7 Mbps using the newly defined 256-QAM modulation. A new non-contiguous 80+80 MHz waveform design is also included in VHT to better fit a 160 MHz transmission into the available spectrum. The maximum number of spatial streams increases from four in 802.11n to eight. With 160 MHz and eight spatial streams, the maximum VHT data rate is 6933.3 Mbps. VHT includes additional smaller increases to data rate with 256-QAM. With the addition of downlink multi-user (MU) MIMO to the 802.11 standard, we now have a single user (SU) and MU packet structure. As we will see, these two packet structures have a common VHT preamble format. This is different from 802.11n, which has both a MF and GF preamble format. This chapter will review the new packet structure and waveform for VHT designed in 802.11ac to support the new features for single user transmission. MU transmission will be addressed in Chapter 14. We will also review minor modifications to features borrowed from 802.11n, including STBC and LDPC.

7.1 Channelization

The channelization for 802.11ac is the same as 802.11n for 20 and 40 MHz, with the addition of channel 144 as illustrated in Figure 7.1. Originally, the 802.11 channel numbers ended at 140 in the 5470–5725 MHz band to leave guard band between it and the 5725–5850 band. However, in recent discussions with the FCC, they indicated that overlap between 5150–5250 MHz and 5250–5350 MHz bands and 5470–5725 MHz and 5725–5850 bands is permitted. Note that regulations regarding maximum transmit power and radar detection must be observed in the respective bands. This new guideline allowed for channel 144 and also for 160 MHz channels.

The design of 80 and 160 MHz channels follows the same philosophy as 802.11n of only allowing non-overlapping channels as seen in Figure 7.1. This results in six non-overlapping 80 MHz channels and two non-overlapping 160 MHz channels.

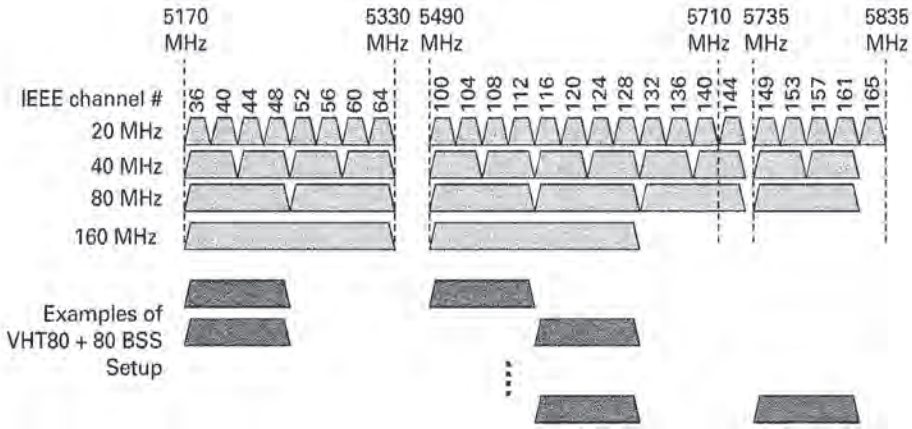

Figure 7.1 802.11ac channelization.

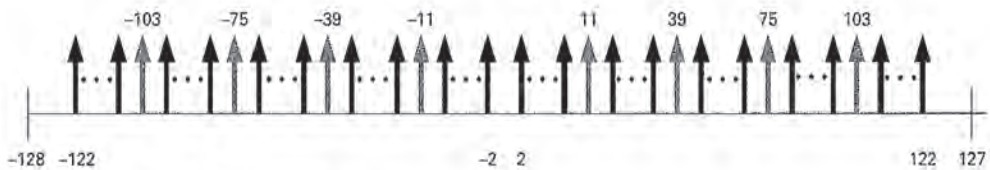

Figure 7.2 80 MHz channelization.

Non-contiguous 160 MHz mode (or 80+80 MHz) is created by selecting any two nonadjacent 80 MHz channels, as illustrated in Figure 7.1. This allows an 80 MHz device to associate with an 80+80 MHz BSS. It also allows a 160 MHz contiguous device to operate as an 80 MHz device and associate with an 80+80 MHz BSS.

The 80 MHz subcarrier design is based on 256 pt FFT and the 160 MHz waveform is based on 512 pt FFT. For 80 MHz, the subcarriers range from −128 to 127, shown in Figure 7.2. There are 14 null subcarriers located at {−128,. . ., −123, −1, 0, 1, 123,. . ., 127} and 242 populated subcarriers located at {−122,. . ., −2, 2,. . ., 122}. The populated subcarriers are comprised of eight pilot subcarriers at positions {−103, −75, −39, −11, 11, 39, 75, 103} and 234 data subcarriers in the remaining populated subcarriers.

The 160 MHz subcarrier structure is made of two 80 MHz portions, as illustrated in Figure 7.3. The lower 80 MHz populated subcarriers in the range of −122 to 122 map to −250 to −6 and the upper 80 MHz populated subcarriers map to 6 to 250. The subcarriers between −256 to −250, −129 to −127, −5 to 5, 127 to 129, and 251 to 255 are null. There are 484 populated subcarriers. Of these, 16 are pilot subcarriers at the corresponding shifted 80 MHz positions, [+/−231, +/−203, +/−167, +/−139, +/−117, +/−89, +/−53, +/−25]. The remaining 486 subcarriers are data, exactly double that of 80 MHz. Though many of the null subcarriers in the center of the channel could have been populated, the key advantage of such a design is that the contiguous 160 MHz and 80+80 MHz subcarrier structures are the same and one could easily build a device compatible with both modes since both are comprised of two 80 MHz subsections.

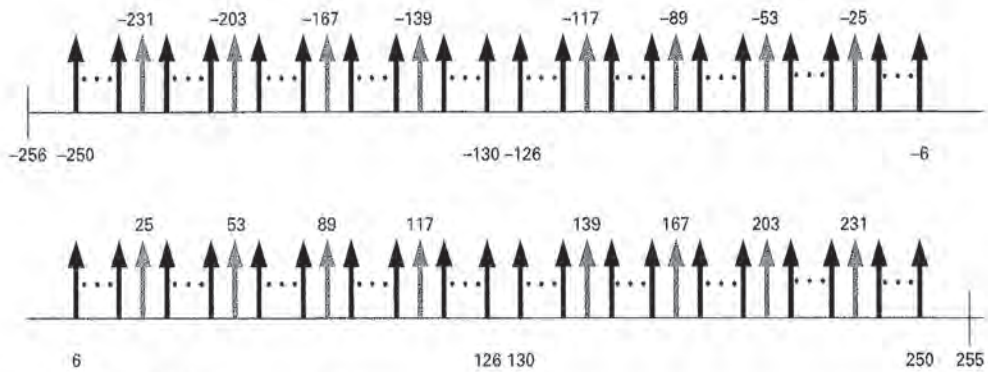

Figure 7.3 160 MHz channelization.

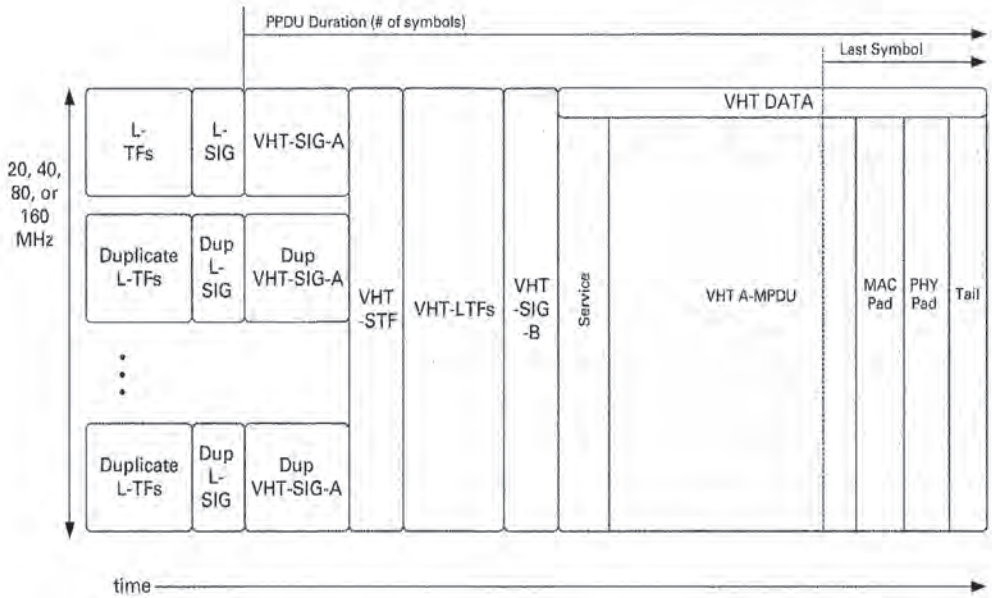

Figure 7.4 SU VHT Packet Structure.

7.2 Single user (SU) VHT packet structure

The SU VHT packet structure is illustrated in Figure 7.4. The SU VHT packet structure begins with parallel legacy training fields, legacy signal field, and the first VHT signal field (VHT-SIG-A) replicated on each 20 MHz sub-channel. The subsequent fields, VHT-LTF, second VHT signal field (VHT-SIG-B) and VHT Data extend the full channel bandwidth. The VHT Data field is comprised of VHT A-MPDU, MAC and PHY padding (if necessary) and tail bits (for BCC).

At this point it is worthwhile to highlight a few changes from 802.11n. In VHT all packets are aggregates, as such are comprised of an A-MPDU. Different from 802.11n, most of the PHY padding was moved to the MAC, where the MAC padding is included

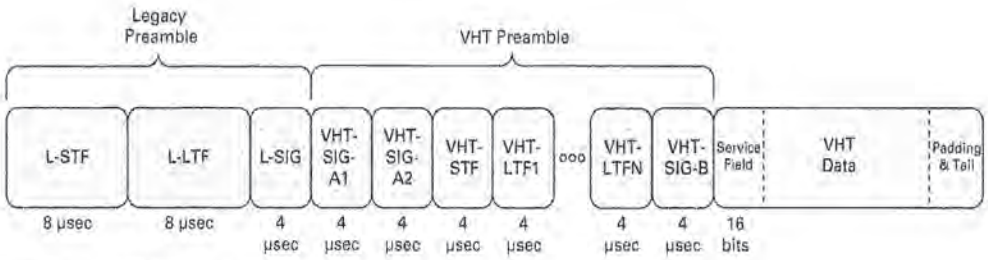

Figure 7.5 VHT Format Preamble.

to fill the frame to the last byte boundary. In addition, PHY padding (0–7 bits) to complete the packet is added and comes before the tail bits. In 802.11n, the tail bits came before the PHY pad bits. In VHT, the L-SIG length and rate fields indicate the PHY packet duration in number of symbols. As we shall see, VHT-SIG-A does not contain length or duration.

7.3 VHT format preamble

The VHT format preamble is illustrated in Figure 7.5. The legacy portion of the preamble has the same format as the legacy portion of the HT MF preamble shown in Figure 4.10. VHT-SIG-A1 and VHT-SIG-A2 replace HT-SIG1 and HT-SIG2, respectively. VHT-STF and VHT-LTF are similar conceptually to HT-STF and HT-LTF, with new sequences for 80 and 160 MHz. There is a modification to VHT-LTF relative to HT-LTF to allow for pilot subcarrier tracking during the VHT-LTFs, which will be discussed in more detail in a subsequent section. The main new field is VHT-SIG-B, added to support MU-MIMO. However, it is also included in the preamble for SU to maintain a single unified preamble format.

7.3.1 Non-VHT portion of the VHT format preamble

Like in 802.11n in Section 4.2.1, the first part of the VHT Format Preamble consists of legacy (non-VHT) training fields. These include the L-STF, L-LTF, and the L-SIG. The subcarrier format and sequences for 20 MHz and 40 MHz for one to four transmit antennas are identical to that of 802.11n given in Sections 4.2.1 and 5.1.3. For greater than four transmit antennas, new cyclic shift values are defined as given in Table 7.1. As noted, the values for one to four transmit antennas are the same as those in Table 4.2. Recall that in Section 5.1.3 for 40 MHz the upper part of the band has a 90° phase rotation, as seen by the "j" multiplication in front of the second summation in Eq. 5.1. For the new 80, 160, and 80+80 MHz bandwidths, new phase rotations are defined as in Eq. (7.2).

The general time domain equation for the L-STF, L-LTF, and L-SIG is given by Eq. (7.1) for transmit chain i_{TX}. For 20, 40, 80, and 160 MHz contiguous, the number

Table 7.1 Cyclic shift values ($T_{CS}^{i_{TX}}$) for L-STF, L-LTF, L-SIG, and VHT-SIG-A fields of the packet (IEEE, 2012)

	Cyclic shift for transmit antenna i_{TX} (in units of ns)								
Total number of transmit antennas (N_{TX})	1	2	3	4	5	6	7	8	>8
1	0	–	–	–	–	–	–	–	–
2	0	−200	–	–	–	–	–	–	–
3	0	−100	−200	–	–	–	–	–	–
4	0	−50	−100	−150	–	–	–	–	–
5	0	−175	−25	−50	−75	–	–	–	–
6	0	−200	−25	−150	−175	−125	–	–	–
7	0	−200	−150	−25	−175	−75	−50	–	–
8	0	−175	−150	−125	−25	−100	−50	−200	–
>8	0	−175	−150	−125	−25	−100	−50	−200	Between −200 and 0 inclusive

Table 7.2 Subcarrier scaling factor (N_{Field}^{Tone}) and highest data subcarrier index (N_{SR}) as a function of bandwidth per frequency segment, and guard interval duration values for L-STF, L-LTF, L-SIG, and VHT-SIG-A

	20 MHz		40 MHz		80 MHz		160 MHz		
Field	N_{Field}^{Tone}	N_{SR}	N_{Field}^{Tone}	N_{SR}	N_{Field}^{Tone}	N_{SR}	N_{Field}^{Tone}	N_{SR}	Guard interval duration
L-STF	12	26	24	58	48	122	96	250	–
L-LTF	52	26	104	58	208	122	416	250	1600 ns
L-SIG	52	26	104	58	208	122	416	250	800 ns
VHT-SIG-A	52	26	104	58	208	122	416	250	800 ns

of frequency segments is one. For 80+80 MHz non-contiguous, there are two frequency segments and Eq. (7.1) is applied to each of the two 80 MHz frequency segments:

$$r_{Field}^{i_{TX}}(t) = \frac{1}{\sqrt{N_{TX} \cdot N_{Field}^{Tone}}} \sum_{k=-N_{SR}}^{N_{SR}} X_{Field,k} \; \Upsilon_{k,BW} \exp\left(j\, 2\pi k \Delta_F \left(t - T_{GI} - T_{CS}^{i_{TX}}\right)\right) \tag{7.1}$$

where $\Delta_F = 312.5$ kHz; $T_{CS}^{i_{TX}}$ represents the cyclic shift for transmit chain i_{TX} with values given by Table 7.1; N_{TX} is the number of transmit chains; $X_{Field,k}$ is the complex value for subcarrier k; N_{Field}^{Tone} is the subcarrier scaling factor given in Table 7.2 for the bandwidth of the frequency segment; N_{SR} is the highest data subcarrier index per frequency segment given in Table 7.2; and $\Upsilon_{k,BW}$ is the phase rotation defined in Eq. (7.2).

The function $\Upsilon_{k,BW}$ is used to represent the phase rotation of the subcarriers for each channel bandwidth:

$$\Upsilon_{k,\mathrm{BW}} = \begin{cases} 1 & 20\ \mathrm{MHz} \\ \begin{Bmatrix} 1 & k<0 \\ j & k\geq 0 \end{Bmatrix} & 40\ \mathrm{MHz} \\ \begin{Bmatrix} 1 & k<-64 \\ -1 & k\geq -64 \end{Bmatrix} & 80\ \mathrm{MHz} \\ \begin{Bmatrix} 1 & k<-192 \\ -1 & -192\leq k<0 \\ 1 & 0\leq k<64 \\ -1 & k\geq 64 \end{Bmatrix} & 160\ \mathrm{MHz} \end{cases} \tag{7.2}$$

For a non-contiguous 80+80 MHz packet transmission, each 80 MHz frequency segment uses the phase rotation for the 80 MHz packet transmission.

7.3.1.1 Non-VHT short training field

The subcarrier sequence $X_{\mathrm{Field},k}$ in Eq. (7.1) given by $S_{-26,26}$ for non-VHT STF (L-STF) for 20 MHz is the same as for the non-HT STF and defined in Section 4.2.1.3. For 40 MHz, $S_{-58,58}$ is the same as for non-HT STF defined in Section 5.1.3, but also given by Eq. (7.3) for clarity. Two new sequences are created for 80 and 160 MHz in Eqs. (7.4) and (7.5), respectively (IEEE, 2012). For 80+80 MHz non-contiguous, each 80 MHz frequency segment uses the L-STF pattern for 80 MHz.

$$S_{-58,58} = \{S_{-26,26}, 0, 0, 0, 0, 0, 0, 0, 0, 0, 0, 0, S_{-26,26}\} \tag{7.3}$$

$$S_{-122,122} = \{S_{-58,58}, 0, 0, 0, 0, 0, 0, 0, 0, 0, 0, 0, S_{-58,58}\} \tag{7.4}$$

$$S_{-250,250} = \{S_{-122,122}, 0, 0, 0, 0, 0, 0, 0, 0, 0, 0, 0, S_{-122,122}\} \tag{7.5}$$

7.3.1.2 Non-VHT long training field

The subcarrier sequence $X_{\mathrm{Field},k}$ in Eq. (7.1) given by $L_{-26,26}$ for non-VHT LTF (L-LTF) for 20 MHz is the same as for the non-HT LTF and defined in Section 4.2.1.4 and Eq. (4.2). For 40 MHz, $L_{-58,58}$ is the same as for non-HT LTF defined in Eq. (5.3) in Section 5.1.3, but also given by Eq. (7.6). Two new sequences are created for 80 and 160 MHz in Eqs. (7.7) and (7.8), respectively (IEEE, 2012). For 80+80 MHz non-contiguous, each 80 MHz frequency segment uses the L-LTF pattern for 80 MHz.

$$L_{-58,58} = \{L_{-26,26}, 0, 0, 0, 0, 0, 0, 0, 0, 0, 0, 0, L_{-26,26}\} \tag{7.6}$$

$$L_{-122,122} = \{L_{-58,58}, 0, 0, 0, 0, 0, 0, 0, 0, 0, 0, 0, L_{-58,58}\} \tag{7.7}$$

$$L_{-250,250} = \{L_{-122,122}, 0, 0, 0, 0, 0, 0, 0, 0, 0, 0, 0, L_{-122,122}\} \tag{7.8}$$

7.3.1.3 Non-VHT signal field

While the structure of the non-VHT Signal Field (L-SIG) is the same for 802.11ac as for 802.11n (see Sections 4.2.1.5 and 5.1.3), the utility is different. In 802.11n the Length field is set such that legacy 802.11a/g devices properly defer based on Eq. (11.4). In

addition, 802.11n devices could ignore L-SIG in an HT packet, see Section 4.2.4.2. As we shall see in the VHT Signal Field A (VHT-SIG-A), there is no length or duration information. Therefore, L-SIG in a VHT packet is used to convey the number of data symbols in the VHT packet, and it is required for a VHT receiver to process L-SIG to determine the PHY packet length.

On transmission, TXTIME (in μs) is computed similarly to 802.11n, but including the new VHT fields, as given in Eq. (7.9):

$$\begin{aligned}\text{TXTIME} = & T_{\text{L-STF}} + T_{\text{L-LTF}} + T_{\text{L-SIG}} + T_{\text{VHT-SIG-A}} + T_{\text{VHT-STF}} \\ & + N_{\text{VHT-LTF}} \cdot T_{\text{VHT-LTF}} + T_{\text{VHT-SIG-B}} + T_{\text{Data}}\end{aligned} \tag{7.9}$$

where

$$T_{\text{Data}} = \begin{cases} T_{\text{SYM}} \cdot N_{\text{SYM}} & \text{for long GI} \\ T_{\text{SYM}} \cdot \left\lceil \dfrac{T_{\text{SYMS}} \cdot N_{\text{SYM}}}{T_{\text{SYM}}} \right\rceil & \text{for short GI} \end{cases}$$

where $T_{\text{L-STF}}$, $T_{\text{L-LTF}}$, $T_{\text{VHT-SIG-A}}$ = 8 μs duration; $T_{\text{L-SIG}}$, $T_{\text{VHT-STF}}$, $T_{\text{VHT-LTF}}$, $T_{\text{VHT-SIG-B}}$ = 4 μs duration; T_{SYM} = 4 μs; T_{SYMS} = 3.6 μs; and $N_{\text{VHT-LTF}}$ is the number of long training symbols determined from the number of space-time streams. The symbol $\lceil x \rceil$ denotes the smallest integer greater than or equal to x, corresponding to the *ceiling* function. N_{SYM} is the number of OFDM symbols in the Data field defined by Eq. (7.10). It is a function of the A-MPDU length prior to end-of-frame MAC padding (A_MPDU_LENGTH):

$$N_{\text{SYM}} = m_{\text{STBC}} \cdot \left\lceil \frac{8 \cdot \text{A\_MPDU\_LENGTH} + 16 + N_{\text{Tail}}}{m_{\text{STBC}} \cdot N_{\text{DBPS}}} \right\rceil \tag{7.10}$$

where m_{STBC} = 2 for STBC, 1 otherwise; N_{DBPS} is the number of data bits per OFDM symbol determined by the selected MCS; and for BCC $N_{\text{Tail}} = 6 \cdot N_{\text{ES}}$ where N_{ES} is the number of encoders, determined by the selected data rate described in Section 7.4, for LDPC $N_{\text{Tail}} = 0$. The "16" term in Eq. (7.10) is for the 16 bits in the Service field.

For LDPC an extra symbol may be added according to Eq. (6.30). If this occurs the LDPC Extra OFDM Symbol bit in VHT-SIG-A is set to one. This is described further below and in Section 7.3.2.1.

The number of total MAC and PHY pad bits is $N_{\text{SYM}} \cdot N_{\text{DBPS}} - 8 \cdot \text{A\_MPDU\_LENGTH} - 16 - 6 \cdot N_{\text{Tail}}$. More information is given on the new VHT padding approach in Section 9.2.4. The PHY payload length (A-MPDU and MAC padding) is computed by Eq. (7.11):

$$\text{PHY\_LENGTH} = \left\lfloor \frac{N_{\text{SYM}} \cdot N_{\text{DBPS}} - 16 - N_{\text{Tail}}}{8} \right\rfloor \tag{7.11}$$

where the symbol $\lfloor x \rfloor$ denotes the largest integer less than or equal to x, corresponding to the *floor* function.

Finally, the Length field set in L-SIG is computed as given in Eq. (7.12) (IEEE, 2012):

$$\text{L\_LENGTH} = \left\lceil \frac{\text{TXTIME} - 20}{4} \right\rceil \cdot 3 - 3 \tag{7.12}$$

The section above computed how to populate the L-SIG based on TXTIME and N_{SYM} on transmission. We go further and examine how the PHY computes N_{SYM} from the L-SIG Length field on reception to understand all the issues involved. First, we compute the RX duration based on the length signaled in L-SIG, as given in Eq. (7.13) (IEEE, 2012):

$$\text{RXTIME } (\mu s) = \left\lceil \frac{\text{L\_LENGTH}+3}{3} \right\rceil \cdot 4 + 20 \tag{7.13}$$

where L_LENGTH is decoded from L-SIG in a VHT packet. Then N'_{SYM} is computed based on RXTIME in addition to information from VHT-SIG-A, as given in Eq. (7.14) (IEEE, 2012):

$$N'_{SYM} = \left\lfloor \frac{\text{RXTIME-}(T_{\text{L-STF}} + T_{\text{L-LTF}} + T_{\text{L-SIG}} + T_{\text{VHT-SIG-A}} + T_{\text{VHT-STF}} + N_{\text{VHT-LTF}} \cdot T_{\text{VHT-LTF}} + T_{\text{VHT-SIG-B}})}{T_{SYM^*}} \right\rfloor \tag{7.14}$$

where $T_{SYM^*} = 4$ μs for long GI and $T_{SYM^*} = 3.6$ μs for short GI. If the packet is encoded with LDPC, the resulting N_{SYM} is given as follows by Eq. (7.15) (IEEE, 2012):

$$N_{SYM} = \begin{cases} N'_{SYM} & \text{if LDPC Extra OFDM Symbol bit} = 0 \text{ in VHT-SIG - A} \\ N'_{SYM} - 1 & \text{if LDPC Extra OFDM Symbol bit} = 1 \text{ and STBC} = 0 \text{ in VHT-SIG-A} \\ N'_{SYM} - 2 & \text{if LDPC Extra OFDM Symbol bit} = 1 \text{ and STBC} = 1 \text{ in VHT-SIG-A} \end{cases} \tag{7.15}$$

This is different from 802.11n, where a receiver had to follow all the LDPC encoder steps (see Section 6.4.1) to determine N_{SYM} and TXTIME, even if the receiver did not support LDPC, for proper deferral.

A problem occurs when receiving a packet with short GI and trying to compute the number of symbols in the Data payload. We first illustrate the problem with an example.

Consider a packet transmission consisting of 20 MHz, single stream, 64-QAM, BCC rate, R = 5/6, no STBC, and short GI. In this case $N_{ES} = 1$, $N_{DBPS} = 260$, and $m_{STBC} = 1$. On transmit, N_{SYM}, TXTIME, and L_LENGTH are computed for a range of A_MPDU_LENGTH values as illustrated in Table 7.3. On reception, RXTIME is computed from L_LENGTH and matches TXTIME. However, N'_{SYM} computed at the receiver is off by one as compared to N_{SYM} at the transmitter.

The problem arises because L-SIG can only indicate time in units of 4 μs, the original symbol duration in 802.11a. As we see in Table 7.3, two N_{SYM} values can map to the same TXTIME and L_LENGTH values. The receiver cannot differentiate between the

Table 7.3 Example of N_{SYM} computation error with short GI

TX				RX	
A_MPDU_LENGTH (Bytes)	N_{SYM}	TXTIME (μs)	L_LENGTH (Bytes)	RXTIME (μs)	N'_{SYM}
1232	38	180	117	180	38
1233	**39**	**184**	**120**	**184**	**40**
1264	**39**	**184**	**120**	**184**	**40**
1265	40	184	120	184	40

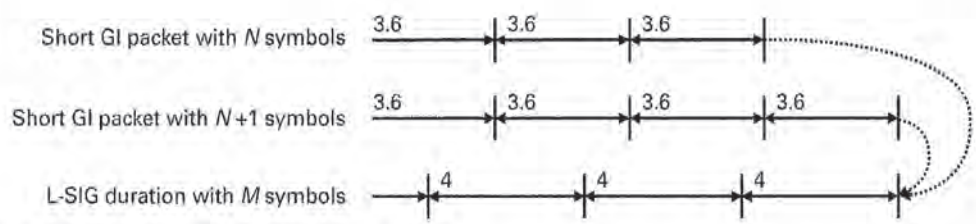

Figure 7.6 L-SIG duration ambiguity with short GI.

two N_{SYM} values. More generally, two 3.6 μs short GI symbol boundaries can map to the same 4 μs long GI boundary indicated by L-SIG, as illustrated in Figure 7.6.

To address this issue, an extra short GI bit is included in VHT-SIG-A. The LSB is set to 1 for short GI. The MSB is set to 1 for short GI AND N_{SYM} mod 10 = 9. Then on receive, N_{SYM} is computed from N'_{SYM} as given in Eq. (7.16). This will correct the example given in Table 7.3 when N_{SYM} is equal to 39.

$$N_{SYM} = \begin{cases} N'_{SYM} - 1 & \text{if short GI} = 11 \text{ in VHT-SIG-A} \\ N'_{SYM} & \text{otherwise} \end{cases} \tag{7.16}$$

We would then use N_{SYM} from Eq. (7.16) to compute the PHY payload length at the receiver with Eq. (7.11).

The waveform for L-SIG is given by Eq. (7.1). The signal field information bits d_k are mapped to subcarrier locations, $X_{\text{Field},k}$, as shown in Eq. (7.17). As with 802.11n for 40 MHz, the L-SIG information only spans 20 MHz and is replicated over the other 20 MHz sub-channels. For VHT, we replicate the L-SIG over each 20 MHz sub-channel for 40, 80, 160, and 80+80 MHz, which is what Eq. (7.17) accomplishes. For 80+80 MHz, Eq. (7.17) is applied for 80 MHz and repeated for each of the two 80 MHz segments:

$$X_{\text{Field},k} = \begin{cases} D_k + p_z P_k & \text{BW} = 20 \text{ MHz} \\ D_{k-\text{sgn}(k)\cdot(\lfloor |k|/64 \rfloor \cdot 64+32)} + p_z P_{k-\text{sgn}(k)\cdot(\lfloor |k|/64 \rfloor \cdot 64+32)} & \text{BW} > 20 \text{ MHz} \end{cases} \tag{7.17}$$

where

$$D_k = \begin{cases} 0 & k = 0, \pm 7, \pm 21, \pm 27, \pm 28, \pm 29, \pm 30, \pm 31, 32 \\ d_{M'(k)} & \text{otherwise} \end{cases}$$

where $M'(k)$ is defined in Eq. (4.15), P_k are the pilot values given in Eq. (4.4), p_z is the polarity of the pilot subcarriers given in Eq. (4.5), and z is equal to 0.

7.3.2 VHT portion of the VHT format preamble

The VHT portion of the VHT format preamble begins with VHT-SIG-A and continues with the VHT-STF, VHT-LTF, and VHT-SIG-B. However, as with HT-SIG in 802.11n, VHT-SIG-A is transmitted with the legacy waveform. The switch to the VHT waveform occurs with the VHT-STF. Any antenna weights are applied starting with VHT-STF, allowing the receiver to recalculate the AGC setting. The cyclic shifts for the VHT portion of the packet also begin with the VHT-STF. The VHT-LTFs are then used to equalize the new VHT-SIG-B and the VHT Data. The new signal field VHT-SIG-B is primarily used to signal multi-user (MU) specific information and it is not required for a single user (SU) device to decode this field. Both VHT-SIG-A and VHT-SIG-B have information specific to a SU or MU packet. In this section, we will focus on signaling for SU. In Chapter 14, we will revisit VHT-SIG-A and VHT-SIG-B and examine their MU signaling.

7.3.2.1 VHT signal field A

The format of VHT-SIG-A for a SU packet is given in Figure 7.7. VHT-SIG-A is comprised of two parts, labeled as VHT-SIG-A1 and VHT-SIG-A2. In VHT-SIG-A1, the BW field is set to 0 for 20 MHz, 1 for 40 MHz, 2 for 80 MHz, and 3 for 160 MHz or 80+80 MHz. The STBC field is only one bit and is set to 0 for no STBC and set to 1 if STBC is applied. Unlike STBC in 802.11n (see Section 6.3.4), the only configuration of STBC in a VHT packet is with the number of space-time streams equal to twice the number of spatial streams.

The Group ID and Partial AID fields are new to VHT. The main utility of Group ID is for MU packets (see Section 14.4). Partial AID is included in SU to provide an earlier indication to the PHY so it can determine if it is the intended recipient of the packet. The MAC configures the PHY with the value that identifies the STA. When the PHY receives a packet where the Partial AID field is not zero and does not match the configured value, it can terminate reception earlier than if the device had waited for receipt of the MAC address. This may provide a small amount of power saving. In an SU packet addressed to an AP, the Group ID is set to 0. If an AP sends an SU packet to one of its STAs, the Group ID is set to 63. In any other SU packet format Group ID is set to 63.

The TXOP_PS_NOT_ALLOWED field supports a new VHT TXOP power save mode. This power save mode is not expected to be widely supported and is not described further in this book. The field is set to 1 by non-AP STAs. In adddition, the field is set to 1 by APs that do not support this feature.

The first bit in VHT-SIG-A2 is the Short GI field, similar to field in HT-SIG in 802.11n. It is set to 1 to indicate that a 400 ns short guard interval is used. The field is set to 0 when the normal 800 ns guard interval is used. The other bit associated with short GI is the

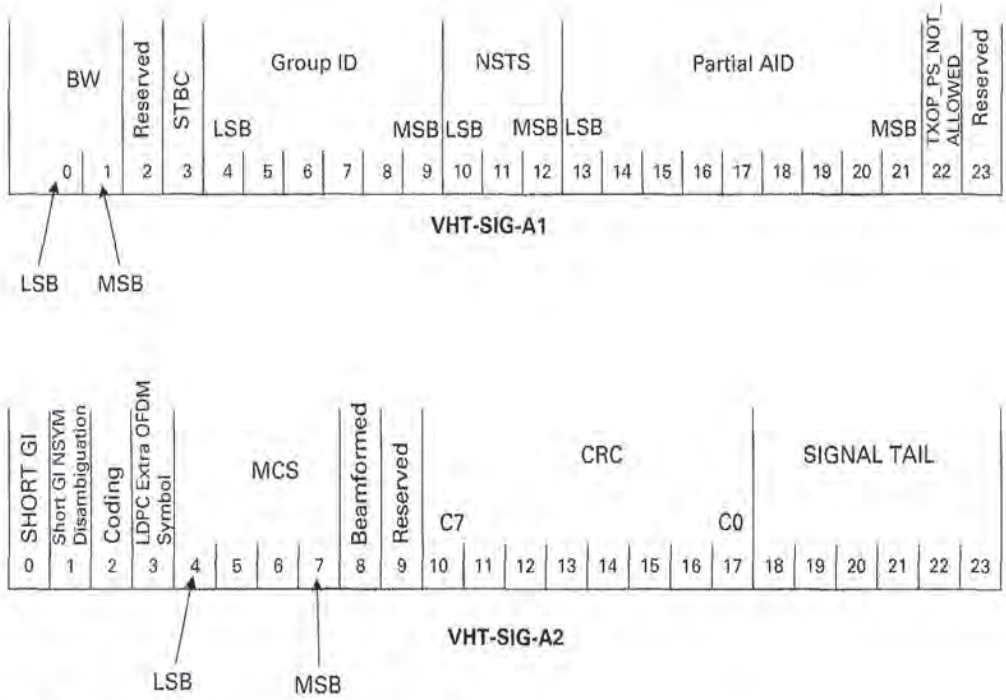

Figure 7.7 VHT-SIG-A structure for SU packet.

Short GI N_{SYM} Disambiguation field. As described in Section 7.3.1.3, this bit is set to 1 if short GI is used and N_{SYM} mod 10 = 9, otherwise the bit is set to 0. Both Short GI bits are used to compute N_{SYM} as discussed in Section 7.3.1.3. The Coding bit is set to 0 for BCC and 1 for LDPC. However, if as described in Section 7.3.3.3, LDPC coding is employed and extra symbol was added in the encoding process, the LDPC Extra OFDM Symbol bit is set to 1. Otherwise, the bit is set to 0.

One can see that the MCS field only has 4 bits compared to 7 bits in HT-SIG for 802.11n. In 802.11ac, MCS only refers to modulation and coding and not to the number of spatial streams. The new N_{STS} field in VHT-SIG-A1 indicates the number of space-time streams. The N_{STS} field is set to 0 for one space-time stream. The field is set to 1 for two space-time streams, etc., up to the value 7 for eight space-time streams. The new MCS table is given in Table 7.10. In VHT, a 256-QAM modulation format was added. The code rates available with this modulation are R = 3/4 and R = 5/6, corresponding to MCS 8 and 9.

As illustrated by Figure 7.7, there is only one bit related to transmit beamforming, whereas in 802.11n HT-SIG there were three. As we shall outline in Section 13.12, only sounding with NDP is permitted in VHT transmit beamforming, therefore there is no need for HT-SIG fields like Not Sounding or Number of Extension Spatial Streams. Furthermore, it was overly complicated to determine how to set the HT-SIG Smoothing bit since the transmitter had to somehow determine the delay spread of the channel. In 802.11ac, we only have the Beamformed field in VHT-SIG-A2. The bit is set to 1 if a beamforming steering matrix is applied to the waveform, otherwise it is set to 0. No determination of the channel delay spread is required. As beamforming may cause a phase discontinuity between adjacent subcarriers, care needs to be taken when applying smoothing when the Beamformed bit is set to 1.

The Reserved bit is set to 1. Both the CRC and the tail are the same as that in HT-SIG in 802.11n, and are described in Section 4.2.2.1.

As depicted in Figure 7.7, VHT-SIG-A consists of a total of 48 bits. These are BCC encoded with rate ½ resulting in 96 bits. These are then split into two symbols, and each one is interleaved. The first symbol is BPSK modulated and the second symbol is QBPSK modulated (BPSK with 90° rotation) and mapped onto the data subcarriers. As with L-SIG, the two VHT-SIG-A symbols span 20 MHz and are duplicated across each additional 20 MHz sub-channel. The time domain waveform for each symbol is given by Eq. (7.1). $X_{\text{Field},k}$ for the first symbol is described in Eq. (7.18):

$$X_{\text{Field},k} = \begin{cases} D_k + p_z P_k & \text{BW} = 20\ \text{MHz} \\ D_{k-\text{sgn}(k)\cdot(\lfloor |k|/64 \rfloor \cdot 64+32)} + p_z P_{k-\text{sgn}(k)\cdot(\lfloor |k|/64 \rfloor \cdot 64+32)} & \text{BW} > 20\ \text{MHz} \end{cases} \tag{7.18}$$

where D_k is given in Eq. (7.17) and z is equal to 1. For the second symbol, $X_{\text{Field},k}$ is described in Eq. (7.19):

$$X_{\text{Field},k} = \begin{cases} \text{j}D_k + p_z P_k & \text{BW} = 20\ \text{MHz} \\ \text{j}D_{k-\text{sgn}(k)\cdot(\lfloor |k|/64 \rfloor \cdot 64+32)} + p_z P_{k-\text{sgn}(k)\cdot(\lfloor |k|/64 \rfloor \cdot 64+32)} & \text{BW} > 20\ \text{MHz} \end{cases} \tag{7.19}$$

where p_z is given in Eq. (4.5) and z is equal to 2. Notice the j term is the 90° rotation.

The reason for the rotation on the second symbol of VHT-SIG-A is for auto-detection between 802.11a, 802.11n MF, and VHT preamble formats. As illustrated in Figure 7.8,

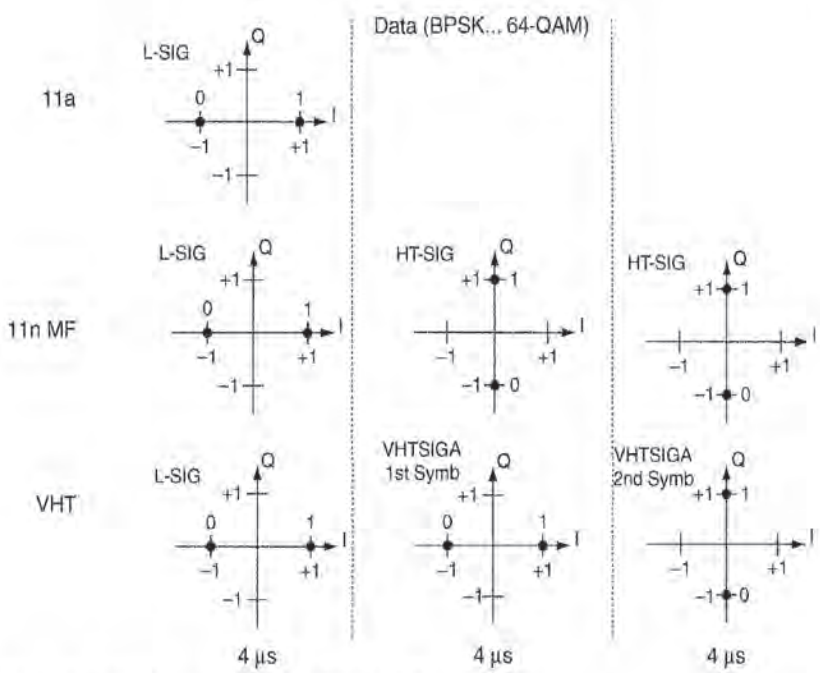

Figure 7.8 Auto-detection between 802.11a, 802.11n MF, and VHT.

L-SIG arrives with BPSK format at the same time in the preamble for all three system types. The next symbol in time, following the L-SIG for all configurations, will be Data for 802.11a, QBPSK modulated HT-SIG for 802.11n, and BPSK for VHT. At this point if the receiver detects QPSK or higher modulation, it knows that packet is 802.11a format. If the modulation is QBPSK, the format is 802.11n MF. However, if the format is BPSK, it could be either 802.11a or VHT. By the next symbol, the receiver can differentiate between 802.11a and VHT since the modulation for the second symbol of VHT-SIG-A is QBPSK.

7.3.2.2 VHT short training field

Signaling of the VHT waveform begins with the VHT-STF. With this field, we switch to the VHT cyclic shifts given in Table 7.4. We see that the cyclic shift values are the same as 802.11n HT cyclic shifts for 1 to 4 spatial streams (Table 4.3).

The time domain waveform of the VHT-STF, VHT-LTF, VHT-SIG-B, and Data fields for transmit chain i_{TX} is represented by Eq. (7.20). The VHT-LTF and Data fields may have multiple symbols indicated by n, otherwise the index n is disregarded. For 80 +80 MHz non-contiguous transmission, there are two frequency segments. In this case Eq. (7.20) is applied to each frequency segment:

$$r_{\text{Field}}^{(i_{\text{TX}},n)}(t) = \frac{1}{\sqrt{N_{\text{STS}} \cdot N_{\text{Field}}^{\text{Tone}}}} \times \sum_{i_{\text{SS}}=1}^{N_{STS}} \sum_{k=-N_{\text{SR}}}^{N_{\text{SR}}} [Q_k]_{i_{\text{TX}},i_{\text{SS}}} X_{\text{Field},k,i_{\text{SS}},n} \Upsilon_{k,\text{BW}} \exp\left(j 2\pi k \Delta_{\text{F}} \left(t - T_{\text{GI}} - T_{\text{CS}}^{i_{\text{SS}}}\right)\right) \tag{7.20}$$

where $\Delta_{\text{F}} = 312.5$ kHz; T_{GI} is the guard interval duration given by Table 7.5; $T_{\text{CS}}^{i_{\text{SS}}}$ represents the cyclic shift for spatial stream i_{SS} with values given by Table 7.4; N_{STS} is the number of space-time streams; $X_{\text{Field},k,i_{\text{SS}},n}$ is the complex value for subcarrier k, spatial stream i_{SS}, and symbol n; $[Q_k]_{i_{\text{TX}},i_{\text{SS}}}$ is the spatial mapping matrix mapping N_{STS}

Table 7.4 Cyclic shift values ($T_{\text{CS}}^{i_{\text{SS}}}$) for VHT-STF, VHT-LTF, VHT-SIG-B, and Data fields of the packet (IEEE, 2012)

Total number of space-time streams (N_{STS})	Cyclic shift for space-time stream i_{SS} (in units of ns)							
	1	2	3	4	5	6	7	8
1	0	–	–	–	–	–	–	–
2	0	−400	–	–	–	–	–	–
3	0	−400	−200	–	–	–	–	–
4	0	−400	−200	−600	–	–	–	–
5	0	−400	−200	−600	−350	–	–	–
6	0	−400	−200	−600	−350	−650	–	–
7	0	−400	−200	−600	−350	−650	−100	–
8	0	−400	−200	−600	−350	−650	−100	−750

Table 7.5 Subcarrier scaling factor ($N_{\text{Field}}^{\text{Tone}}$) and highest data subcarrier index (N_{SR}) as a function of bandwidth per frequency segment, and guard interval duration values for VHT-STF, VHT-LTF, VHT-SIG-B, and Data fields

	20 MHz		40 MHz		80 MHz		160 MHz		
Field	$N_{\text{Field}}^{\text{Tone}}$	N_{SR}	$N_{\text{Field}}^{\text{Tone}}$	N_{SR}	$N_{\text{Field}}^{\text{Tone}}$	N_{SR}	$N_{\text{Field}}^{\text{Tone}}$	N_{SR}	Guard interval duration T_{GI}
VHT-STF	12	28	24	58	48	122	96	250	–
VHT-LTF	56	28	114	58	242	122	484	250	800 ns
VHT-SIG-B	56	28	114	58	242	122	484	250	800 ns
Data	56	28	114	58	242	122	484	250	800 ns or 400 ns

space-time streams to N_{TX} transmit chains; $N_{\text{Field}}^{\text{Tone}}$ is the subcarrier scaling factor given in Table 7.5 for the bandwidth of the frequency segment; N_{SR} is the highest data subcarrier index per frequency segment given in Table 7.5; and $\Upsilon_{k,\text{BW}}$ is the phase rotation defined in Eq. (7.2).

The time domain representation of VHT-STF is given by Eq. (7.20), with $X_{\text{Field},k}$ identical to that used for L-STF in Section 7.3.1.1 and the respective parameter values in Eq. (7.20) taken from Table 7.5.

7.3.2.3 VHT long training field

The construction of VHT-LTF is similar to that of HT-LTF illustrated in Figure 4.20, with some notable differences: (1) up to eight spatial streams, (2) up to 160 MHz, and (3) allowance for phase tracking during VHT-LTF.

The VHT-LTF has been expanded to accommodate up to eight spatial streams with the number of symbols (N_{LTF}) given by

$$N_{\text{LTF}} = \begin{cases} N_{\text{STS}} & \text{if } N_{\text{STS}} = 1,2,4,6,8 \\ N_{\text{STS}} + 1 & \text{if } N_{\text{STS}} = 3,5,7 \end{cases} \tag{7.21}$$

For simplicity, the 20 and 40 MHz sequences for HT-LTF in Eqs. (4.18) and (5.4), respectively, are used for corresponding VHT bandwidths. The new sequence for 80 MHz is as follows in Eq. (7.22) (IEEE, 2012):

$$\begin{aligned} &\text{VHTLTF}_{-122,122} = \\ &\quad \{\text{LTF}_{\text{left}}, 1, \text{LTF}_{\text{right}}, -1, -1, -1, 1, 1, -1, 1, -1, 1, 1, -1, \text{LTF}_{\text{left}}, 1, \text{LTF}_{\text{right}}, \\ &\qquad 1, -1, 1, -1, 0, 0, 0, 1, -1, -1, 1, \\ &\quad \text{LTF}_{\text{left}}, 1, \text{LTF}_{\text{right}}, -1, -1, -1, 1, 1, -1, 1, -1, 1, 1, -1, \text{LTF}_{\text{left}}, 1, \text{LTF}_{\text{right}}\} \end{aligned} \tag{7.22}$$

where

$$\text{LTF}_{\text{left}} = \{1, 1, -1, -1, 1, 1, -1, 1, -1, 1, 1, 1, 1, 1, 1, -1, -1, 1, 1, -1, 1, -1, 1, 1, 1, 1\}$$
$$\text{LTF}_{\text{right}} = \{1, -1, -1, 1, 1, -1, 1, -1, 1, -1, -1, -1, -1, -1, 1, 1, -1, -1, 1, -1, 1, -1, 1, 1, 1, 1\}$$

LTF_{left} is the same sequence of values as the left most 26 elements in Eq. (4.2) and LTF_{right} is the same sequence of values at the 26 right most elements in Eq. (4.2). The new sequence for 160 MHz is comprised of the 80 MHz sequences as given in Eq. (7.23) (IEEE, 2012):

$$VHTLTF_{-250,250} = \{VHTLTF_{-122,122}, 0, 0, 0, 0, 0, 0, 0, 0, 0, 0, 0, VHTLTF_{-122,122}\} \tag{7.23}$$

Referring again to Figure 4.20, the +1/–1 multiplier values are from the orthogonal mapping matrix (the P matrix in Eq. (4.19)). In 802.11n, these values are applied to subcarriers indexes corresponding to both data and pilot. Therefore we have different pilot sequence values for different space-time streams. However, this also means there are no pilot subcarriers in the HT-LTF for phase tracking. In the worst case in 802.11n for four spatial streams, the receiver is not able to perform phase tracking to mitigate phase noise and carrier frequency drift during the 4 HT-LTF symbols (or 16 μs).

With up to eight spatial streams in 802.11ac, the VHT-LTF duration can be twice as long, up to 32 μs. Analysis in Shi *et al.* (2010), reported that the average channel estimation SNR can degrade to 24.5 dB due to –41dBc integrated phase noise at both TX and RX and a residual frequency offset of 1 kHz. To mitigate this degradation, pilot subcarriers are inserted into VHT-LTF symbols that allow the receiver to track the phase during the VHT-LTFs. This is achieved by using identical pilot values for all space-time streams for VHT-LTF and the Data field by not multiplying the subcarriers at pilot locations by the P matrix.

During the VHT-LTFs, the receiver estimates the channel on the pilot subcarriers during the first long training symbols. Then during subsequent long training symbols, the pilot subcarriers are equalized and the phase rotation is tracked and corrected. However, phase tracking during the VHT-LTFs is not required.

Figures 7.9 and 7.10 demonstrate the benefit of phase tracking during the VHT-LTFs. The simulations are conducted with channel model D, NLOS, and with the physical layer impairments described in Section 3.5.5. The equalizer is based on MMSE. Synchronization, channel estimation, and phase tracking are included in the simulation to give an accurate model for algorithm degradations. The packet length is 3000 bytes. Three spatial streams are transmitted, and four antennas are used at the receiver. In Figure 7.9, the data is modulated with 64-QAM and BCC encoded with a code rate of 5/6. In Figure 7.10, the data is modulated with 256-QAM and BCC encoded with a code rate of 5/6. The frequency offset is modeled by an initial offset ramping to zero after 100 μsec, to model LO pull-in.

With 64-QAM and no phase tracking during the VHT-LTFs, performance degrades 3 dB at a 1% PER with a 5 kHz offset (dashed line with diamonds in Figure 7.9). With phase tracking, the performance only degrades by 1 dB for a 2 dB improvement (solid line with diamonds in Figure 7.9). With 256-QAM, a frequency error of 2 kHz degrades the 1% PER by 3.5 dB when there is no phase tracking during the VHT-LTFs (the dashed line with diamonds in Figure 7.10). However, with phase tracking, the degradation is only 0.5 dB, demonstrating an improvement of 3 dB (the solid line with diamonds in Figure 7.10).

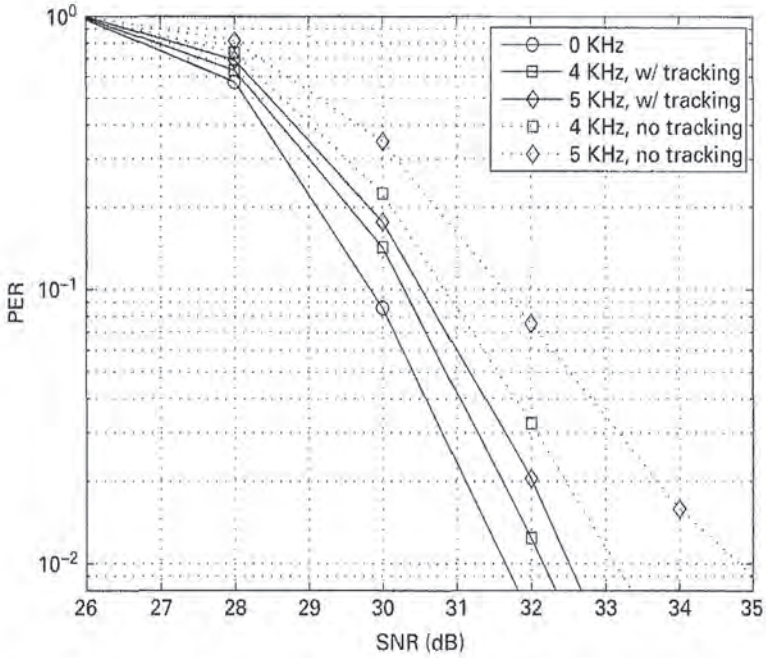

Figure 7.9 Benefit of phase tracking during VHT-LTF, with 64-QAM.

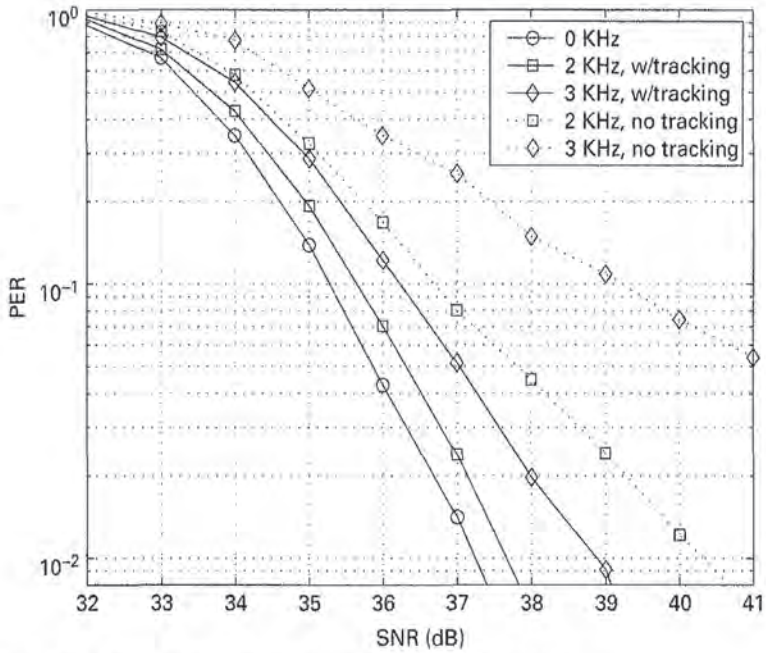

Figure 7.10 Benefit of phase tracking during VHT-LTF, with 256-QAM.

By applying the P matrix to pilot subcarriers in 802.11n, the receiver was able to perform per-stream phase tracking during the data symbols. Without the P matrix on the pilot subcarriers in 802.11ac, this is not possible unless the receiver performs MIMO channel estimation for pilot subcarrier locations via frequency domain interpolation. Furthermore, for TxBF feedback the pilot subcarrier locations are skipped in 802.11ac.

The P matrix for the data subcarrier locations for four or less space-time streams ($P_{\text{VHTLTF},4\times4}$) is the same as 802.11n in Eq. (4.20). For five and six space-time streams, the P matrix is defined in Eq. (7.24) (IEEE, 2012):

$$P_{\text{VHTLTF},6\times6} = \begin{bmatrix} 1 & -1 & 1 & 1 & 1 & -1 \\ 1 & -w^1 & w^2 & w^3 & w^4 & -w^5 \\ 1 & -w^2 & w^4 & w^6 & w^8 & -w^{10} \\ 1 & -w^3 & w^6 & w^9 & w^{12} & -w^{15} \\ 1 & -w^4 & w^8 & w^{12} & w^{16} & -w^{20} \\ 1 & -w^5 & w^{10} & w^{15} & w^{20} & -w^{25} \end{bmatrix} \tag{7.24}$$

where

$$w = \exp(-j2\pi/6)$$

For seven and eight space-time streams, the P matrix is given in Eq. (7.25) (IEEE, 2012):

$$P_{\text{VHTLTF},8\times8} = \begin{bmatrix} P_{\text{VHTLTF},4\times4} & P_{\text{VHTLTF},4\times4} \\ P_{\text{VHTLTF},4\times4} & -P_{\text{VHTLTF},4\times4} \end{bmatrix} \tag{7.25}$$

The mapping matrix (B matrix) for the pilot subcarrier locations is derived from the first column of the P matrix and is defined in Eq. (7.26):

$$\left[B_{\text{VHTLTF},N_{\text{LTF}}\times N_{\text{LTF}}}\right]_{i_{\text{SS}},n} = \left[P_{\text{VHTLTF},N_{\text{LTF}}\times N_{\text{LTF}}}\right]_{1,n} \tag{7.26}$$

The resulting $X_{\text{Field},k,i_{\text{SS}},n}$ value for subcarrier k, spatial stream i_{SS}, and symbol n in the time domain waveform in Eq. (7.20) for VHT-LTF is defined in Eq. (7.27):

$$X_{\text{VHTLTF},k,i_{\text{SS}},n} = \left[A_{\text{VHTLTF},N_{\text{LTF}}\times N_{\text{LTF}}}\right]_{i_{\text{SS}},n} \text{VHTLTF}_k \tag{7.27}$$

where

$$\left[A_{\text{VHTLTF},N_{\text{LTF}}\times N_{\text{LTF}}}\right]_{i_{\text{SS}},n} = \begin{cases} \left[B_{\text{VHTLTF},N_{\text{LTF}}\times N_{\text{LTF}}}\right]_{i_{\text{SS}},n} & \text{if } k \in K_{\text{Pilot}} \\ \left[P_{\text{VHTLTF},N_{\text{LTF}}\times N_{\text{LTF}}}\right]_{i_{\text{SS}},n} & \text{otherwise} \end{cases}$$

$1 \le n \le N_{\text{LTF}}$,

$$K_{\text{Pilot}} = \begin{cases} \pm7, \pm21 & \text{for 20 MHz} \\ \pm11, \pm25, \pm53 & \text{for 40 MHz} \\ \pm11, \pm39, \pm75, \pm103 & \text{for 80 MHz} \\ \pm25, \pm53, \pm89, \pm117, \pm139, \pm167, \pm203, \pm231 & \text{for 160 MHz} \end{cases}$$

7.3.2.4 VHT signal field B

While the primary usage of VHT-SIG-B is for signaling user specific information in a MU packet, it is still included in all packets to maintain a single unified preamble format for VHT packets. For SU, however, the receiver is not required to process VHT-SIG-B.

Since VHT-SIG-B comes after VHT-STF and VHT-LTF, it is formatted differently than VHT-SIG-A, e.g. there is no repetition of the 20 MHz sub-channel into the other sub-channels. Instead, for 40, 80, and 160 MHz bandwidths the bits are repeated including the tail bits. In this way, processing gain is achieved at the receiver by averaging repeated soft values at the decoder input.

VHT-SIG-B is comprised of a single 4 μsec OFDM symbol with single stream, BPSK, BCC rate ½ modulation. Therefore in 20 MHz mode, 26 bits are available. Twenty bits are used to convey signaling information and six bits are tail. For higher bandwidths, additional bits are available due to extra subcarriers. With 40 MHz, there are 21 information bits and six tail bits, each repeated twice. With 80 MHz there are 23 information bits and six tail bits each repeated four times, with a single pad bit appended at the end. For 160 MHz and 80+80 MHz, the 80 MHz bit sequence is repeated twice. This is illustrated in Figure 7.11.

The fields in VHT-SIG-B for a SU packet are VHT-SIG-B Length and tail. The number of bits allocated for VHT-SIG-B Length is 17, 19, and 21 for 20, 40, and 80 MHz bandwidth, respectively. The additional length bits for the larger bandwidths are to accommodate larger packet sizes that are possible in 5.46 ms (max packet duration in L-SIG). There are six tail bits, set to zero, for each bandwidth. The remaining bits are filled with reserved bits that are set to one. The locations of the fields in VHT-SIG-B for each bandwidth are shown in Figure 7.12.

The purpose of VHT-SIG-B Length is to indicate the length of the useful data in the packet. It provides the length of the A-MPDU pre-EOF padding in units of 4 bytes, as

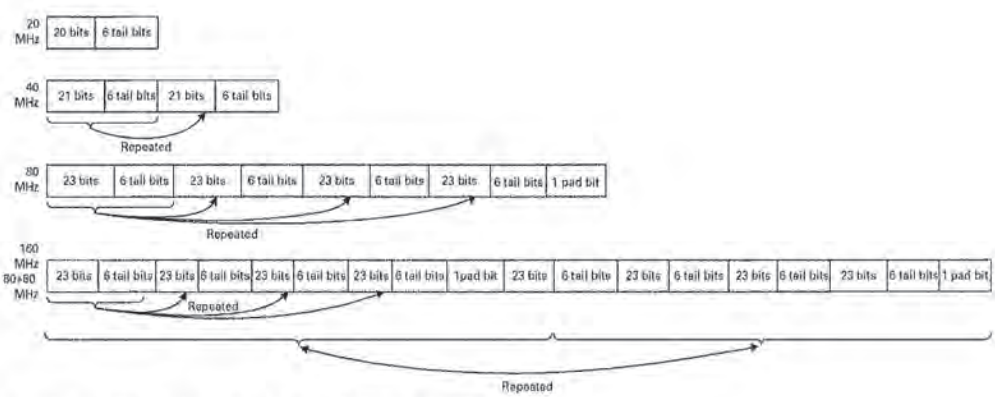

Figure 7.11 Repetition of bits in VHT-SIG-B (IEEE, 2012).

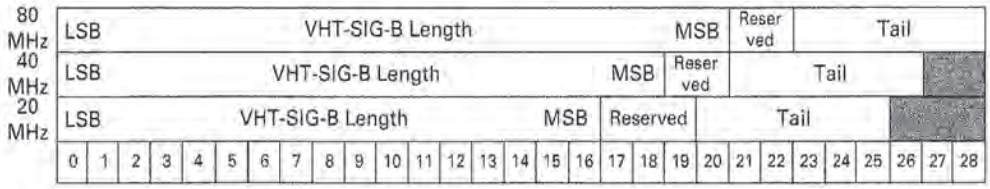

Figure 7.12 Fields in VHT-SIG-B for SU packet.

defined in Eq. (7.28). This allows receivers to shut off PHY processing after receiving useful data and thereby saving some power. Since the length of the packet as calculated by receiver with L-SIG and VHT-SIG-A information with Eq. (7.11) is only greater than VHT-SIG-B Length by at most a few bits less than those contained in a single symbol, the utility of this in SU operation is minimal. The main purpose is for multi-user operation where padding between different users can result in many extra symbols, refer to Chapter 14 for more information. Furthermore, since there are only enough bits in VHT-SIG-B to provide length in units of 4 bytes, the PHY still does not have the exact packet length and the MAC needs to determine this from the A-MPDU length information in the delimiters:

$$\text{VHT\_SIG\_B\_LENGTH} = \left\lceil \frac{\text{A\_MPDU\_LENGTH}}{4} \right\rceil \tag{7.28}$$

It may happen that the A-MPDU pre-EOF padding is not a multiple of 4 bytes, requires less than 4 bytes of EOF padding to fill the PSDU, and further that the total length of the A-MPDU including the padding is also not a multiple of 4 bytes. In this case the value placed in the VHT-SIG-B Length field, when rounded up to the next 4 octet boundary, would indicate a length that is slightly longer than the PHY payload length calculated by receiver with L-SIG and VHT-SIG-A information with Eq. (7.11). VHT_SIG_B_LENGTH may exceed the PHY payload length by up to 3 bytes.

For example, consider SU packet with 80 MHz, single stream, BPSK, rate ½, and A-MPDU pre-EOF padding length of 14 621 bytes. VHT_SIG_B_LENGTH is computed to be 14 624 bytes with Eq. (7.28) (IEEE, 2012). However, the PHY payload length is calculated as 14 622 bytes with Eq. (7.11).

The waveform for VHT-SIG-B is created as follows. There is no frequency repetition of 20 MHz sub-channels into other sub-channels, instead the bits are repeated as illustrated in Figure 7.11. As indicated by Table 7.5, the 800 ns guard interval is always used to compose the VHT-SIG-B symbol regardless of the Short GI field setting in VHT-SIG-A. Since VHT-SIG-B only consists of one spatial stream, the VHT-SIG-B constellation points are mapped to N_{STS} space-time streams by the first column of the P matrix. The resulting $X_{\text{Field},k,i_{\text{SS}},n}$ value for subcarrier k, spatial stream i_{SS}, and symbol n in the time domain waveform in Eq. (7.20) for VHT-SIG-B is defined in Eq. (7.29):

$$X_{\text{VHT-SIG-B},k,i_{\text{SS}}} = [P_{\text{VHTLTF}}]_{i_{\text{SS}},1} D_{k,\text{BW}} + p_z P_0^k \tag{7.29}$$

where p_z is given in Eq. (4.5) and z is equal to 3, $D_{k,\text{BW}}$ is defined in Section 7.3.3.11, and P_n^k is defined in Section 7.3.3.8.

7.3.3 VHT data field

The Data field encoding process for single user transmission with BCC and 20, 40, 80 MHz and 160 MHz bandwidth are for the most part the same as in 802.11n and described in Section 4.2.3. The only difference is the order of the padding and the tail bits, as described

in Section 7.2. The LDPC encoding process is modified as compared to 802.11n. The BCC encoder parsing has been expanded to encompass more than two encoders in 802.11ac to support the higher data rates. The stream parser is expanded to eight spatial streams. The major new modification to the processing steps is for 160 MHz, which includes a frequency segment parser. The interleaver is modified to encompass up to eight spatial streams and 80 MHz. In addition, the Service field has been modified to include a CRC for VHT-SIG-B. These changes are described in detail in the subsequent sections.

7.3.3.1 PHY transmitter flow

The transmitter block diagram for the HT Data field for 802.11n is illustrated in Figure 4.21, and still mostly applies for 20, 40, and 80 MHz bandwidths. The modifications to the padding, tail, and VHT-SIG-B are illustrated for BCC in Figure 7.13.

For 160 MHz, the data is encoded across 160 MHz, but interleaved over only 80 MHz. Therefore a frequency segment parser is inserted before the interleaver block. For contiguous

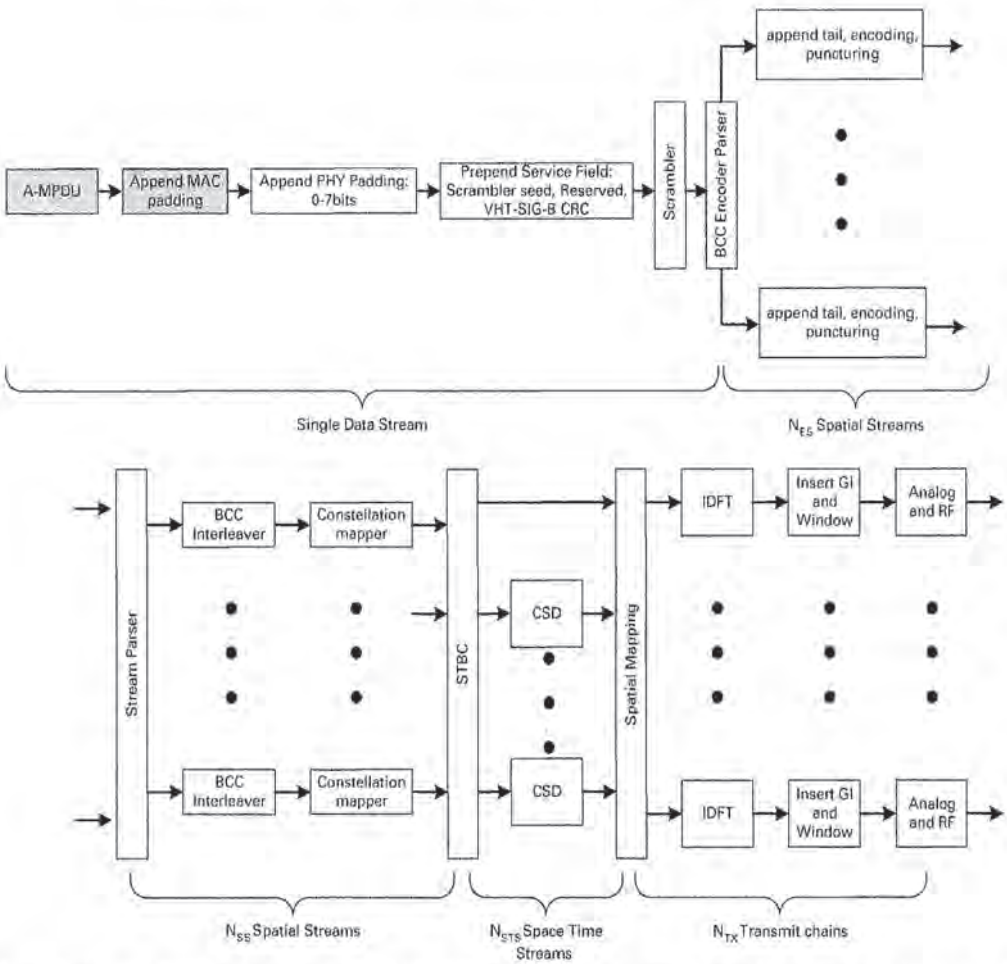

Figure 7.13 SU Transmitter block diagram for VHT Data field for 20, 40, and 80 MHz with BCC. Reproduced with permission from Asai (2012).

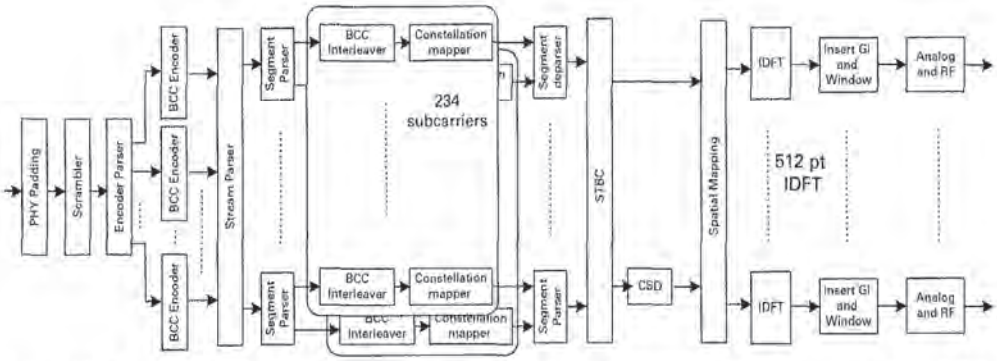

Figure 7.14 Transmitter block diagram for VHT Data field for contiguous 160 MHz transmission with BCC. Reproduced with permission from Asai (2012).

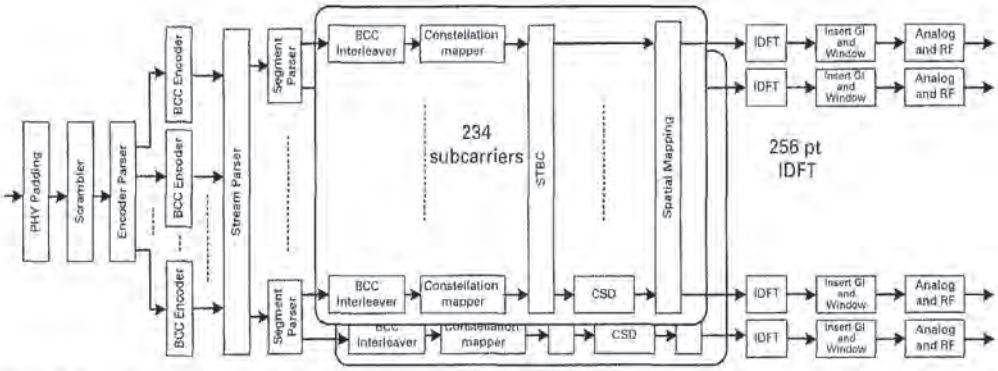

Figure 7.15 Transmitter block diagram for VHT Data field for non-contiguous 80+80 MHz transmission with BCC. Reproduced with permission from Asai (2012).

160 MHz transmission, a 512 pt IDFT is used, as shown in Figure 7.14. However, as illustrated in Figure 7.15 for non-contiguous 80+80 MHz operation, each frequency segment follows the 80 MHz format with a 256 pt IDFT for each frequency segment.

7.3.3.2 Service field

As seen in Figure 7.12, there is no CRC in VHT-SIG-B since there were not enough available bits. Instead, the CRC for VHT-SIG-B is included in the Service field. The transmitter computes an 8-bit CRC based on VHT-SIG-B "information bits," i.e. not including repetition, tail, or pad. These are the initial 17, 20, and 23 bits for 20, 40, and 80 MHz bandwidths, respectively (160 MHz and 80+80 MHz are processed the same as 80 MHz). The 8-bit CRC is inserted in the 8 MSB's of the Service field. In addition, the 7 Scrambler bits and the one remaining Reserved bit are also not included in the CRC computation. This is illustrated in Figure 7.16. The CRC calculation is the same as for VHT-SIG-A and defined in Section 4.2.2.1, with C7 of the CRC mapped to B8 of the Service field, C6 to B7,. . ., C0 to B15. The resulting Service field and data is scrambled as in 802.11n, and described in Section 4.2.3.2.

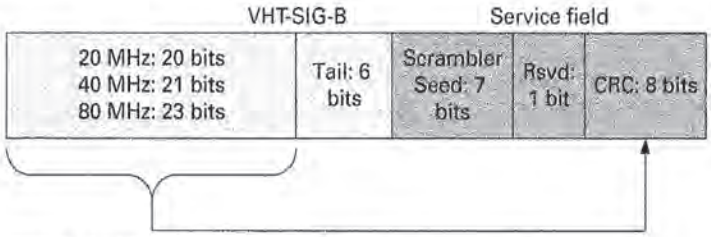

Figure 7.16 CRC for VHT-SIG-B in Service field.

Even though the scrambler bits are not included in the CRC computation, they are still protected by the CRC. Any error in the scrambler seed field will result in a corrupted CRC field after descrambling. Checking the CRC field against the contents of VHT-SIG-B will then fail. However, since it is optional to parse VHT-SIG-B in a SU packet at the receiver, it is also optional to check the CRC. Even so, an error in the scrambler seed would also cause the entire packet to be in error, which would be detected by the MAC with the FCS in the MPDU.

7.3.3.3 Encoding

BCC encoder parser for SU

In 802.11n, only one or two BCC encoders were used. With the gigabit data rates in 802.11ac, up to 12 encoders are possible as seen in Table 7.12. The BCC encoder parser for 802.11n in Eq. (5.7) is expanded for 802.11ac. The ith bit is sent to the jth encoder, where b is the data string in Eq. (7.30) (IEEE, 2012):

$$x_i^{(j)} = \begin{cases} b_{N_{ES} \cdot i+j} & 0 \le i < N_{SYM} \frac{N_{DBPS}}{N_{ES}} - 6, \quad 0 \le j \le N_{ES} - 1 \\ 0 & N_{SYM} \frac{N_{DBPS}}{N_{ES}} - 6 \le i \le N_{SYM} \frac{N_{DBPS}}{N_{ES}}, \quad 0 \le j \le N_{ES} - 1 \end{cases} \tag{7.30}$$

Also note that in 802.11n, six scrambled "zero" tail bits following the end of the message bits in each BCC are replaced by unscrambled "zero" bits. This step is not necessary in 802.11ac since the tail bits are at the end of the packet. The tail bits are appended to each data bit flow after the encoder parser.

LDPC coding for SU

For the most part the LDPC encoder/decoder processing is the same as 802.11n. Due to the change in the padding (see Section 7.2), there is a change to the computation of the number of encoded bits, as follows.

In Section 6.4.1.1, N_{SYM} computed in Eq. (6.16) is replaced by Eq. (7.10) in 802.11ac. Then N_{pld} in Eq. (6.17) is replaced by Eq. (7.31), as follows (IEEE, 2012):

$$N_{pld} = N_{SYM} N_{DBPS} \tag{7.31}$$

If after following Steps 1–5 in Sections 6.4.1.1–6.4.1.5, N_{SYM} computed in Eq. (6.30) is greater than that computed with Eq. (7.10), then the LDPC Extra Symbol field in VHT-SIG-A is set to 1.

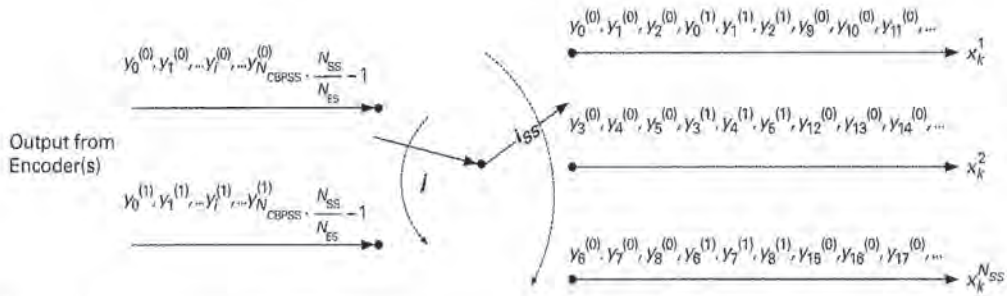

Figure 7.17 Stream parser for N_{ES} encoders.

7.3.3.4 Stream parsing

Stream parsing for VHT is similar to HT. For VHT data rates with one encoder, the stream parser for VHT will follow Section 4.2.3.3. For VHT data rates with two encoders, VHT stream parsing is the same as Section 5.1.4.3. For data rates with higher number of encoders, we generalize the equations in those sections as follows in Eq. (7.32) and illustrated in Figure 7.17:

$$\begin{aligned} s &= \max\left\{1, \frac{N_{BPSCS}}{2}\right\} \\ x_k^{i_{SS}} &= y_i^{(j)} \\ j &= \left\lfloor \frac{k}{s} \right\rfloor \bmod N_{ES} \\ i &= (i_{SS} - 1) \cdot s + s \cdot N_{SS} \cdot \left\lfloor \frac{k}{N_{ES} \cdot s} \right\rfloor + k \bmod s \end{aligned} \tag{7.32}$$

where $1 \le i_{SS} \le N_{SS}$; and $k = 0, 1, \ldots, N_{CBPSS} - 1$.

In 802.11n, the stream parser also needs to accommodate unequal modulation as described in Section 13.4. There is no unequal modulation in 802.11ac, so this is not necessary for VHT transmissions.

There is an exception for the following 160 MHz MCSs, where the number of coded bits per symbol is not evenly divisible into blocks of bits for each stream and encoder. These MCSs include:

- 160 MHz, $N_{SS} = 5$, MCS = 5
- 160 MHz, $N_{SS} = 5$, MCS = 6
- 160 MHz, $N_{SS} = 7$, MCS = 5
- 160 MHz, $N_{SS} = 7$, MCS = 6

In these cases, the residual bits are distributed to the streams as described by Eqs. (7.33), (7.34), and (7.35) (IEEE, 2012):

$$j = \begin{cases} \left\lfloor \frac{k}{s} \right\rfloor \bmod N_{ES} & k = 0, 1, \ldots, N_{Block} \cdot N_{ES} \cdot s - 1 \\ \left\lfloor \frac{L}{M} \right\rfloor & k = N_{Block} \cdot N_{ES} \cdot s, \ldots N_{CBPSS} - 1 \end{cases}$$

$$i = \begin{cases} (i_{SS} - 1) \cdot s + s \cdot N_{SS} \cdot \left\lfloor \frac{k}{N_{ES} \cdot s} \right\rfloor + k \bmod s & k = 0, 1, \ldots, N_{Block} \cdot N_{ES} \cdot s - 1 \\ (L \bmod M) \cdot s + N_{Block} \cdot s \cdot N_{SS} + k \bmod s & k = N_{Block} \cdot N_{ES} \cdot s, \ldots N_{CBPSS} - 1 \end{cases} \tag{7.33}$$

where

$$N_{\text{Block}} = \left\lfloor \frac{N_{\text{CBPS}}}{N_{\text{ES}} \cdot N_{\text{SS}} \cdot s} \right\rfloor \tag{7.34}$$

and

$$\begin{aligned} M &= \frac{N_{\text{CBPS}} - N_{\text{Block}} \cdot N_{\text{ES}} \cdot N_{\text{SS}} \cdot s}{N_{\text{ES}} \cdot s} \\ L &= \left\lfloor \frac{k - N_{\text{Block}} \cdot N_{\text{ES}} \cdot s}{s} \right\rfloor \cdot N_{\text{SS}} + (i_{\text{SS}} - 1) \end{aligned} \tag{7.35}$$

7.3.3.5 160 MHz frequency segment parsing

As described in Section 7.3.3.1 and illustrated in Figure 7.14 and Figure 7.15, the 160 MHz and 80+80 MHz transmissions are divided into two 80 MHz frequency segments by the new segment parser. The output bits of each stream parser are first divided into blocks of N_{CBPSS} bits. Then each block is further divided into two sub-blocks ($l = 0,1$) of $N_{\text{CBPSS}}/2$ bits. If N_{CBPSS} is not divisible by $2s \cdot N_{\text{ES}}$, there will be residual bits that need to be accounted for. The entire segment parsing operation is mathematically described by Eq. (7.36) (IEEE, 2012):

$$y_{k,l} = x_j$$

$$j = \begin{cases} 2s \cdot N_{\text{ES}} \left\lfloor \frac{k}{s \cdot N_{\text{ES}}} \right\rfloor + l \cdot s \cdot N_{\text{ES}} + k \bmod (s \cdot N_{\text{ES}}) & k = 0, 1, \ldots \left\lfloor \frac{N_{\text{CBPSS}}}{2s \cdot N_{\text{ES}}} \right\rfloor \cdot s \cdot N_{\text{ES}} - 1 \\ 2s \cdot N_{\text{ES}} \left\lfloor \frac{k}{s \cdot N_{\text{ES}}} \right\rfloor + l \cdot s + k \bmod s & k = \left\lfloor \frac{N_{\text{CBPSS}}}{2s \cdot N_{\text{ES}}} \right\rfloor \cdot s \cdot N_{\text{ES}}, \ldots, \frac{N_{\text{CBPSS}}}{2} - 1 \\ \quad + 2s \cdot \left\lfloor \frac{k \bmod (s \cdot N_{\text{ES}})}{s} \right\rfloor & \text{only if } N_{\text{CBPSS}} \text{ is not divible by } 2s \cdot N_{\text{ES}} \end{cases} \tag{7.36}$$

where x_j is the jth bit of a block of N_{CBPSS} bits, $j = 0, 1, \ldots, N_{\text{CBPSS}} - 1$, and $y_{k,l}$ is the kth bit of the lth frequency sub-block.

For 20, 40, and 80 MHz channel bandwidths, this operation is skipped as illustrated in Figure 7.13.

7.3.3.6 BCC interleaving

The BCC interleaver for 802.11ac for 20 and 40 MHz and up to four spatial streams is the same as 802.11n as given in Sections 4.2.3.4 and 5.1.4.4. There are new permutation parameters for 80 MHz and for more than four spatial streams. The interleaver parameters are summarized in Table 7.6.

Table 7.6 VHT interleaver parameters

Parameter	20 MHz	40 MHz	80 MHz
N_{COL}	13	18	26
N_{ROW}	$4 \cdot N_{\text{BPSCS}}$	$6 \cdot N_{\text{BPSCS}}$	$9 \cdot N_{\text{BPSCS}}$
N_{ROT} ($N_{\text{SS}} \leq 4$)	11	29	58
N_{ROT} ($N_{\text{SS}} > 4$)	6	13	28

We generalize the first permutation from Eq. (4.25) for all bandwidths and spatial streams in Eq. (7.37) (IEEE, 2012):

$$i = N_{\mathrm{ROW}} \cdot (k \bmod N_{\mathrm{COL}}) + \left\lfloor \frac{k}{N_{\mathrm{COL}}} \right\rfloor \tag{7.37}$$

where $1 \le i_{\mathrm{SS}} \le N_{\mathrm{SS}}$, $k = 0,1,\ldots, N_{\mathrm{CBPSSI}} - 1$. For 160 MHz we divide N_{CBPSS} into two segments. Therefore, N_{CBPSSI} is equal to N_{CBPSS} for 20, 40, and 80 MHz, and N_{CBPSSI} is equal to $N_{\mathrm{CBPSS}}/2$ for 160 and 80+80 MHz.

The second permutation in Eq. (4.26) is generalized by Eq. (7.38) (IEEE, 2012):

$$j = s \cdot \left\lfloor \frac{k}{s} \right\rfloor + \left(k + N_{\mathrm{CBPSSI}} - \left\lfloor \frac{N_{\mathrm{COL}} \cdot k}{N_{\mathrm{CBPSSI}}} \right\rfloor \right) \bmod s \tag{7.38}$$

where $1 \le i_{\mathrm{SS}} \le N_{\mathrm{SS}}$, $k = 0,1,\ldots, N_{\mathrm{CBPSSI}} - 1$, and s is the same block size as with the stream parser, defined by Eq. (7.32).

If there is more than one spatial stream the third permutation is performed as described by Eq. (7.39) (IEEE, 2012). Furthermore, with more than four spatial streams, an extra frequency rotation is applied (in the form of $J(i_{\mathrm{SS}})$ given in Table 7.7):

$$r = \begin{cases} \left(k - \left(((i_{\mathrm{SS}} - 1) \cdot 2) \bmod 3 + 3 \cdot \left\lfloor \frac{i_{\mathrm{SS}}-1}{3} \right\rfloor\right) \cdot N_{\mathrm{ROT}} \cdot N_{\mathrm{BPSCS}}\right) \bmod N_{\mathrm{CBPSSI}} & 2 \le N_{\mathrm{SS}} \le 4 \\ \left(k - J(i_{\mathrm{SS}}) \cdot N_{\mathrm{ROT}} \cdot N_{\mathrm{BPSCS}}\right) \bmod N_{\mathrm{CBPSSI}} & N_{\mathrm{SS}} > 4 \end{cases} \tag{7.39}$$

where $1 \le i_{\mathrm{SS}} \le N_{\mathrm{SS}}$, and $k = 0,1,\ldots, N_{\mathrm{CBPSSI}} - 1$.

At the receiver, the deinterleaver reverses these steps. The first permutation reverses the third interleaver permutation if there is more than one spatial stream. Equation (4.40) is generalized for all channel bandwidths in Eq. (7.40) (IEEE, 2012) when $N_{\mathrm{SS}} \le 4$:

$$r = \left(k + \left(((i_{\mathrm{SS}} - 1) \cdot 2) \bmod 3 + 3 \cdot \left\lfloor \frac{i_{\mathrm{SS}} - 1}{3} \right\rfloor \right) \cdot N_{\mathrm{ROT}} \cdot N_{\mathrm{BPSCS}} \right) \bmod N_{\mathrm{CBPSSI}} \tag{7.40}$$

Table 7.7 $J(i_{\mathrm{SS}})$ values (IEEE, 2012)

i_{SS}	$J(i_{\mathrm{SS}})$
1	0
2	5
3	2
4	7
5	3
6	6
7	1
8	4

where $1 \le i_{SS} \le N_{SS}$, $k = 0,1,\ldots, N_{CBPSSI} - 1$. When $N_{SS} > 4$, the reversal of the third interleaver permutation is given by Eq. (7.41) (IEEE, 2012):

$$r = (k + J(i_{SS}) \cdot N_{ROT} \cdot N_{BPSCS}) \bmod N_{CBPSSI} \tag{7.41}$$

The second deinterleaver permutation reverses the second interleaver permutation. Equation (4.41) is generalized for all channel bandwidths in Eq. (7.42) (IEEE, 2012):

$$j = s \cdot \left\lfloor \frac{k}{s} \right\rfloor + \left(k + \left\lfloor \frac{N_{COL} \cdot k}{N_{CBPSSI}} \right\rfloor \right) \bmod s \tag{7.42}$$

The third deinterleaver permutation reverses the first interleaver permutation. Equation (4.42) is generalized for all channel bandwidths in Eq. (7.43) (IEEE, 2012):

$$i = N_{COL} \cdot k - (N_{CBPSSI} - 1) \cdot \left\lfloor \frac{k}{N_{ROW}} \right\rfloor \tag{7.43}$$

7.3.3.7 256-QAM modulation mapping

BPSK, QPSK, 16-QAM, and 64-QAM are modulated the same as in 802.11n. As one method to increase the data rate and spectral efficiency, 256-QAM is introduced in 802.11ac. The mapping is shown in Figure 7.18. The normalization factor is $1/\sqrt{170}$.

7.3.3.8 LDPC subcarrier mapper

As described in Zheng *et al.* (2010), an interleaver was not used in 802.11n with LDPC since with a 1944 bit LDPC code word the bits are spread over all the streams and subcarriers within an OFDM symbol for most 802.11n data rates. In addition, LDPC has an intrinsic pseudo-randomness property that protects it against burst errors. However, since we use the same code words for 802.11ac with gigabit data rates, the LDPC code word may only occupy a few of the subcarriers and not achieve full frequency diversity. Simulation results in Zheng *et al.* (2010) showed that the required SNR for 64-QAM, rate ¾, four spatial streams, 80 MHz improved by one dB when including a subcarrier mapper. Therefore a subcarrier mapper is added in the transmitter flow when an LDPC encoder is used, as shown in Figure 7.19.

As described in Zheng *et al.* (2010), the objective of the LDPC tone mapper is to map consecutive QAM symbols to non-consecutive subcarriers. The separation distance of the subcarriers (D_{TM}) is a function of bandwidth, given in Table 7.8.

The output of the constellation mapper is $d_{k,l,n}$, similar to that defined in Eq. (4.28) for 802.11n. Each of the n OFDM symbols consists of N_{SD} subcarriers (defined in Table 7.11) indexed by k and N_{SS} spatial streams indexed by l. The output of the LDPC mapper is $d'_{k,l,n}$, defined by Eq. (7.44) for 20, 40, 80, and 80+80 MHz:

$$d'_{k,l,n} = d_{r(k),l,n}$$

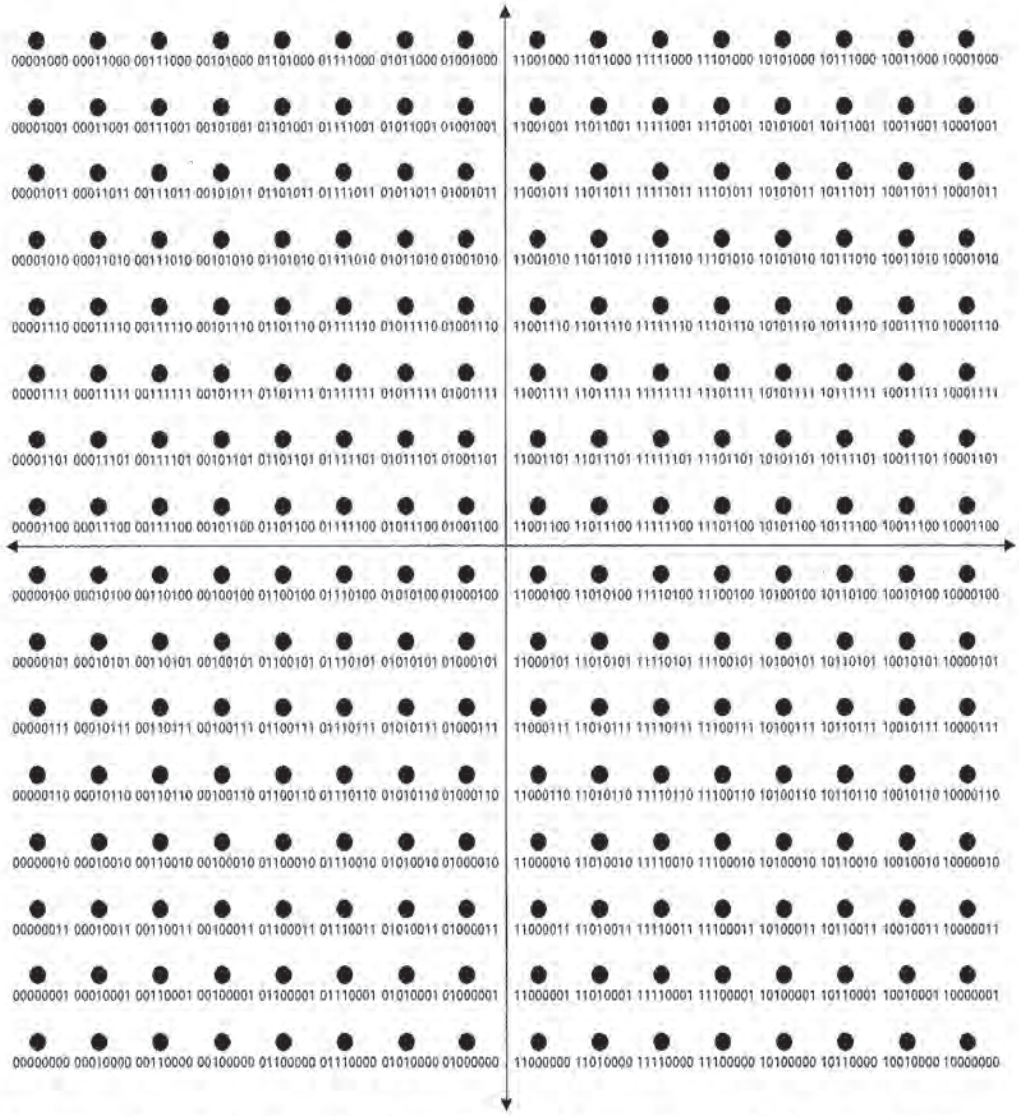

Figure 7.18 Constellation bit encoding for 256-QAM. Reproduced with permission from Stacey (2011).

where

$$t(k) = D_{\mathrm{TM}} \cdot (k \bmod \frac{N_{\mathrm{SD}}}{D_{\mathrm{TM}}}) + \left\lfloor \frac{k \cdot D_{\mathrm{TM}}}{N_{\mathrm{SD}}} \right\rfloor \tag{7.44}$$
$$k = 0, 1, \ldots, N_{\mathrm{SD}} - 1,\ l = 1, \ldots, N_{\mathrm{SS}},\ n = 0, 1, \ldots, N_{\mathrm{SYM}} - 1$$

For 160 MHz, the N_{SD} value for 80 MHz is used. The subcarrier mapping operation is repeated for each 80 MHz frequency segment for both 160 MHz and 80+80 MHz.

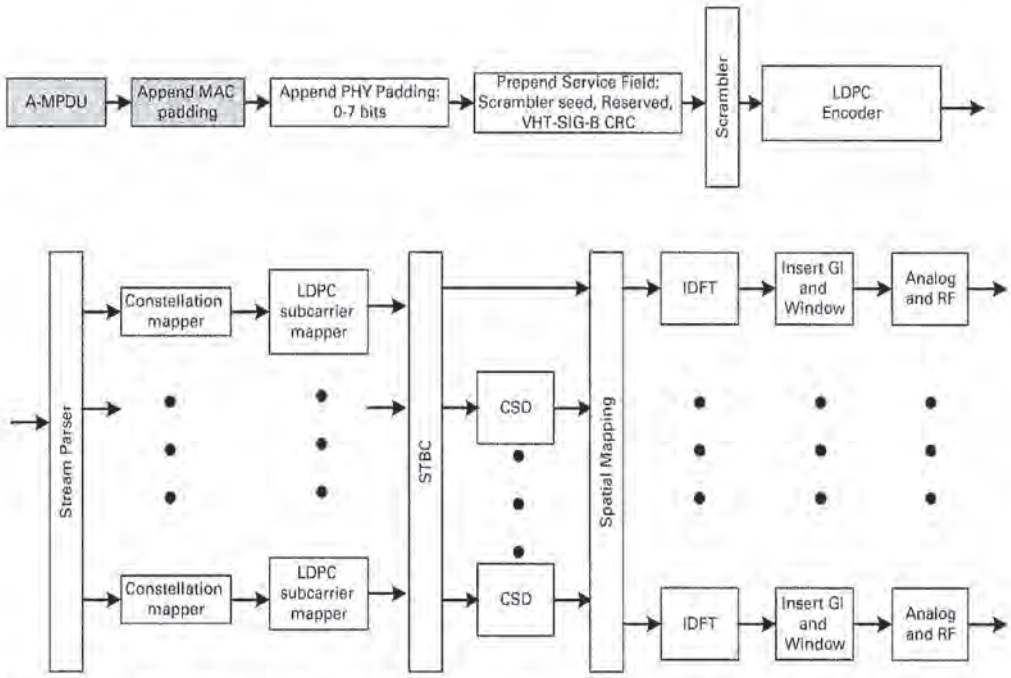

Figure 7.19 Transmitter block diagram for VHT Data field for 20, 40, and 80 MHz with LDPC.

Table 7.8 LDPC subcarrier mapping distance for each bandwidth (IEEE, 2012)

Parameter	20 MHz	40 MHz	80, 160, 80+80 MHz
D_{TM}	4	6	9

7.3.3.9 Segment deparser for 160 MHz

As illustrated in Figure 7.14, the segment deparser operation follows the constellation mapper for BCC (or subcarrier mapper for LDPC). This takes the output of each 80 MHz frequency segment and combines them back into a single 160 MHz segment. The 80 MHz frequency segment corresponding to $l = 0$ in Eq. (7.36) maps to data values 0 to 233 and the 80 MHz frequency segment corresponding to $l = 1$ in Eq. (7.36) maps to data values 234 to 467. This operation is skipped for 20 MHz, 40 MHz, 80 MHz, and 80+80 MHz transmissions.

7.3.3.10 Pilot subcarriers

As described in Section 7.3.2.3, pilot values are identical for all space-time streams. Therefore, the pilot subcarrier values are defined for one spatial stream and are copied across all space-time streams. The pilot subcarriers are inserted into the waveform prior to application of the cyclic shifts.

Table 7.9 Pilot values for 80 MHz (IEEE, 2012)

Ψ_0	Ψ_1	Ψ_2	Ψ_3	Ψ_4	Ψ_5	Ψ_6	Ψ_7
1	1	1	−1	−1	1	1	1

For 20 MHz, the pilot values are the same as the first row of Table 4.4. The pilot mapping P_n^k for symbol n and subcarrier k is given by Eq. (7.45) (IEEE, 2012):

$$\begin{aligned} P_n^{\{-21,-7,7,21\}} &= \left\{\Psi^{(1)}_{1,n\oplus 4}, \Psi^{(1)}_{1,(n+1)\oplus 4}, \Psi^{(1)}_{1,(n+2)\oplus 4}, \Psi^{(1)}_{1,(n+3)\oplus 4}\right\} \\ P_n^{k\notin\{-21,-7,7,21\}} &= 0 \end{aligned} \tag{7.45}$$

For 40 MHz, the pilot values are the same as the first row of Table 5.1. The pilot mapping is given by Eq. (7.46) (IEEE, 2012):

$$\begin{aligned} P_n^{\{-53,-25,-11,11,25,53\}} &= \left\{\Psi^{(1)}_{1,n\oplus 6}, \Psi^{(1)}_{1,(n+1)\oplus 6}, \Psi^{(1)}_{1,(n+2)\oplus 6}, \Psi^{(1)}_{1,(n+3)\oplus 6}, \Psi^{(1)}_{1,(n+4)\oplus 6}, \Psi^{(1)}_{1,(n+5)\oplus 6}\right\} \\ P_n^{k\notin\{-53,-25,-11,11,25,53\}} &= 0 \end{aligned} \tag{7.46}$$

For 80 MHz, the pilot values are defined in Table 7.9.

The pilot mapping is given by Eq. (7.47) (IEEE, 2012):

$$\begin{aligned} P_n^{\{-103,-75,-39,-11,11,39,75,103\}} &= \{\Psi_{n\oplus 8}, \Psi_{(n+1)\oplus 8}, \Psi_{(n+2)\oplus 8}, \Psi_{(n+3)\oplus 8}, \\ &\quad \Psi_{(n+4)\oplus 8}, \Psi_{(n+5)\oplus 8}, \Psi_{(n+6)\oplus 8}, \Psi_{(n+7)\oplus 8}\} \\ P_n^{k\notin\{-103,-75,-39,-11,11,39,75,103\}} &= 0 \end{aligned} \tag{7.47}$$

For 160 MHz, the 80 MHz pilot values in Table 7.9 are replicated in each 80 MHz frequency segment according to Eq. (7.48) (IEEE, 2012):

$$\begin{aligned} &P_n^{\{-231,-203,-167,-139,-117,-89,-53,-25,25,53,89,117,139,167,203,231\}} \\ &= \{\Psi_{n\oplus 8}, \Psi_{(n+1)\oplus 8}, \Psi_{(n+2)\oplus 8}, \Psi_{(n+3)\oplus 8}, \Psi_{(n+4)\oplus 8}, \Psi_{(n+5)\oplus 8}, \Psi_{(n+6)\oplus 8}, \Psi_{(n+7)\oplus 8}, \\ &\Psi_{n\oplus 8}, \Psi_{(n+1)\oplus 8}, \Psi_{(n+2)\oplus 8}, \Psi_{(n+3)\oplus 8}, \Psi_{(n+4)\oplus 8}, \Psi_{(n+5)\oplus 8}, \Psi_{(n+6)\oplus 8}, \Psi_{(n+7)\oplus 8}\} \\ &P_n^{k\notin\{-231,-203,-167,-139,-117,-89,-53,-25,25,53,89,117,139,167,203,231\}} = 0 \end{aligned} \tag{7.48}$$

For non-contiguous 80+80 MHz, each frequency segment follows the pilot subcarrier format as 80 MHz.

7.3.3.11 Time domain waveform

The resulting $X_{\text{Field},k,i_{\text{SS}},n}$ value for the Data field for subcarrier k, spatial stream i_{SS}, symbol n in the time domain waveform in Eq. (7.20) is defined by Eq. (7.49):

$$X_{\text{VHT-Data},k,i_{\text{SS}},n} = D_{k,i_{\text{SS}},n} + p_{n+z}P_n^k \tag{7.49}$$

where p_z is given in Eq. (4.5) and z is equal to 4, and P_n^k is defined in Section 7.3.3.10. $D_{k,i_{SS},n}$ for 20 MHz is equivalent to Eq. (4.30). $D_{k,i_{SS},n}$ for 40 MHz is equivalent to Eq. (5.2). For 80 MHz (IEEE, 2012),

$$D_{k,i_{SS},n} = \begin{cases} 0 & k = 0, \pm 1, \pm 11, \pm 39, \pm 75, \pm 103 \\ d_{M^r(k),i_{SS},n} & \text{otherwise} \end{cases}$$

$$M^r(k) = \begin{cases} k+122 & -122 \le k \le -104 \\ k+121 & -102 \le k \le -76 \\ k+120 & -74 \le k \le -40 \\ k+119 & -38 \le k \le -12 \\ k+118 & -10 \le k \le -2 \\ k+115 & 2 \le k \le 10 \\ k+114 & 12 \le k \le 38 \\ k+113 & 40 \le k \le 74 \\ k+112 & 76 \le k \le 102 \\ k+111 & 104 \le k \le 122 \end{cases} \tag{7.50}$$

For 160 MHz (IEEE, 2012),

$$D_{k,i_{SS},n} = \begin{cases} 0 & k = 0, \pm 1, \pm 2, \pm 3, \pm 4, \pm 5, \pm 25, \pm 53, \pm 89, \pm 117, \pm 127, \pm 128, \pm 129, \pm 139, \pm 167, \pm 203, \pm 231 \\ d_{M^r(k),i_{SS},n} & \text{otherwise} \end{cases}$$

$$M^r(k) = \begin{cases} k+250 & -250 \le k \le -232 \\ k+249 & -230 \le k \le -204 \\ k+248 & -202 \le k \le -168 \\ k+247 & -166 \le k \le -140 \\ k+246 & -138 \le k \le -130 \\ k+243 & -126 \le k \le -118 \\ k+242 & -116 \le k \le -90 \\ k+241 & -88 \le k \le -54 \\ k+240 & -52 \le k \le -26 \\ k+239 & -24 \le k \le -6 \\ k+228 & 6 \le k \le 24 \\ k+227 & 26 \le k \le 52 \\ k+226 & 54 \le k \le 88 \\ k+225 & 90 \le k \le 116 \\ k+224 & 118 \le k \le 126 \\ k+221 & 130 \le k \le 138 \\ k+220 & 140 \le k \le 166 \\ k+219 & 168 \le k \le 202 \\ k+218 & 204 \le k \le 230 \\ k+217 & 232 \le k \le 250 \end{cases} \tag{7.51}$$

For non-contiguous 80+80 MHz, each frequency segment follows the subcarrier format as 80 MHz.

7.4 Modulation coding scheme

The new VHT MCS indices are listed in Table 7.10. In 802.11n, MCS referred to modulation, coding, and spatial streams. In 802.11ac, MCS only refers to modulation and coding. MCS 0 – 7 are the same set of modulation and codes rates as in 11n. The two new MCSs in 802.11ac are 256-QAM, rate 3/4 and 256-QAM, rate 5/6. The number of coded bits per subcarrier per spatial stream (N_{BPSCS}) is also given in Table 7.10.

The number of coded data bits per symbol (N_{CBPS}) is defined by Eq. (7.52), and the number of data bits per symbol (N_{DBPS}) is defined by Eq. (7.53):

$$N_{CBPS} = N_{SD} \cdot N_{FS} \cdot N_{SS} \cdot N_{BPSCS} \tag{7.52}$$

$$N_{DBPS} = N_{CBPS} \cdot R \tag{7.53}$$

with the number of complex data numbers per frequency segment (N_{SD}) and the number of frequency segments (N_{FS}) given in Table 7.11. N_{SD} for 20 and 40 MHz is the same as 802.11n.

Table 7.10 VHT MCS index

MCS index	Modulation	Rate (R)	N_{BPSCS}
0	BPSK	1/2	1
1	QPSK	1/2	2
2	QPSK	3/4	2
3	16-QAM	1/2	4
4	16-QAM	3/4	4
5	64-QAM	2/3	6
6	64-QAM	3/4	6
7	64-QAM	5/6	6
8	256-QAM	3/4	8
9	256-QAM	5/6	8

Table 7.11 Number of complex data numbers per frequency segment (N_{SD}) and number of frequency segments (N_{FS})

BW (MHz)	N_{SD}	N_{FS}
20	52	1
40	108	1
80	234	1
160	468	1
80+80	234	2

The resulting data rate for each combination of bandwidth, modulation, code rate, number of spatial streams, and guard interval duration is given by Eq. (7.54):

$$\text{Data rate (Mbps)} = \begin{cases} \dfrac{N_{\text{DBPS}}}{4} & \text{for normal GI} \\ \dfrac{N_{\text{DBPS}}}{3.6} & \text{for short GI} \end{cases} \tag{7.54}$$

Like 802.11n for 40 MHz, the data rate per BCC encoder is restricted to minimize the decoder complexity. In 802.11ac, the data rate per encoder is up to 600 Mbps. The number of BCC encoders for each combination of bandwidth, modulation, code rate, and number of spatial streams is given by Eq. (7.55). This equation applies to either normal GI or short GI.

$$N_{\text{ES}} = \left\lceil \frac{N_{\text{DBPS}}/3.6}{600} \right\rceil \tag{7.55}$$

Examples of calculations of N_{DBPS}, N_{CBPS}, N_{ES}, and data rate are provided in Table 7.12.

However, there are some exceptions to Eq. (7.55). For the 802.11ac transmitter data flow, N_{DBPS} and N_{CBPS} must be an integer value for each BCC encoder. This is also true for 802.11a and 802.11n, but this is always the case for all 802.11a data rates and 802.11n MCSs. New conditions in 802.11ac: (1) 80 MHz with 234 data subcarriers, (2) 160 MHz with 468 data subcarriers, (3) 256-QAM, and (4) more than two encoders, leads to fractional N_{DBPS} and N_{CBPS} per encoder in some instances.

Mathematically, if the remainder of $N_{\text{DBPS}}/N_{\text{ES}}$ is not equal to zero OR if the remainder of $N_{\text{CBPS}}/N_{\text{ES}}$ is not equal to zero, then the MCS is excluded from 802.11ac for the particular combination of bandwidth, modulation, code rate, and number of spatial streams. However, this leads to many MCS "holes." Many of these MCS holes can be filled with an expeditious choice of N_{ES}. Hart (2011) suggests that devices implementing seven spatial streams will also implement eight spatial streams, and that devices implementing greater than four spatial streams will implement 256-QAM. Given these

Table 7.12 Example calculations of MCS parameters

							Data Rate (Mbps)	
BW (MHz)	N_{SS}	Modulation	Rate (R)	N_{DBPS}	N_{CBPS}	N_{ES}	Normal GI	Short GI
20	1	BPSK	1/2	26	52	1	6.5	7.22
40	2	QPSK	1/2	216	432	1	54	60
80	3	QPSK	3/4	1053	1404	1	263.25	292.5
160, 80+80	4	16-QAM	1/2	3744	7488	2	936	1040
40	5	16-QAM	3/4	1620	2160	1	405	450
80	6	64-QAM	2/3	5616	8424	3	1404	1560
160, 80+80	7	64-QAM	3/4	14742	19656	7	3685.5	4095
40	8	64-QAM	5/6	4320	5184	2	1080	1200
80	8	256-QAM	3/4	11232	14976	6	2808	3120
160, 80+80	8	256-QAM	5/6	24960	29952	12	6240	6933.33

Table 7.13 MCSs that do not follow N_{ES} formula in Eq. (7.55)

BW (MHz)	N_{SS}	Modulation	Rate (R)	N_{ES}
80	7	QPSK	3/4	3
80	7	64-QAM	5/6	6
80	7	256-QAM	3/4	6
80	8	64-QAM	5/6	6
160	4	64-QAM	5/6	6
160	5	256-QAM	3/4	8
160	6	64-QAM	5/6	8
160	7	16-QAM	3/4	6
160	7	64-QAM	5/6	9
160	7	256-QAM	3/4	12
160	7	256-QAM	5/6	12
160	8	64-QAM	2/3	8
160	8	256-QAM	3/4	12

Table 7.14 Excluded MCSs

BW (MHz)	N_{SS}	Modulation	Rate (R)
20	1	256-QAM	5/6
20	2	256-QAM	5/6
20	4	256-QAM	5/6
20	5	256-QAM	5/6
20	7	256-QAM	5/6
20	8	256-QAM	5/6
80	3	64-QAM	3/4
80	6	256-QAM	5/6
80	7	64-QAM	3/4
160	3	256-QAM	5/6

assumptions, an MCS that would have been excluded can be included by selecting an N_{ES} value that does not exceed that which would have already been implemented by the device. These are given in Table 7.13.

Table 7.14 lists all the excluded combinations of bandwidth, modulation, code rate, and number of spatial streams that are not permitted in 802.11ac.

LDPC has the same MCS exclusions to make the set of allowable data rates equivalent between BCC and LDPC.

The receiver minimum sensitivity for 802.11ac is given in Table 7.15. Note that MCS indexes 0–7 for 20 and 40 MHz are the same as 802.11n given in Table 5.3.

Figure 5.12 gives PER performance for 802.11n MCS 0–7 in AWGN and no impairments. These results will be the same for 802.11ac. Figure 7.20 provides the additional PER curves for 256-QAM.

Table 7.15 Receiver minimum sensitivity for 802.11ac

MCS index	Modulation	FEC code rate	Minimum sensitivity (dBm) (20 MHz channel spacing)	Minimum sensitivity (dBm) (40 MHz channel spacing)	Minimum sensitivity (dBm) (80 MHz channel spacing)	Minimum sensitivity (dBm) (160 MHz or 80+80 MHz channel spacing)
0	BPSK	1/2	−82	−79	−76	−73
1	QPSK	1/2	−79	−76	−73	−70
2	QPSK	3/4	−77	−74	−71	−68
3	16-QAM	1/2	−74	−71	−68	−65
4	16-QAM	3/4	−70	−67	−64	−61
5	64-QAM	2/3	−66	−63	−60	−57
6	64-QAM	3/4	−65	−62	−59	−56
7	64-QAM	5/6	−64	−61	−58	−55
8	256-QAM	3/4	−59	−56	−53	−50
9	256-QAM	5/6	−57	−54	−51	−48

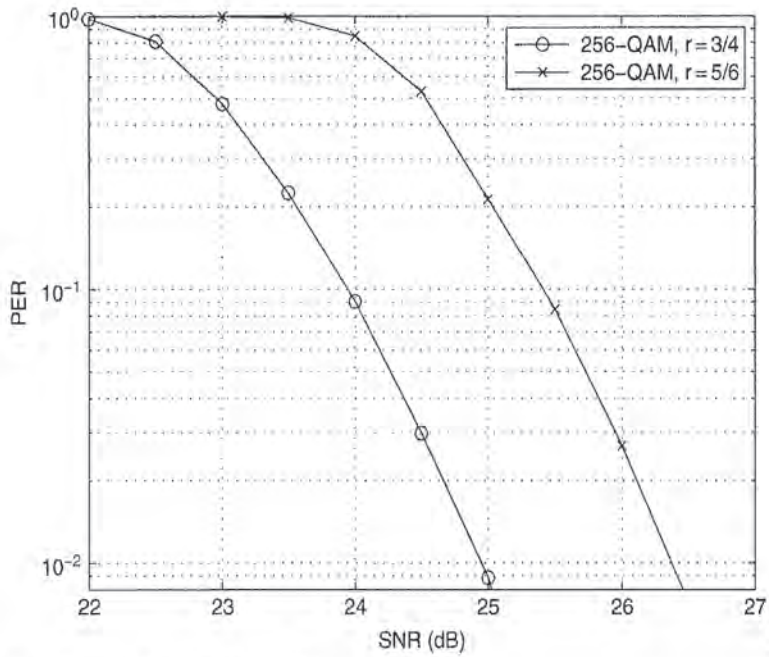

Figure 7.20 256-QAM performance in AWGN.

Figure 7.21 provides PER results for 256-QAM, R = 5/6 in channel model D with the same simulation parameters as in Figure 5.14.

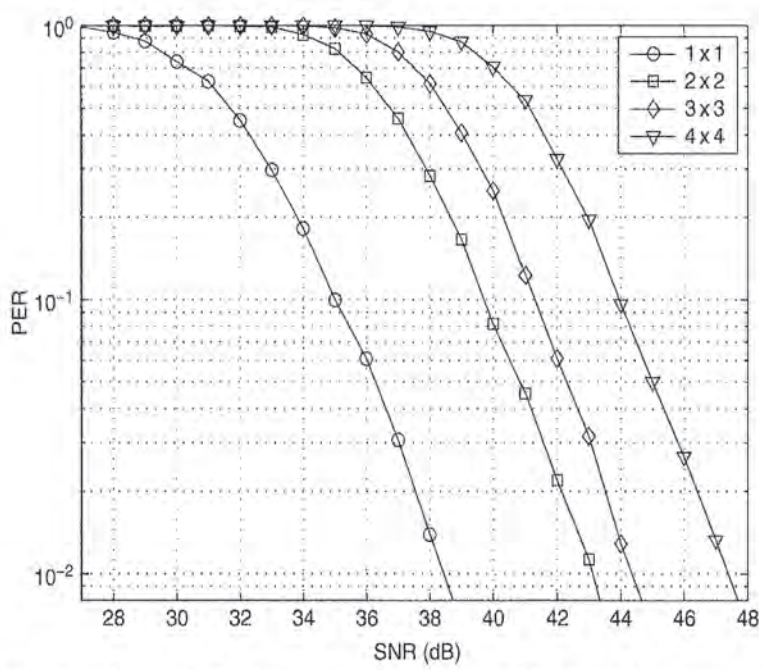

Figure 7.21 Simulated 256-QAM, R = 5/6 results with channel model D, NLOS, and impairments for 80 MHz.

References

Asai, Yusuke (2012). *Proposed resolutions to comments on transmitter block diagram*, IEEE 802.11-12/525r3.

Hart, B. (2011). D0.1 *Comment Resolution, brianh, part 4*, IEEE 802.11–10/0577r1.

IEEE (2012). *IEEE P802.11acTM/D3.00, Draft Amendment to STANDARD for Information Technology – Telecommunications and Information Exchange Between Systems – Local and Metropolitan Networks – Specific Requirements – Part 11: Wireless LAN Medium Access Control (MAC) and Physical Layer (PHY). Amendment 5: Enhancements for Very High Throughput for Operation in Bands below 6 GHz.*

Shi, K., Kim, Y., Zhang, N., *et al.* (2010). *Phase Tracking During VHT-LTF*, IEEE 802.11-10/0771r0.

Stacey, R. *et al.* (2011). *Proposed TGac draft amendment*, IEEE 802.11-10/1361r3.

Zheng, J., Erceg, V., Vermani, S. *et al.* (2010). *LDPC for 11ac*, IEEE 802.11-10/1300r0.